The activity of chromite in multicomponent spinels: An experimental study with implications for the metamorphic history of equilibrated ordinary chondrites

Thesis by
Ronit Kessel

In Partial Fulfillment of the Requirements
For the Degree of
Doctor of Philosophy

California Institute of Technology
Pasadena, California
2002

(Submitted November 14, 2001)

Acknowledgements

I would like to thank all the people, close-by and faraway, whose advice, encouragement, and friendship helped me during my Ph.D. at Caltech and contributed to my scientific development and personal happiness.

First of all, I would like to thank my advisor, Ed Stolper, for his insights and guidance. I thank him for teaching me that every problem I encounter is not a step back but a step forward in understanding the subject and for constantly questioning every assumption. I am indebted to John Beckett for his constant encouragement and enthusiasm and his endless desire to teach me, and to Mike Baker for his interest, advice, and support. I thank them both for never taking my 'quitting' threats seriously.

I am grateful for George Rossman for many scientific and non-scientific discussions. John Eiler, Don Burnett, Paul Asimow, and Peter Wyllie are appreciated for always having an open door and curiosity about my research. Harry McSween is greatly appreciated for the discussions and interest he showed in my work.

I would also like to thank many in the administrative and technical staff for their friendly attitude. Ma Chi is especially thanked for his helpful assistance and advice working on the electron probe. Gary Huss, Lauri Lishin and Yunbin Guan are thanked for their help working on the ion probe at ASU.

I would like to express my deep gratitude for many new friends I found at Caltech and old friends from Israel for their constant support and love. Yulia Goreva is especially thanked for her friendship and support through happy as well as difficult hours. I am

grateful for the sharing and nourishing between us both scientifically and non-scientifically.

I would like to thank Yehoshua Kolodny (Yeshu) for taking the time to convince me to pursue a Ph.D. at Caltech and together with Oded Navon, Avraham Starniski (Stari), and Amitai Katz, continuously inquiring about my progress and my well being all these years.

Abstract

An experimental technique for evaluating the activity of chromite in multicomponent spinels was developed by equilibrating the spinel of interest with a Pt-alloy under a controlled temperature and oxygen fugacity. The thermodynamic properties of the ternary Pt-Fe-Cr system was evaluated, such that activities of Cr and Fe in an equilibrated Pt-alloy can be used to calculate the activity of chromite in the spinel of interest.

The ternary activity model formulation used is based on the characterization of each bounding binary system, Pt-Fe, Pt-Cr, Fe-Cr, with the addition of ternary interaction terms. The Pt-Fe and Pt-Cr systems are described as asymmetric regular solutions with interaction parameters of W_{PtFe}=–138.0±3.3, W_{FePt}=–90.8±24.0, and W_{PtCr}=–129.1±1.2, W_{CrPt}=–80.9±4.4, and D_{PtCr}=+94.4±2.5 kJ/mol (1σ), respectively. Combined with literature thermodynamic properties for the Fe-Cr system, the ternary interaction parameters in the Pt-Fe-Cr system were found to be C_{Cr}=0, C_{Pt}=+115.7, and C_{Fe}=–68.6 kJ/mol.

Using this technique, the metamorphic history of equilibrated ordinary chondrites was evaluated by examining the compositions and textures of olivines, pyroxenes, spinels, and alloys. Equilibrium temperatures based on Fe-Mg exchange between olivine and spinel exhibit a range of 680-796°C in H, L, and LL ordinary chondrites spanning petrographic type 4 to 6. Type 4 chondrites in all groups record variable temperatures that are lower than or equal to those of types 5 and 6 chondrites, implying decoupling of metamorphic temperature from petrographic type. Cooling rates near 800°C were found

to be 1-3 K/Ma, slow enough to allow continous re-equilibration of spinel grains from peak metamorphic temperatures to the olivine-spinel equilibration temperature.

The temperature-oxygen fugacity relationships in equilibrated H chondrites were constrained from spinel-alloy and olivine-pyroxene-alloy phase assemblages based on the mineral compositions and activity-composition models. $\mathrm{Log}_{10} f_{O_2}$ values based on the assemblage olivine-pyroxene-alloy are –1.75±0.02 log units below Iron-Wüstite (IW) buffer, regardless of petrographic type. The $\log_{10} f_{O_2}$ values calculated based on the spinel-alloy coexistence are at least ~1.5 log units more oxidizing than those based on the olivine-pyroxene-alloy if olivine-spinel equilibration temperatures (728-820°C) are assumed. This probably indicates that closure for spinel-alloy equilibria occurred under retrograde conditions at temperatures below 700°C.

Table of Contents

List of Tables

Chapter 1

Chapter 2

Chapter 3

Chapter 4

List of Figures

Chapter 1

Chapter 2

INTRODUCTION

Spinel is a common accessory mineral in a wide variety of igneous and metamorphic rocks, making it a potentially important indicator of petrologic processes. For example, changes in the Cr or Ti contents of spinel are linked to the degree of partial melting and fractionation of mantle–derived rocks from the Earth and Moon (Arai, 1987; Dick and Bullen, 1984; El Goresy, 1976), variations in metamorphic grade in serpentinites (e.g., Evans and Frost, 1975), and both crystallization and subsolidus reduction processes in meteorites (Haggerty, 1972). Equilibria involving spinel and other coexisting phases in a rock can be used to constrain the equilibrium conditions of the assemblage. An appropriate reaction for the equilibrium assemblage can be written, and based on the thermodynamic properties of the phases, an expression is obtained relating the observed mineral compositions to temperature, pressure, and/or oxygen fugacity.

For example, a common thermometer involving spinel is based on the coexistence of spinel and olivine, represented by the reaction:

$$\underset{fayalite}{Fe_2SiO_4^{olivine}} + 2\underset{picrochromite}{MgCr_2O_4^{spinel}} = 2\underset{chromite}{FeCr_2O_4^{spinel}} + \underset{forsterite}{Mg_2SiO_4^{olivine}} \quad . \tag{1a}$$

Provided the activities of fayalite and forsterite in olivine and chromite and picrochromite in spinel are known, this reaction can be used to constrain the equilibrium temperature according to the expression:

$$K_1 = \exp[-\Delta G_1^{\circ} / RT] = \frac{\left(a_{FeCr_2O_4}^{spinel}\right)^2 a_{MgSi_2O_4}^{olivine}}{\left(a_{MgCr_2O_4}^{spinel}\right)^2 a_{FeSi_2O_4}^{olivine}}, \tag{1b}$$

where a_i^j refers to the activity of component i in phase j, K_1 is the temperature-dependent equilibrium constant, R is the gas constant, T is the temperature in Kelvin, and ΔG_1^o is the free energy of reaction 1a.

The coexistence of olivine, pyroxene, and alloy is commonly used to constrain the temperature-oxygen fugacity (f_{O_2}) relationship, according to the reaction:

$$Fe^{alloy} + \underset{ferrosilite}{FeSiO_3^{pyroxene}} + \frac{1}{2}O_2^{gas} = \underset{fayalite}{Fe_2SiO_4^{olivine}} \quad , \tag{2a}$$

which can rearranged to yield an expression for f_{O_2}:

$$f_{O_2} = \left(\frac{a_{Fe_2Si_2O_4}^{olivine}}{K_2 a_{Fe}^{alloy} a_{FeSiO_3}^{pyroxene}} \right)^2 . \tag{2b}$$

Provided $a_{Fe_2Si_2O_4}^{olivine}$, $a_{Fe_2Si_2O_4}^{olivine}$, and a_{Fe}^{alloy}, and the equilibrium constant for reaction 2a are known, f_{O_2} can be determined at any given temperature.

Calculations of temperature and f_{O_2} using the above method are possible only if the activity-composition relationships of the phases of interest are well constrained. Natural spinels are complex solid solutions in the compositional space $(Fe^{2+},Mg)(Al,Cr,Fe^{3+})_2O_4$-$(Fe^{2+},Mg)_2TiO_4$. Ordering of cations between two crystallographically distinct sites, tetrahedral and octahedral, can be a strong function of composition and temperature (e.g., Sack and Ghiorso, 1991a,b) and the frequent presence of Fe in two valence states complicates matters even further. Experimental studies designed to obtain activity-composition models for spinels are, however, limited to binary and rarely ternary subsystems and mostly involve magnetite as an end-member [e.g., Fe_3O_4-$FeAl_2O_4$ (Mason and Bowen, 1981); Fe_3O_4-$MgFe_2O_4$, Fe_3O_4-Fe_2TiO_4 (Woodland and Wood, 1994); Fe_3O_4-$FeCr_2O_4$ (Petric and Jacob, 1982); $MgAl_2O_4$-Fe_3O_4-$\gamma Fe_{3/8}O_4$

(Mattioli et al., 1987)]. The use of magnetite as an end-member spinel in these experiments is problematic, due to its nonstoichiometric composition at high temperatures (Dieckmann, 1982). Lacking an accurate knowledge of Fe^{2+}/Fe^{3+} in the spinel of interest results in an incorrect assessment of the magnetite mole fraction in the spinel. The lack of direct experimentation on multicomponent spinels led to the development of activity-composition models for natural spinels that are based on the binary systems extrapolated to multicomponent spinels (e.g., Sack, 1982; Sack and Ghiorso, 1991a,b). The usage of these models add an additional uncertainty in determining spinel activities, since such models are poorly constrained in precisely those regions of composition space that are of greatest interest for applications to natural occurrences.

In this work, an experimental technique is developed for evaluating the activity of chromite, $FeCr_2O_4$, in multicomponent spinels (chapter 1 and 2). The technique is applied to evaluate the metamorphic conditions experienced by equilibrated ordinary chondrites (chapter 3 and 4).

The experimental technique developed here is based on equilibrating a spinel of interest with a Pt-alloy under a controlled temperature and oxygen fugacity. Cations from the oxides are reduced and dissolved into the alloy until equilibrium is reached according to the experimental conditions. The activity of $FeCr_2O_4$ in the spinel can then be determined from the knowledge of the activities of Fe and Cr in the equilibrated Pt-alloy and the equilibrium constant. A model is developed from which the Fe and Cr contents of the Pt-alloys can be converted to activities. A wide range of alloy compositions is produced by equilibrating them with Cr_2O_3 and simple Cr-, Fe-bearing spinels at a range of temperatures and oxygen fugacities. The compositions are fitted to a Pt-Fe-Cr ternary

activity model formulation based on the characterization of each bounding binary system, Pt-Fe, Pt-Cr, Fe-Cr, with the addition of ternary interaction terms.

The activity-composition relationship of alloys in the Pt-Fe system is evaluated in chapter 1 by equilibrating Pt wires with Fe-oxides at a range of temperatures and f_{O_2}. At a given experimental condition, the chemical potential, and thus the activity, of Fe in the Pt alloy is fixed by the chemical potential of O_2 (i.e., by the f_{O_2}) and of the Fe-oxide. By equilibrating alloys and oxides over a range of temperatures and f_{O_2} and analyzing the metal at each set of conditions, the relationship between metal composition, temperature, and iron activity is determined. This chapter has been recently published (Kessel et al., 2001a).

In chapter 2, the activity-composition in the Pt-Cr system is determined by equilibrating Pt wires with Cr_2O_3 at 1300°C and a range of f_{O_2}'s, and an activity-composition model is fit to the results. For the Fe-Cr system activity-composition results from Andersson and Sundman (1987) are used. The activity-composition relationships for these two binary systems together with Pt-Fe system (chapter 1) are combined to construct a ternary model in the Pt-Fe-Cr system. Compositions of Pt-alloys equilibrated with $FeCr_2O_4$+Cr_2O_3 and $(Fe,Mg)Cr_2O_4$+Cr_2O_3 at 1300°C and a range of f_{O_2} are used to constrain the ternary interaction parameters based on the knowledge of the interaction parameters for the three bounding binaries. Using the ternary activity model developed for the Pt-Fe-Cr system, the free energy of formation of $FeCr_2O_4$ at 1300°C is evaluated based on the activities of Fe and Cr in Pt-alloys in equilibrium with $FeCr_2O_4$+Cr_2O_3. The free energy of formation of chromite from Fe+Cr_2O_3+O_2 is also determined. The activity-composition relationship of $(Fe,Mg)Cr_2O_4$ chromites is evaluated from a set of

experiments in which Pt-alloys were equilibrated with spinel+Cr_2O_3. This chapter is ready for submission (Kessel et al., 2001b).

The experimental technique for evaluating the activity of chromite in multicomponent spinels is applied to evaluate the metamorphic conditions experienced by equilibrated ordinary chondrites. Ordinary chondrites are primitive meteorites showing variable degrees of metamorphism ranging from negligible to intensities sufficient to completely obliterate the original phases. Based on the coexistence of olivine, pyroxene, spinel, and alloy, the metamorphic temperatures and oxygen fugacities recorded by chondrites spanning the range of observed metamorphic grades are evaluated. The thermal history of equilibrated ordinary chondrites from H, L, and LL groups spanning petrographic types 4 to 6 are examined in chapter 3. Olivine-spinel equilibration temperatures (reaction 1a) are determined by equating expressions for the chemical potentials of Fe-Mg exchange in olivine and spinel using the formulation of Sack and Ghiorso (1991a,b). The relation between the petrographic type, chemical and textural maturation, and temperature is evaluated, and the cooling rates near peak metamorphic conditions are constrained.

The oxidation state experienced by H chondrites is determined in chapter 4. First, chromite activities in spinels whose compositions approximate those in equilibrated ordinary chondrites are evaluated using the technique developed in Kessel et al. (2001a,b) and compared to existing models. The activity of chromite in spinels, combined with activity-composition model for Fe-metal (Miettinen, 1999), are used to constrain the T-f_{O_2} relationships for spinel0alloy coexistence in equilibrated H chondrites. Additional T-f_{O_2} relationships are derived from the coexistence of olivine, pyroxene, and alloy, using

activity models for the ferromagnesian silicates incorporated into the program MELTS (Ghiorso and Sack, 1995). Based on the evaluated peak metamorphic temperatures, absolute f_{O_2} values for equilibrated H chondrites are evaluated. Chapter 3 is ready for submission (Kessel et al., 2001c) and chapter 4 is currently being prepared for publication.

REFERENCES

Andersson J. O. and Sundman B. (1987) Thermodynamic properties of the Cr-Fe system. *CALPHAD* **11**, 83-92.

Arai S. (1987) An estimation of the least depleted spinel peridotite on the basis of olivine-spinel mantle array. *Neues Jahrb. Mineral. Mh.* **1987**, 347-357.

Dick H. J. B. and Bullen T. (1984) Chromian spinel as a petrogenetic indicator in abyssal and alpine-type peridotites and spatially associated lavas. *Contributions to Mineralogy and Petrology* **86**, 54-76.

Dieckmann R. (1982) Defects and cation diffusion in magnetite (IV): Nonstoichiometry and point defect structure of magnetite ($Fe_{3-\delta}O_4$). *Berichte der Bunsen Gesellschaft für Physikalische Chemie* **86**, 112-118.

El Goresy A. (1976) Oxide minerals in lunar rocks. In *Oxide Minerals*, Vol. 3 (ed. D. Rumble). Southern Printing Company.

Evans B. W. and Frost B. R. (1975) Chrome-spinel in progressive metamorphism - a preliminary analysis. *Geochimica et Cosmochimica Acta* **39**, 959-972.

Ghiorso M. S. and Sack R. O. (1995) Chemical mass transfer in magmatic processes IV. A revised and internally consistent thermodynamic model for the interpolation and extrapolation of liquid-solid equilibria in magmatic systems at elevated temperatures and pressures. *Contributions to Mineralogy and Petrology* **119**, 197-212.

Haggerty S. E. (1972) Solid solution, subsolidus reduction and compositional characteristics of spinels in some Apollo 15 basalts. *Meteoritics* **7**, 353-370.

Kessel R., Beckett J. R., and Stolper E. M. (2001) Thermodynamic properties of the Pt-Fe system. *American Mineralogist.* **86**, 1003-1014.

Kessel R., Beckett J. R., and Stolper E. M. (2001b) Chromite activities in multicomponent spinels. Part I: Experimental technique. *Geochimica et Cosmochimica Acta.*

Kessel R., Beckett J. R., and Stolper E. M. (2001c) The thermal history of equilibrated ordinary chondrites and the relationship between textural maturity and temperature. *Geochimica et Cosmochimica Acta.*

Mason T. O. and Bowen H. K. (1981) Electric conduction and thermopower of magnetite and iron-aluminate spinels. *Journal of American Ceramic Society* **64**, 237-242.

Mattioli G. S., Wood B. J., and Carmichael I. S. E. (1987) Ternary-spinel volume in the system $MgAl_2O_4$-Fe_3O_4-$\gamma Fe_{3/8}O_4$: Implications for the effect of P on intrinsic f_{O2} measurements of mantle-xenolith spinels. *American Mineralogist* **72**, 468-480.

Miettinen J. (1999) Thermodynamic reassessment of Fe-Cr-Ni system with emphasis on the iron-rich corner. *CALPHAD* **23**, 231-248.

Petric A. and Jacob K. T. (1982) Thermodynamic properties of Fe_3O_4-FeV_2O_4 and Fe_3O_4-$FeCr_2O_4$ spinel solid solutions. *Journal of the American Ceramic Society* **65**, 117-122.

Sack R. O. (1982) Spinels as petrogenetic indicators: Activity-composition relations at low pressures. *Contribution to Mineralogy and Petrology* **79**, 169-180.

Sack R. O. and Ghiorso M. S. (1991a) Chromium spinels as petrogenetic indicators: thermodynamics and petrological applications. *American Mineralogist* **76**, 827-847.

Sack R. O. and Ghiorso M. S. (1991b) An internally consistent model for the thermodynamic properties of Fe-Mg titanomagnetite-aluminate spinels. *Contribution to Mineralogy and Petrology* **106**, 474-505.

Woodland A. B. and Wood B. J. (1994) Fe_3O_4 activities in Fe-Ti spinel solid solutions. *European Journal of Mineralogy* **6**, 23-37.

Chapter 1. Thermodynamic properties of the Pt-Fe system

(Reprinted from Kessel R., Beckett J. R., and Stolper E. M. (2001) Thermodynamic properties of the Pt-Fe system. *American Mineralogist*. 86, 1003-1014).

Abstract–We determined activity-composition relationships for the Pt-Fe system by equilibrating Fe-oxides with Pt-Fe alloys at temperatures in the range of 1200-1400°C and oxygen fugacities from 1.6 to 7.7 log units above the iron-wüstite (IW) buffer. The system is characterized by strong negative deviations from ideality throughout the investigated temperature range (e.g., γ_{Fe}^{alloy}<0.02 for X_{Fe}^{alloy}<0.3). Our data are consistent with an asymmetric regular solution of the form: $RT\ln\gamma_{Fe}^{alloy} = [W_{G_1} + 2(W_{G_2} - W_{G_1})X_{Fe}^{alloy}](X_{Pt}^{alloy})^2$, where W_{G1} = -138.0±3.3 kJ/mol and W_{G2} = -90.8±24.0 kJ/mol (1σ). Based on experiments at 1200°C-1400°C, variations in the activity coefficients at a given composition are consistent with $\ln\gamma_{Fe}^{alloy}(T_1) / \ln\gamma_{Fe}^{alloy}(T_2) = T_2 / T_1$.

The Pt-Fe alloy composition in equilibrium with a FeO-bearing silicate liquid can be obtained from: $\log_{10} f_{O_2} = \log\{\exp[\ln a_{Fe_2SiO_4}^{liq} - \ln a_{SiO_2}^{liq} - 2\ln a_{Fe}^{alloy} - (\frac{-\Delta G_r^0}{RT})]\}$ where ΔG_r^0 is the standard state free energy for the reaction $2Fe^{alloy} + O_2^{gas} + SiO_2^{liq} = Fe_2SiO_4{}^{liq}$. We obtained values of a_{Fe}^{alloy} from our model and used the program MELTS together with the thermodynamic properties of these elements to evaluate activities of SiO_2 and Fe_2SiO_4 components in the liquid and ΔG_r^0. We provide sample calculations showing how to

predict the optimum Fe concentrations for pre-saturation of Pt-bearing containers to reduce Fe loss from the charge during experiments on magmatic liquids at high temperatures and pressures from 1 atm to 40 kbar.

1. INTRODUCTION

Among the primary goals of experimental petrology are the simulation of processes within the earth and other terrestrial planets and the determination of physical and thermodynamic properties of relevant solid and liquid phases. Iron is an ubiquitous element in these systems and there continues to be a search for suitable container materials for experimentation involving Fe-bearing samples. Some prospective materials are limited by their low melting points (e.g., Ag, Au) and/or their tendency to interact with the sample (e.g., SiO_2, Al_2O_3, Mo), while others can only be used under relatively reducing conditions (e.g., Mo, graphite). In many respects, Pt is an ideal container material: it can be used at high temperatures (e.g., 1600°C); it is stable over a wide range of f_{O_2}; and, in many systems, it is essentially inert. Unfortunately, the use of Pt for Fe-bearing systems is complicated by a complete solid solution that stretches across the Pt-Fe join between 1350 and 1500°C and by both solid solutions and stable intermetallic compounds at lower temperatures (Hultgren et al. 1973). This can lead to serious problems since Fe-loss from a sample in contact with Pt can significantly change the phase equilibria (e.g., Bowen and Schairer 1932; Presnall and Brenner 1974). In addition, for experiments in sealed capsules, loss of Fe to a Pt capsule leads to the release of O_2 and a change in the oxidation state of the sample (Merrill and Wyllie 1973; Stern and Wyllie 1975). A less widely recognized potential problem in gas-mixing furnaces is the possible contamination of thermocouples

and of electrodes for oxygen sensors because of Fe vaporizing from samples, which could lead to errors in the measurement of temperature and f_{O_2}.

The problems associated with loss of Fe to a Pt sample container can be minimized by using a pre-saturated Pt-Fe alloy that, at the oxygen fugacity of the experiment, has a Fe content close to that of an alloy in equilibrium with the experimental charge. Grove (1981) showed through characterization of Fe partitioning between Pt-Fe alloys and coexisting phases how the alloy composition can be customized such that Fe gain or loss from the charge is minimized. Pt-Fe alloys can also be used to determine the thermodynamic properties of coexisting Fe-bearing phases if the activity-composition relations of the alloy are known. Moreover, if the oxygen fugacity is known, Pt-Fe alloys can also be used to determine the activities of iron oxide components (e.g., FeO, Fe_3O_4) in coexisting oxide and silicate phases (e.g., Nolan 1977; Gudmundsson and Holloway 1993). Alternatively, Pt-Fe alloys can be used to monitor redox conditions in experiments including Fe-bearing phases (e.g., Jamieson et al. 1992; Gudmundsson and Holloway 1993; Wasylenki 1998).

In each of the examples given above, the amount of Fe dissolved in the alloy is related to the activity-composition relationships of the Pt-Fe system, and these have therefore received considerable attention (e.g., Heald 1967; Petric et al. 1981; Petric and Jacob 1982; Gudmundsson and Holloway 1993). There are, however, substantial discrepancies among these previous studies, so an internally consistent characterization of activities in the Pt-Fe system is not yet available. Possible sources of differences between results of previous studies include different experimental conditions (T, f_{O_2}) and experimental and analytical methods and in some cases inappropriate techniques used to calculate the activity of Fe in the alloy.

In this paper, we determine the relationship between the activity of Fe in a Pt-Fe alloy and its composition by equilibrating Pt with Fe-oxides at 1200 -1400°C over a wide range of oxygen fugacities. In such experiments, the chemical potential (and thus the activity) of Fe in the alloy is fixed by the chemical potential of O_2 (i.e., by the f_{O_2}) and of the Fe-oxide, which is independently known (Darken and Gurry 1945; Dieckmann 1982; O'Neill 1988). Thus by equilibrating alloys and oxides over a range of temperatures and oxygen fugacities and analyzing the metal at each set of conditions, the relationship between metal composition, temperature, and iron activity can be precisely determined. Our procedures are similar to those of some previous studies, but we have used modern analytical techniques to reduce errors in the determination of alloy composition. In addition, we have fit our data to a functional form for the thermodynamic properties of the Pt-Fe alloys that is readily transportable to applications that require precise calculations of Fe and Pt activities in Pt-Fe alloys.

2. PREVIOUS WORK

In Figure 1, run conditions of experiments to constrain the activity-composition relationships of Pt-Fe alloys for this and previous studies are shown on the T-$\log_{10} f_{O_2}$ plane superimposed on the 1 atm phase relations of the Fe-O system (Darken and Gurry 1946). For clarity, the temperatures for our experiments are displaced upward by 10°C. Although wide ranges of conditions have been explored experimentally, there is considerable disagreement among the various data sets, which were assembled using a variety of experimental and analytical techniques. This has made it difficult to produce a definitive assessment of activity-composition relations for the Pt-Fe system. Larson and Chipman

(1954) equilibrated CaO-FeO-Fe_2O_3 and FeO-Fe_2O_3 melts with Pt at known f_{O_2} and calculated the activity of Fe in Pt using previously determined Fe activities in the oxide melts (Fetters and Chipman 1940). Heald (1967), Petric et al. (1981), and Petric and Jacob (1982) equilibrated Pt foils with Fe-oxides in the wüstite or magnetite stability fields at known f_{O_2} and measured the Fe concentration in the Pt by wet chemistry. Taylor and Muan (1962) did similar experiments but used a thermogravimetric technique and determined the compositions of Pt-Fe alloys indirectly by measuring weight changes in the sample as a function of f_{O_2}. Gudmundsson and Holloway (1993) equilibrated Pt wire or powder with Fe or Fe_2O_3 powders in the magnetite or wüstite stability fields and determined compositions of the Pt-Fe alloys by electron microprobe.

The variability in techniques and conditions among previous studies is matched by differences in data treatments, some of which are demonstrably incorrect. Petric and coworkers (Petric and Jacob 1982; Petric et al. 1981) used the free energy of formation of magnetite from Spencer and Kubaschewski (1978) to calculate Fe activities in all of their experiments. Larson and Chipman (1954) used a Gibbs-Duhem integration for liquid Fe-oxides introduced by Darken and Gurry (1946) to calculate the activities of Fe in Fe-oxide and Fe-, Ca-oxide liquids. The interpretation of experiments in each of these studies is in our view sound. On the other hand, Taylor and Muan (1962), Heald (1967), and Gudmundsson and Holloway (1993) all used an integration method developed by Darken and Gurry (1945) for experiments in the wüstite field. Yet, as shown in Figure 1, many of their experiments were actually conducted in the magnetite stability field where the Darken and Gurry (1945) algorithm does not apply. Heald (1967) compounded the problem by combining all the results of his experiments (ranging in temperature from 1131 to 1347°C)

with the 1300°C data of Taylor and Muan (1962) and fitting them to an isothermal Redlich-Kister solution model. This led to a widely-used expression for Fe activities that incorporates both correctly and incorrectly determined activities and ignores the possible temperature dependence of the activity coefficients. The results of later workers who used Heald's (1967) expression (e.g., Grove 1981; Jamieson et al. 1992; Van der Laan and Koster van Groos 1991) or depended on activities from Gudmundsson and Holloway (1993) (e.g., Gudmundsson and Wood (1995), Wasylenki (1998)) may therefore require reexamination.

3. EXPERIMENTAL PROCEDURES AND ANALYTICAL TECHNIQEUS

Experiments were conducted at 1 atm in a Deltech DT-31 furnace or a home-built $MoSi_2$ furnace with gas-mixing capability. Oxygen fugacity was set by mixing CO_2 and H_2 gases and measured using an yttria-doped-zirconia solid electrolyte oxygen sensor ($SIRO_2$®, Ceramic Oxide Fabricators, Ltd., Australia). The sensor was calibrated at two points encompassing the range of oxygen fugacities imposed in this study: air, for which agreement with the Nernst equation was checked (Williams and Mullins 1981), and the Iron-Wüstite (IW) buffer, which was determined by measuring the resistance of high-purity Fe wire as a function of f_{O_2} (details given in Mendybaev et al. (1998)). Since all of our experiments were conducted under conditions significantly more oxidizing than IW, no correction for electronic conduction of the electrolyte was required (Mendybaev et al. 1998). During the experiments, the EMF was maintained to within ±1 mV, leading to an uncertainty of ±0.05 (1σ) in $\log_{10} f_{O_2}$, except for the most oxidizing experiments (Pt/Fe 17 and Pt/Fe 17R, see Table 1), where larger fluctuations in EMF during the experiments led

to an uncertainty of ±0.1 (1σ). Temperatures were measured using a Pt-$Pt_{90}Rh_{10}$ (type S) thermocouple calibrated against the melting point of gold and are estimated to be accurate to within ±3°C.

For each experiment, a pellet (7 mm diameter) was prepared by pressing analytical grade Fe_2O_3 powder (99.999%, Johnson Matthey) around 3-5 mm long, 75 μm diameter Pt wires (99.9999%, Alfa® ÆSAR). The pellet was placed in a crucible constructed from 1/4" diameter Al_2O_3 rods (Vesuvius McDanel) and suspended in the hot spot of the vertical tube furnace.

Experiments were conducted at 1200-1400°C and oxygen fugacities from IW+1.56 to IW+7.70. The experiments were run for 4-5 days at 1200°C, 2 days at 1300°C, and 1 day at 1400°C. These run durations were at least twice the characteristic time required to homogenize the Pt-Fe alloys based on the diffusion data of Berger and Schwartz (1978); they also ensured complete conversion of Fe_2O_3 pellets to magnetite or wüstite with equilibrium concentrations of defects, which occurs in significantly less than half the run time (Darken and Gurry 1945; Darken and Gurry 1946). Experiments were terminated by raising the crucible into the cold area of the furnace, with quench times on the order of seconds; this time scale was sufficient to avoid significant changes in Pt-Fe alloy composition. To test the approach to equilibrium, reversals were also performed by equilibrating Pt wires with Fe-oxide at a given f_{O_2} and temperature, quenching, removing any adhering oxide from the equilibrated Pt-Fe wires, pressing them with a new batch of Fe_2O_3 powder, and then reequilibrating the wires with oxide at the same temperature but a higher f_{O_2} than the initial equilibration for a time sufficient to reequilibrate the sample.

After quenching, samples were removed from the furnace. The pellet was taken from the crucible and the Pt-Fe wires physically separated from oxides. Four to five wires were mounted in epoxy. Al_2O_3 impregnated papers were used to expose the wires, and diamond powder (<0.25 μm) to achieve the final polished surfaces.

The Pt-Fe wires were analyzed using a JEOL733 Superprobe with an accelerating voltage of 20 KeV, a beam current of 25 nA, and a takeoff angle of 40°. X-ray counts were collected for 30 seconds on peak and 15 seconds at each background position. Pure metals were used as standards and a ZAF correction procedure (Armstrong 1988) was applied. The wires were checked for homogeneity by analyzing one or two traverses of 3-4 points each across each wire from each run. Note that by having removed the wires from the enclosing oxides, we avoided the possibility of Fe excitation from oxides adjacent to the wires.

The identity of Fe-oxides in equilibrium with the wires was confirmed for selected experiments using x-ray diffraction. In every case, the phase was magnetite or wüstite, and corresponded to the expected equilibrium oxide based on Figure 1.

4. EXPERIMENTAL RESULTS

The experimental conditions and results are listed in Table 1. Compositions of alloys as a function of $\log_{10} f_{O_2}$ are shown in Figure 2. Most experiments were done at 1300°C, encompassing a wide range of oxygen fugacities (from $\log_{10} f_{O_2}$ = -9.14 to -3.20), leading to a correspondingly large range in mole fraction of Fe in the Pt-Fe alloy (X_{Fe}^{alloy} = 0.082-0.539). A smaller number of experiments were done at 1200°C and 1400°C to determine the dependence of the mixing properties of the alloy on temperature and to

facilitate comparison with literature data. The curves plotted in Figure 2 are based on a regular solution model of the alloy described below.

4.1. Results

Values of X_{Fe}^{alloy} were calculated from the measured wt% Fe by averaging all of the analyses made on wires from each experiment. The averages and their uncertainties (the standard deviation of the distribution of measured alloy compositions from each experiment) are listed in Table 1. The uncertainties (reported throughout this work as 1σ) are less than 2% of the average concentration for most of the experiments.

The stable Fe-oxide in our experiments was either wüstite or magnetite. Neither of these phases is stoichiometric over all of the conditions of our experiments and this must be taken into account in determining Fe activities. In the following two subsections, we show how this can be done for wüstite- and magnetite-saturated experiments. The first subsection is essentially a brief reprise of Darken and Gurry's (1945) procedure for wüstite. In the second, we take advantage of measurements by Dieckmann and coworkers of magnetite stoichiometry as a function of temperature and f_{O_2} in evaluating the effect of varying cation to oxygen ratios in the phase on resulting calculated alloy activities. To our knowledge, this has not previously been done for magnetite. In the third and final subsection we calculate free energies of formation of stable defect-bearing magnetite, Fe_3O_4, and compare these values with those in the literature for metastable, essentially defect-free magnetite under the same conditions.

4.1.1. Activity of iron in Pt-Fe alloys in equilibrium with wüstite

For experiments conducted in the wüstite stability field, activities of Fe in the alloy in equilibrium with wüstite were calculated using Darken and Gurry's (1945) procedure.

In this approach a Gibbs-Duhem equation of the form $\sum_i N_i^j d\mu_i^j = \sum_i X_i^j d\ln a_i^j = 0$, where N_i^j, μ_i^j, X_i^j, and a_i^j are the number of moles, chemical potential, mole fraction, and activity of component i in phase j, is used to relate wüstite composition to f_{O_2} at a given temperature. For wüstite in the system Fe-O, this equation becomes $X_{Fe}^{\text{wüstite}} d\ln a_{Fe}^{\text{wüstite}} + X_O^{\text{wüstite}} d\ln a_O^{\text{wüstite}} = 0$ or where wüstite coexists with a Pt-Fe alloy $X_{Fe}^{\text{wüstite}} d\ln a_{Fe}^{alloy} + X_O^{\text{wüstite}} d\ln a_O^{alloy} = 0$, which assumes the reference state for the pure Fe and O components in wüstite and metal are the same. The activity of Fe in the alloy is expressed as

$$d\ln a_{Fe}^{alloy} = -\frac{X_O^{\text{wüstite}}}{X_{Fe}^{\text{wüstite}}} d\ln f_{O_2}^{1/2}. \qquad (1a)$$

Integrating Equation 1a results in

$$\int_{a_{Fe}^{alloy}@IW}^{a_{Fe}^{alloy}@\text{wüstite}} d\ln a_{Fe}^{alloy} = -\int_{f_{O_2}@IW}^{f_{O_2}@\text{wüstite}} \left(\frac{X_O}{X_{Fe}}\right)^{\text{wüstite}} d\ln f_{O_2}^{1/2}, \qquad (1b)$$

where $(X_O/X_{Fe})^{\text{wüstite}}$ refers to the oxygen/iron ratio of wüstite. Integration on the wüstite composition is performed starting from an assumed Fe activity of 1 for wüstite coexisting with pure Fe at the IW buffer (i.e., ignoring the small solubility of oxygen in the metal (Darken and Gurry 1946, and references therein)) and proceeding to the wüstite composition (and, therefore, the f_{O_2}) of interest. Activities of Fe in Pt-Fe alloys for our wüstite-bearing experiments were calculated numerically using this procedure and are given in Table 1.

Activities of FeO in the wüstite field in our experiments were calculated from the equilibrium of wüstite with Pt-Fe alloy according to the reaction:

$$Fe^{alloy} + \tfrac{1}{2}O_2^{gas} = FeO^{\text{wüstite}}, \quad (2)$$

which can be described by the following equilibrium constant

$$K_2 = \frac{a_{FeO}^{\text{wüstite}}}{(a_{Fe}^{alloy})\,(f_{O_2})^{1/2}}, \quad (3)$$

and rearranged to

$$a_{FeO}^{\text{wüstite}} = K_2 (f_{O_2})^{1/2} a_{Fe}^{alloy}. \quad (4)$$

Using the equilibrium constant from O'Neill (1988), Equation 4 can be used to calculate $a_{FeO}^{\text{wüstite}}$ for each experiment. Contours of constant $a_{FeO}^{\text{wüstite}}$ in the wüstite field are shown in Figure 1.

4.1.2. Activity of iron in Pt-Fe alloys in equilibrium with magnetite

Most of our experiments were conducted within the magnetite stability field so Darken and Gurry's (1945) experimental results within wüstite stability field could not be used and the composition of the magnetite needs to be considered. Although the metal equilibrates with magnetite in these experiments, it is not necessarily appropriate to assume that the magnetite is fixed in composition throughout its stability field since magnetite can be significantly non-stoichiometric (Dieckmann 1982). For temperatures below 1438°C, the stability limit of wüstite (see Fig. 1), an appropriate Gibbs-Duhem integration to evaluate the effect of changes in magnetite composition with f_{O_2} on a_{Fe}^{alloy}, is given by (Darken and Gurry 1945):

$$\int_{a_{Fe}^{alloy}@WM}^{a_{Fe}^{alloy}@magnetite} d\ln a_{Fe}^{alloy} = -\int_{f_{O_2}@WM}^{f_{O_2}@magnetite} \left(\frac{X_O}{X_{Fe}}\right)^{magnetite} d\ln f_{O_2}^{1/2}, \quad (5)$$

(cf. Eq. 1b) where the integration is performed on the magnetite composition starting from the wüstite-magnetite (WM) boundary (and the corresponding a_{Fe}^{alloy} value at this f_{O_2} calculated from Eq. 1b) and proceeding to the magnetite composition (and, therefore, f_{O_2}) of interest. The following paragraphs explain how we calculated the magnetite compositions and corresponding activities in our experiments.

Dieckmann and coworkers (Dieckmann 1982; Dieckmann 1998; Dieckmann et al. 1978; Dieckmann and Schmalzried 1977a; Dieckmann and Schmalzried 1977b) showed that magnetite deviates from Fe_3O_4 primarily due to Fe interstitials towards its more reduced stability limit at the WM boundary and cation vacancies towards its more oxidized stability limit at the magnetite–hematite (MH) boundary. By combining equilibria for these two kinds of defects, the stoichiometry of magnetite, as expressed in the formula $Fe_{3-\delta}O_4$, can be determined from (Dieckmann 1982)

$$\delta = [\frac{(1-3\delta)^3}{(2+2\delta)^2} K_{vac} f_{O_2}{}^{2/3}] - [\frac{(2+2\delta)^2}{(1-3\delta)^3} K_{\text{int}} f_{O_2}{}^{-2/3}], \quad (6)$$

where K_{vac} is an equilibrium constant for the formation of cation vacancies and K_{int} is an equilibrium constant for the formation of cation interstitials. Values of δ in our experiments were determined by iteration using Equation 6 and at 1300°C range from -0.003 at the WM boundary ($\log_{10} f_{O_2}$ = -7.69), to 0 at $\log f_{O_2} \cong -5.67$, to +0.101 at the MH boundary ($\log_{10} f_{O_2}$ = -1.70). Since $(X_O / X_{Fe})^{magnetite}$=4/(3-$\delta$), the activity of Fe at any given composition can be obtained through Equation 5. Activities of Fe in Pt-Fe alloys for our magnetite-bearing experiments calculated using this procedure are given in Table 1.

The activity of Fe_3O_4 in magnetite in equilibrium with a Pt-Fe alloy can be related to a_{Fe}^{alloy} and f_{O_2} based on the reaction:

$$3Fe^{alloy} + 2O_2^{gas} = Fe_3O_4^{magnetite}, \tag{7}$$

which can be described by the equilibrium constant

$$K_7 = \frac{a_{Fe_3O_4}^{magnetite}}{(a_{Fe}^{alloy})^3 (f_{O_2})^2}. \tag{8}$$

Rearranging Equation 8 gives

$$a_{Fe3O4}^{magnetite} = K_7 (f_{O2})^2 (a_{Fe}^{alloy})^3. \tag{9}$$

Differentiating Equation 9 yields $d\ln a_{Fe3O4}^{magnetite} = 3d\ln a_{Fe}^{alloy} + 2d\ln f_{O_2}$, which can be converted (cf. Eq. 5) to $d\ln a_{Fe3O4}^{magnetite} = -3(\frac{X_O}{X_{Fe}})^{magnetite} d\ln f_{O_2}^{1/2} + 4d\ln f_{O_2}^{1/2}$. Integrating this form of Gibbs-Duhem equation results in the following expression for $a_{Fe_3O_4}^{magnetite}$:

$$\ln a_{Fe_3O_4}^{magnetite} = \int_{\substack{@Fe_3O_4 \\ (\delta=0)}}^{@Fe_{3-\delta}O_4} \left[4 - 3(\frac{X_O}{X_{Fe}})^{magnetite}\right] d\ln f_{O_2}^{1/2} \tag{10}$$

as given by Darken and Gurry (1946). We performed the integration across the magnetite field at constant temperature starting from Fe_3O_4 (i.e., $\delta = 0$ and $a_{Fe_3O_4}^{magnetite}=1$, which corresponds to a particular f_{O_2} in the magnetite field based on Dieckmann's results) to the f_{O_2} and hence $Fe_{3-\delta}O_4$ of interest. Curves of constant $a_{Fe_3O_4}^{magnetite}$ in the magnetite stability field are shown in Figure 1.

Calculated values of $a_{Fe_3O_4}^{magnetite}$ at 1300°C equal or exceed 0.988 for f_{O_2}'s between the WM buffer and $\log_{10} f_{O_2}$ = -3.2, the most oxidizing condition for our experiments, but can be as low as $a_{Fe_3O_4}^{magnetite}$ = 0.895 at the MH buffer ($\log_{10} f_{O_2}$ = -1.7). At 1200°C, $a_{Fe_3O_4}^{magnetite}$ ranges from 0.996 at the WM buffer to 0.925 at the MH buffer but is >0.998 for our experiments. At 1400°C, greater deviations from stoichiometry are physically accessible, such that $a_{Fe_3O_4}^{magnetite}$ = 0.846 at the MH buffer; however, based on these calculations, $a_{Fe_3O_4}^{magnetite}$ in our experiments is >0.999. Based on this analysis, the minimum value of $a_{Fe_3O_4}^{magnetite}$ in our experiments is thus estimated to be 0.988.

The difference in calculated values of a_{Fe}^{alloy} between using the above procedure and simply assuming a magnetite activity of 1 in Equation 8 is smaller than the deviations in $a_{Fe_3O_4}^{magnetite}$ from unity because a_{Fe}^{alloy} scales with the cube root of $a_{Fe_3O_4}^{magnetite}$ (cf. Eq. 9). For experiments at the MH boundary, assuming $a_{Fe_3O_4}^{magnetite}$ = 1 leads to values of a_{Fe}^{alloy} that are too high by 2.7% at 1200°C, 3.7% at 1300°C, and 5.7% at 1400°C. The largest error in a_{Fe}^{alloy} for data in the literature resulting from assuming $a_{Fe_3O_4}^{magnetite}$=1 would be 5.7% for an experiment at 1400°C and $\log_{10} f_{O_2}$=-0.68 (at the MH boundary) reported by Gudmundsson and Holloway (1993). Even here, there is only 0.8% error in the calculated value of $\ln \gamma_{Fe}^{alloy}$ which is less than likely 1σ errors due to other sources of uncertainty (see below).

Although the effect of nonstoichiometry of magnetite on calculated values of a_{Fe}^{alloy} is generally small, we have nevertheless incorporated it into our calculations of a_{Fe}^{alloy} for both our own data and those from previous studies. Given a_{Fe}^{alloy}, the activity coefficient of Fe, γ_{Fe}^{alloy}, can be obtained by dividing a_{Fe}^{alloy} by X_{Fe}^{alloy}. Values of $\ln \gamma_{Fe}^{alloy}$ are listed for our experiments in Table 1. Uncertainties on $\ln \gamma_{Fe}^{alloy}$ were calculated by propagating errors on

the temperature (±3°C), $\log_{10} f_{O_2}$ (±0.05-0.10), and X_{Fe}^{alloy} (0.5-3%, see Table 1); the propagated uncertainties on $\ln \gamma_{Fe}^{alloy}$ for our experiments are ±1-6% (1σ).

4.1.3. Free energy of formation of stable, non-stoichiometric magnetite

The free energy of formation of stable, non-stoichiometric Fe_3O_4 (i.e., $\delta = 0$ with equal but non-negligible amounts of Fe interstitials and Fe vacancies) at high temperature was evaluated and compared to the free energy of formation of metastable, stoichiometric magnetite given by O'Neill (1988). Stoichiometric magnetite ($\delta = 0$ and defect population approaches zero) is metastable above ~560°C, and O'Neill's (1988) values for the free energy of formation of stoichiometric magnetite at higher temperatures are based on an extrapolation of electrochemical measurements obtained at 477-560°C. The free energy of formation of stable non-stoichiometric Fe_3O_4 at 1200-1400°C was evaluated from $\Delta G_7^0 = -RT \ln K_7$ using the calculated values of a_{Fe}^{alloy} in equilibrium with Fe_3O_4 and the f_{O_2} corresponding to $\delta = 0$ (via Eqs. 5 and 6). The free energy of formation of Fe_3O_4 from the elements is –645.88 kJ/mol at 1200°C (0.73 kJ/mol lower than O'Neill's (1988) value), –615.84 kJ/mol at 1300°C (0.91 kJ/mol lower than O'Neill's (1988) value), and –585.65 kJ/mol at 1400°C (1.36 kJ/mol lower than O'Neill's (1988) value). The increasing deviation between our values and those of O'Neill with increasing temperature is consistent with increasing defect concentrations, but all of these differences are within the uncertainty (±1.0-1.5 kJ/mol) based on propagated errors on the calculated a_{Fe}^{alloy} (taken as ±0.2% on a_{Fe}^{alloy} (Darken and Gurry 1945)).

4.2. Activity-composition model for the Pt-Fe system

As shown in Table 1, activity-composition relations for the Pt-Fe system are characterized by negative deviations from ideality (i.e., $\gamma_{Fe}^{alloy}<1$) over the full range of compositions we have investigated. Other binary alloys involving Pt show a similar or even more extreme behavior (e.g., Pt-Mn, (Garbers-Craig and Dippenar 1997); Pt-Cr, Pt-V, (Pretorius and Muan 1992)), and this pattern is also common to other platinum group element alloys (e.g., Pd-Si, Pd-Mg, Pd-Al, (Chamberlin et al. 1994); Pd-Th, Pd-Sn, etc., (Schaller 1989); Nb-Rh, (Kleykamp 1982); U-Pd, U-Rh, (Kleykamp and Kang 1991); Ir-Fe, Rh-Fe, (Schwerdtfeger and Zwell 1968)). Several effects are thought to contribute to the non-ideal behavior of such systems. Schaller and coworkers (see detailed discussion in Schaller (1989) and references therein) emphasize a lattice distortion introduced by the size difference of the components and an electronic effect common to Pt and Pd alloys, which accounts for both charge transfer between solute and solvent atoms and the resulting rise in Fermi energy through filling of holes in the electron bands. In Pt-alloys with non-noble metals, the electronic effect dominates and the non-ideality scales with the number of valence electrons in the solute and its electronegativity. An alternative view (e.g., Brewer 1981) is that the non-ideality reflects acid-base interactions between nonbonding electrons in Pt and empty orbitals in the solute. Either approach can be used to rationalize the negative deviations from ideality.

Thompson (1967) summarized the use of one form of polynomial excess function to describe the thermodynamics of non-ideal binary solid solutions. By assuming ideal configurational entropy but non-zero enthalpy of mixing (i.e., a regular solution) and expressing the excess free energy as a Taylor expansion truncated to a third-order

polynomial in terms of composition, the activity coefficients have the form (written in terms of the Pt-Fe system):

$$RT\ln\gamma_{Fe}^{alloy} = [W_{G_1} + 2(W_{G_2} - W_{G_1})X_{Fe}^{alloy}](X_{Pt}^{alloy})^2 \qquad (11a)$$

and

$$RT\ln\gamma_{Pt}^{alloy} = [W_{G_2} + 2(W_{G_1} - W_{G_2})X_{Pt}^{alloy}](X_{Fe}^{alloy})^2 \qquad (11b)$$

at constant pressure. The W_G's in Equation 11a and 11b are temperature- and composition-independent constants referred to as Margules parameters (Hildebrand 1929) that correspond to the difference between the molar Gibbs free energy of component i in the solution and the molar Gibbs free energy of pure component i. Symmetric solutions are characterized by only one parameter (i.e., $W_{G1}=W_{G2}=W_G$), while asymmetric solutions are described by two constants.

A best fit of our data to Equation 11a using a weighted least-squares method (Reed 1992) resulted in W_{G1} = –138.0±3.3 kJ/mol and W_{G2} = –90.8±24.0 kJ/mol. Other binary alloys involving Pt and a transition element show W_G's values in the same range (e.g., –179.1 and –73.68 kJ/mol for the Pt-Cr system, and –225.63 and –153.87 kJ/mol for Pt-V, (Pretorius and Muan 1992)). Figure 3 shows our data for $RT\ln\gamma_{Fe}^{alloy}$ plotted against X_{Fe}^{alloy} compared to the best fits assuming asymmetric and symmetric regular solution behavior (the best fit W_G assuming a symmetric regular solution is -116.6±2.4 kJ/mol). Our data are clearly poorly fit by a symmetric regular solution but well described by an asymmetric solution. The deviations of our data from best fits for both models are shown as an inset in Figure 3 as a function of composition. Deviations from an asymmetric regular solution

model are independent of X_{Fe}^{alloy}. Most data points plot within 1σ of the predicted curve. In contrast, absolute deviations from the best fit to a symmetric regular solution model show a systematic increase with increasing X_{Fe}^{alloy}.

In describing the system as a regular solution (i.e., one in which the excess Gibbs free energy is a function only of composition), we implicitly adopt the assumption that $RT\ln\gamma_{Fe}^{alloy}$ is independent of temperature for a given alloy composition; i.e.,

$$\frac{\ln\gamma_{Fe}^{alloy}(T_1)}{\ln\gamma_{Fe}^{alloy}(T_2)} = \frac{T_2}{T_1} \tag{12}$$

where temperature is in degrees K. Figure 3 demonstrates that this is a valid approximation in that all of our data at 1200, 1300, and 1400°C can be fit by a single set of temperature-independent Margules parameters. This is shown more clearly in Figure 2, where the variation of $\log_{10} f_{O_2}$ as a function of X_{Fe}^{alloy} given by our data is well described by the calculated curves at 1200°C, 1300°C, and 1400°C based on the asymmetric regular solution fit with its temperature-independent Margules parameters. We conclude that our data are consistent with asymmetric regular solution behavior of the Pt-Fe system over the range of temperature and composition explored in this study. Calculated activities of Fe and Pt at 1300°C as functions of alloy composition based on Equations 11a and 11b are shown in Figure 4. The strong negative deviations from ideality are apparent.

4.3. Comparison with previous studies

Figure 5 compares the compositions of Pt-Fe alloys in equilibrium with Fe oxides versus $\log_{10} f_{O_2}$ at 1300°C from our study and from earlier work. A similar pattern is observed for 1400°C. Our alloy compositions plot near the upper bound of the literature

data; i.e., they are generally more Fe-rich at a given f_{O_2} than those reported in most other studies; overall agreement is best between our results and those of Gudmundsson and Holloway (1993), especially at 1400°C (not shown), in the range of compositions on which our model is based, although deviations of their results from our fit are observed at lower and higher Fe contents. In spite of greater scatter in some of the earlier data sets, the results define an overall trend in Figure 5 that is consistent with the asymmetric regular solution mixing model to which our data have been fit.

Figures 6a and b show $\ln\gamma_{Fe}^{alloy}$ values from this study and previous work as a function of X_{Fe}^{alloy}. Also shown are the calculated trends using Equation 11a and our best fit model parameters. Where necessary, activity coefficients given by Taylor and Muan (1962), Heald (1967), and Gudmundsson and Holloway (1993), which implicitly assumed wüstite saturation, were recalculated to be consistent with magnetite saturation. We accepted the authors' stated T- f_{O_2} conditions and X_{Fe}^{alloy} and obtained a corresponding value of a_{Fe}^{alloy} based on modeling of oxide defect equilibria as described above. The correction yielded changes in $\ln\gamma_{Fe}^{alloy}$ relative to those given in the original papers as large as 0.25 log units for Gudmundsson and Holloway's (1993) experiments, 0.33 log units for data of Taylor and Muan (1962) and 1.0 log units for experiments of Heald (1967). As explained earlier, the effect of magnetite nonstoichiometry on calculated values of $\ln\gamma_{Fe}^{alloy}$ is negligible (<0.01), except for the most oxidizing of Gudmundsson and Holloway (1993) experiments (at 1400°C close to MH) where the effect is as much as 0.06 log units, corresponding to 0.8%. We also corrected the standard state of Fe for the 1550°C data of Larson and Chipman (1954) from liquid to solid Fe, which decreases their reported values of $\ln\gamma_{Fe}^{alloy}$ by 0.014 (~0.5% difference). Figures 5 and 6 show that recalculated values for

Gudmundsson and Holloway's (1993) experiments agree reasonably well with our data and thus with the model trend; the deviations are largest for X_{Fe}^{alloy}>0.4 at 1400°C. For other studies, however, values of $\ln\gamma_{Fe}^{alloy}$ at a given X_{Fe}^{alloy} are generally higher than obtained in our study, as expected given the generally lower X_{Fe}^{alloy} at constant $\log_{10} f_{O_2}$ (Fig. 5).

We are uncertain about the cause(s) of systematic differences shown in Figures 5 and 6 between our data (and those of Gudmundsson and Holloway (1993)) versus other data in the literature. Errors in determining f_{O_2} or temperature are unlikely candidates as deviations of 0.5-1.5 log units in f_{O_2} or ~100°C would be required and this is well outside likely errors even in the earliest studies. An exception may be Heald's (1967) experiments at temperatures below 1200°C, which could have been prone to systematic errors of this magnitude in f_{O_2} due to disequilibrium in the H_2-CO_2 gas mixtures (e.g., Beckett and Mendybaev 1997; Huebner 1975). Although Heald (1967) did not give run times, the experiments of Taylor and Muan (1962) and Petric and coworkers (Petric and Jacob 1982; Petric et al. 1981) were, according to the diffusion data of Berger and Schwartz (1978), long enough to homogenize the Pt-Fe alloys. We consider the most likely explanation for the systematically lower Fe contents of the alloys reported by the older studies to reflect either inaccuracies in the analytical procedures or inclusion of incompletely equilibrated (i.e., Fe-poor) alloys in the analyzed metal. Analytical procedures were very different in our study and that of Gudmundsson and Holloway (1993) compared to those of Taylor and Muan (1962), Heald (1967), Petric et al. (1981), and Petric and Jacob (1982). In particular, a modern microanalytical procedure, (i.e., electron microprobe analysis) was used in our work and that of Gudmundsson and Holloway (1993) whereas either bulk analytical techniques (Heald 1967; Petric and Jacob 1982; Petric et al. 1981) or an indirect

measurement of composition via weight change (Taylor and Muan 1962) were used in the older studies. Without access to the run products from the other studies it is difficult to pinpoint the source of the systematic discrepancies, but the agreement between our results and those of Gudmundsson and Holloway (1993), both of which used spatially resolved, modern electron microprobe methods to analyze the alloys, and the fact that both studies are reversed, gives us considerable confidence in these data and the thermodynamic model based upon them.

Grove (1981), Jamieson et al. (1992), and Wasylenki (1998) all used Heald's (1967) model to determine a_{Fe}^{alloy} when evaluating the f_{O_2} of reactions containing Fe-bearing phases in equilibrium with a Pt-Fe alloy. As shown in Figures 5 and 6, our results differ substantially from those of Heald (1967). For Fe-poor alloys (corresponding to highly oxidizing conditions and/or FeO-poor liquids), our model for the alloy leads to much higher calculated oxygen fugacities for the reaction $Fe^{alloy} + \frac{1}{2}O_2 = FeO^{liquid}$, up to 2.07 log units at 1300°C as the alloy composition approaches pure Pt, compared to the oxygen fugacities calculated using the model of Heald (1967). For more Fe-rich alloys (corresponding to lower oxygen fugacities and/or FeO-rich liquids), the models are in better agreement (e.g., for X_{Fe}^{alloy}>0.45, the deviation is less than 0.1 log units). These curves of calculated oxygen fugacities for the two models reflects the cross-over in $\ln\gamma_{Fe}^{alloy}$-X_{Fe}^{alloy} slopes (Fig. 6a) and the fact that a_{Fe}^{alloy} must approach 1 as the alloy approaches pure Fe (i.e., all models must agree as $X_{Fe}^{alloy} \rightarrow 1$). As shown in Figure 4, small changes in X_{Fe}^{alloy} for Pt-rich alloys can lead to order of magnitude changes in a_{Fe}^{alloy} while at high Fe contents a_{Fe}^{alloy} is a relatively weak function of composition. Heald's expression of $\ln\gamma_{Fe}^{alloy}$ is

temperature-independent, while ours scales with temperature according to Equation 12 and therefore, differences between the two models diminish at higher temperatures and become greater at lower temperatures. Since experiments under most conditions of interest to experimental geochemists and as conducted by Jamieson et al. (1992), and Wasylenki (1998) generally yield $X_{Fe}^{alloy}<0.5$, the use of our activity-composition expression for Pt-Fe alloys in place of the widely used Heald's (1967) expression can have noticeable effects on the calculated X_{Fe}^{alloy} or redox conditions.

5. APPLICATIONS OF THE ACTIVITY-COMPOSITION MODEL

As described in the Introduction, there are currently two major geochemical applications for a thermodynamic model of Pt-Fe alloys. The first is to predict the appropriate composition of an alloy to be used as a container in an experiment so that changes in sample composition are minimized. Second, given the composition of an alloy equilibrated with an experimental charge, the alloy model can be used to determine the oxygen fugacity in an experiment provided activities of iron oxide components are fixed by the coexisting phase assemblage. Previous workers (e.g., Grove 1981, Jamieson et al. 1992, Gudmundsson and Holloway 1993, Wasylenki 1998) have performed such calculations only for olivine±pyroxene-saturated melts. In this section, we show how it is possible using our model for Pt-Fe alloys together with the program MELTS for silicate liquids (Ghiorso and Sack 1995) to perform calculations of this type for a wider range of melt compositions. In particular, we show that equilibrium alloy compositions are readily calculated for liquids that are not saturated with crystalline silicates or oxide. We begin by showing how the apparent free energies of liquid components obtained from MELTS can be modified to accommodate reactions involving alloys. We then provide examples of how

to use MELTS with our alloy model to calculate appropriate Fe contents for pre-saturation of Pt-Fe containers, both at 1 bar and in high-pressure experiments, or given alloy compositions, to calculate the oxygen fugacity of an experiment.

The program MELTS recasts liquid compositions expressed in terms of oxides into an alternative set of components including Fe_2SiO_4, Mg_2SiO_4, $CaSiO_3$, and SiO_2. It is, therefore, convenient to write exchange reactions between the solid alloy and silicate liquid in terms of the MELTS component set. For a Pt-Fe alloy this leads to

$$2Fe^{alloy} + O_2^{gas} + SiO_2^{liq} = Fe_2SiO_4{}^{liq}, \tag{13}$$

which has a free energy of reaction

$$\Delta G_r^{13} = 0 = \Delta G_r^0 + RT\ln\left[\frac{a_{Fe_2SiO_4}^{liq}}{a_{SiO_2}^{liq}(a_{Fe}^{alloy})^2 f_{O_2}}\right], \tag{14}$$

where ΔG_r^0 is the standard state free energy of reaction. If standard state free energies for SiO_2 and Fe_2SiO_4 in the liquid are referenced to the elements at the temperature of interest and 1 bar, then $\Delta G_r^0 = G_{f,T,1}^{Fe_2SiO_4,liq} - G_{f,T,1}^{SiO_2,liq}$. Unfortunately, for our purposes, free energies for liquid components given by MELTS are apparent values relative to the elements at 298.15 K and 1 bar. To use Equation 14 with MELTS output, we must, therefore, first correct the standard state from 298.15 K to the temperature of interest, which can be done via

$$G_{T,P}^j = G_{298,1}^j + \sum_i^{\#ele} \nu_i^j\left[(H_{T_1}^i - H_{298}^i) + \int_{T_1}^{T} C_p^i\,dT - T(S_{T_1}^i + \int_{T_1}^{T}\frac{C_p^i}{T}dT) + V^i(P-1)\right], \tag{15}$$

where ν_i^j is the stoichiometry of element i in phase j (e.g., $\nu_{Fe}^{Fe_2SiO_4} = 2$), $G_{298,1}^j$ is the apparent free energy of formation of j as given by MELTS, and T_1 is either 298K or the 1

bar temperature of transition for element i that is closest to but less than the temperature of interest, T (e.g., for Si, solid Si is stable between 298 K and the melting point at 1685 K; if T = 1600 K, then T_1= 298K; if T = 1700 K, then T_1= 1685 K). $(H^i_{T_1} - H^i_{298})$ is the difference in enthalpy between a mole of element i at T_1 and 298 K, $S^i_{T_1}$ is the third law entropy of element i at T_1, C^i_p is the heat capacity of element i, V^i is the molar volume of element i and P is the pressure in bars. Values for $(H^i_{T_1} - H^i_{298})$ and $S^i_{T_1}$ are 1 bar values taken either at 298 K or at the high temperature side of T_1 if it represents a transition. Values of $(H^i_{T_1} - H^i_{298})$, $S^i_{T_1}$, and V^i are obtained directly from Robie et al. (1978). Temperature dependent expressions for C^i_p were taken from Robie et al. (1978) except for Fe, which were interpolated from the tabulation because Robie et al. (1978) lacks expressions for C^{Fe}_p as a function of temperature.

All of our applications involve the use of Equation 14 for which the liquid composition, possibly excepting Fe^{2+}/Fe^{3+}, is known. For a known liquid composition and temperature, MELTS can provide $a^{liq}_{Fe_2SiO_4}$ and $a^{liq}_{SiO_2}$. Using Equation 15, apparent free energies of SiO_2^{liq} and $Fe_2SiO_4^{liq}$ are converted to free energies of formation at temperature, allowing ΔG^0_r to be computed. If the alloy composition is known, then a^{alloy}_{Fe} is obtained from Equation 11a and f_{O_2} can then be obtained from Equation 14. Alternatively, if f_{O_2} is known, then a^{alloy}_{Fe} can be calculated and the alloy composition can be determined. Figure 7 compares calculated $\log_{10} f_{O_2}$ for selected olivine-saturated experiments by Grove (1981) using MELTS and the measured $\log_{10} f_{O_2}$. We note the good agreement (within ±0.5 log units) between the calculated values based on the liquid and equilibrated Pt-Fe alloy compositions and the values determined by the gas ratio imposed during the experiments.

The principle advantage of using MELTS for these types of calculations is that olivine need not be present and, therefore, a much broader spectrum of liquid compositions can be evaluated than would have been possible using the formulations of previous workers. Suppose, for example, that we were interested in doing equilibrium or dynamic crystallization experiments on the calc-alkaline andesite, ET80, from Elat massif, southern Israel, analyzed by Kessel et al. (1998). Taking the composition of ET80 on an anhydrous basis and assuming oxygen fugacities between 1 log unit above the Quartz-Fayalite-Magnetite buffer (QFM) and 1 log unit below it, plagioclase (Plag) is the liquidus phase according to MELTS at 1155°C. Plagioclase is followed by pyroxene (px) and either spinel (sp) or ilmenite (il) during equilibrium or fractional crystallization. Note that olivine does not appear anywhere in the liquid line of descent and therefore previous formulations for determining equilibrium alloy compositions for this liquid would be inapplicable. Using activities and apparent free energies of SiO_2^{liq} and $Fe_2SiO_4^{liq}$ as given by MELTS, we calculated ΔG_r^0 using Equation 15, solved Equation 14 for a_{Fe}^{alloy} and then used Equation 11a to obtain X_{Fe}^{alloy}. The results are shown in Figure 8 for both equilibrium and fractional crystallization paths. For equilibrium and fractional crystallization at QFM+1 and temperature above 1000°C, alloy compositions would be virtually identical, but under more reducing conditions, alloy compositions diverge slightly below ~1100°C. Optimal pre-saturation compositions for an isothermal experiment can be read directly from the figure. For example, the sample container for an experiment at QFM+1 and 1100°C should be pre-saturated with X_{Fe}^{alloy}=0.26, while at QFM-1, the appropriate composition would be X_{Fe}^{alloy}=0.38. Choosing the best pre-saturation level for a dynamic crystallization experiment would be more difficult because X_{Fe}^{alloy} changes with temperature, and both the

liquid line of descent and the rate of exchange between the container and sample will depend on the length of time at the maximum temperature, T_{max}, the cooling rate, relative weights and geometry of sample and container, and the desired quench temperature, T_q. Figure 8 nevertheless provides a quantitative basis for choosing an initial X_{Fe}^{alloy}.

Similar calculations can be done for experiments conducted at high pressure. ΔG_r^0 at a given temperature and pressure can be calculated as described above since MELTS provides the apparent free energies of SiO_2^{liq} and $Fe_2SiO_4^{liq}$ at temperature and pressure and Equation 15 can be used with an additional pressure term to convert these values to free energies of formation for the components. The pressure effect on liquid components is significant due to compressibility of the liquids, but the effect on alloy activities can be ignored for experiments below ~40 kbar because excess volumes are small in the Pt-Fe system (see discussions on the pressure effect on $\ln\gamma_{Fe}^{alloy}$ for X_{Fe}^{alloy}<0.35 in Gudmundsson and Holloway (1993); we performed similar calculations using the unit-cell data of Cabri (1975) for X_{Fe}^{alloy}<0.7 and came to the same conclusion). To illustrate the effect of pressure, we computed equilibrium alloy compositions at 10 kbar for liquid compositions produced at 1100 and 1200°C via equilibrium crystallization at 1 bar of an andesitic liquid (Fig. 8). The Fe^{2+}/Fe^{3+} of these same liquids was recalculated using MELTS (i.e., assuming constant relative f_{O_2}) and the equilibrium alloy composition was then calculated using Equations 11a, 14 and 15. The Pt-Fe alloys produced under these conditions are enriched in Fe by 3-4 mole% compared to values at 1 bar (e.g., the 1200°C, QFM liquid has X_{Fe}^{alloy}=0.30 at 1 bar and 0.33 at 10 kbar).

An EXCEL spreadsheet that can be used in conjunction with the MELTS supplemental calculator to perform calculations described above is available from the

authors upon request. As a caveat, note that the current version of the MELTS supplemental calculator incorporates f_{O_2} through deviations relative to a buffer (e.g., QFM±x log units) at 1 bar no matter what the total pressure might be (i.e., for the 10 kbar calculations discussed here, we entered QFM+$\frac{0.05(P(bar)-1)}{T(K)}$ to "fool" the MELTS supplemental calculator into giving results for QFM at 10 kbar).

Acknowledgements – This work was supported by NASA grant NAG5-4318. Discussions with M. Baker and R. Mendybaev greatly improved the quality of this study. Ma Chi is thanked for his help with the analytical work. C. Capobianco and J. Jones are thanked for their constructive reviews.

REFERENCES

Armstrong, J.T. (1988) Quantitative analysis of silicate and oxide materials: Comparison of Monte Carlo, ZAF, and $\phi(\rho Z)$ procedures. In D.E. Newbury, Ed. MicroBeam Analysis, p. 239-246. San Francisco Press, Inc., California.

Beckett, J.R. and Mendybaev, R.A. (1997) The measurement of oxygen fugacities in flowing gas mixtures at temperatures below 1200°C. Geochimica et Cosmochimica Acta, 61, 4331-4336.

Berger, D. and Schwartz, K. (1978) Zur Fremddiffusion in Platin. Neue Huette, 23, 210-212.

Bowen, N.L. and Schairer, J.F. (1932) The FeO-SiO_2 system. American Journal of Science 5th series, 24, 177-213.

Brewer, L. (1981) The role and significance of empirical and semiempirical correlations. In M. O'Keefe and A. Navrotsky, Eds. Structure and Bonding in Crystals. v. 1. p. 155-174. New York, Academic Press.

Cabri, L.J. and Feather, C.E. (1975) Platinum-iron alloys: A nomenclature based on a study of natural and synthetic alloys. The Canadian Mineralogist, 13,117-126.

Chamberlin, L., Beckett, J.R., and Stolper, E. (1994) Pd-oxide equilibrium: a new experimental method for the direct determination of oxide activities in melts and minerals. Contributions to Mineralogy and Petrology, 116, 169-181.

Darken, L.S. (1967) Thermodynamics of binary metallic solutions. Transactions of the Metallurgical Society of AIME, 239, 80-89.

Darken, L.S. and Gurry, R.W. (1945) The system Iron-Oxygen. I. The wüstite field and related equilibria. Journal of the American Chemical Society, 67, 1398-1412.

——— (1946) The system Iron-Oxygen. II. Equilibrium and thermodynamics of liquid oxide and other phases. Journal of the American Chemical Society, 68, 798-816.

Dieckmann, R. (1982) Defects and cation diffusion in magnetite (IV): Nonstoichiometry and point defect structure of magnetite ($Fe_{3-\delta}O_4$). Berichte der Bunsen Gesellschaft für Physikalische Chemie, 86, 112-118.

——— (1998) Point defects and transport in non-stoichiometric oxides: solved and unsolved problems. Journal of Physics and Chemistry of Solids, 59, 507-525.

Dieckmann, R., Mason, T.O., Hodge, J.D., and Schmalzried, H. (1978) Defects and cation diffusion in magnetite (III). Tracer diffusion of foreign tracer cations as a function of temperature and oxygen potential. Berichte der Bunsen Gesellschaft für Physikalische Chemie, 82, 778-783.

Dieckmann, R. and Schmalzried, H. (1977a) Defects and cation diffusion in magnetite (I). Bereits Bunsengesellschaft für Physikalische Chemie, 81, 344-347.

——— (1977b) Defects and cation diffusion in magnetite (II). Berichte der Bunsen Gesellschaft für Physikalische Chemie, 81, 414-419.

Fetters, K.L. and Chipman, J. (1940) Slag-metal relationships in the basic open-hearth furnace. Transactions of the Metallurgical Society of AIME, 140, 170-203.

Garbers-Craig, A.M. and Dippenar, R.J. (1997) Thermodynamic properties of solid Pt-Mn, Pt-Cr, and Pt-Mn-Cr alloys at 1500°C. Metallurgical and Materials Transactions, 28B, 547-552.

Ghiorso, M.S., and Sack, R.O. (1995) Chemical mass transfer in magmatic processes IV. A revised and internally consistent thermodynamic model for the interpolation and extrapolation of liquid-solid equilibria in magmatic systems at elevated temperatures and pressures. Contribution to Mineralogy and Petrology, 119, 197-212.

Grove, T.L. (1981) Use of FePt alloys to eliminate the iron loss problem in 1 atmosphere gas mixing experiments: Theoretical and practical considerations. Contributions to Mineralogy and Petrology, 78, 298-304.

Gudmundsson, G. and Holloway, J. (1993) Activity-composition relationships in the system Fe-Pt at 1300 and 1400°C and at 1 atm and 20 kbar. American Mineralogist, 78, 178-186.

Gudmundsson, G. and Wood, B.J. (1995) Experimental tests of garnet peridotite oxygen barometry. Contribution to Mineralogy and Petrology, 119, 56-67.

Heald, E.F. (1967) Thermodynamics of iron-platinum alloys. Transactions of the Metallurgical Society of AIME, 239, 1337-1340.

Hildebrand, J.H. (1929) Solubility XII, Regular solutions. Journal of American Chemical Society, 51, 66-80.

Huebner, J.S. (1975) Oxygen fugacity values of furnace gas mixtures. American Mineralogist, 60, 815-823.

Hultgren, R., Desai, P.D., Hawkins, D.T., Gleiser, M., Kelley, K.K., and Wagman, D.D. (1973) Selected values of the thermodynamic properties of binary alloys. American Society for Metals, Metals Park, Ohio.

Jamieson, H.E., Roeder, P.L., and Grant, A.H. (1992) Olivine-pyroxene-PtFe alloy as an oxygen geobarometer. Journal of Geology, 100, 138-145.

Kessel, R., Stein, M., and Navon, O. (1998) Petrogenesis of late Neoproterozoic dikes in the northern Arabian-Nubian Shield: Implications for the origin of A-type granites. Precambrian Research, 92, 195-213.

Kleykamp, H. (1982) On the thermodynamics in the Nb-Rh and Nb-Rh-O systems. Journal of the Less-Common Metals, 83, 105-113.

Kleykamp, H. and Kang, S.-G. (1991) The constitution of the uranium-palladium and uranium-rhodium-palladium systems. Z. Metalkd., 82, 544-552.

Larson, H.R. and Chipman, J. (1954) Activity of iron in iron-platinum solid solutions. Acta Metallurgica, 2, 1-2.

Mendybaev, R.A., Beckett, J.R., Stolper, E.M., and Grossman, L. (1998) Measurement of oxygen fugacities under reducing conditions; non-Nernstian behavior of Y_2O_3-doped zirconia oxygen sensors. Geochimica et Cosmochimica Acta, 62, 3131-3139.

Merrill, R.B. and Wyllie, P.J. (1973) Absorption of iron by platinum capsules in high pressure rock melting experiments. American Mineralogist, 58, 16-20.

Nolan, J. (1977) Determination of specific component activities in tholeiitic melts; principles and techniques. Philosophical Transactions of the Royal Society of London, Series A: Mathematical and Physical Sciences, 286, 343-351.

O'Neill, H.St.C. (1988) Systems Fe-O and Cu-O: thermodynamic data for the equilibria Fe-"FeO", Fe-Fe_3O_4, "FeO"-Fe_3O_4, Fe_3O_4-Fe_2O_3, Cu-Cu_2O, and Cu_2O-CuO from emf measurements. American Mineralogist, 73, 470-486.

Petric, A. and Jacob, K.T. (1982) Thermodynamic properties of Fe_3O_4-FeV_2O_4 and Fe_3O_4-$FeCr_2O_4$ spinel solid solutions. Journal of the American Ceramic Society, 65, 117-122.

Petric, A., Jacob, K.T., and Alcock, C.B. (1981) Thermodynamic properties of Fe_3O_4-$FeAl_2O_4$ spinel solid solutions. Journal of the American Ceramic Society, 64, 632-639.

Presnall, D.C. and Brenner, N.L. (1974) A method for studying iron silicate liquids under reducing conditions with negligible iron loss. Geochimica et Cosmochimica Acta, 38, 1785-1788.

Pretorius, E.B. and Muan, A. (1992) Activity-composition relations in platinum-chromium and platinum-vanadium alloys at 1500°C. Journal of the American Ceramic Society, 75, 1361-1363.

Reed, B.C. (1992) Linear least-squares fits with errors in both coordinates: II: comments on parameter variances. American Journal of Physics, 60, 59-62.

Robie, R.A. and Hemingway, B.S. (1978) Thermodynamic properties of minerals and related substances at 298.15 K and 1 bar (10^5 Pascals) pressure and at higher temperatures Geological Survey Bulletin, 1452: 456 pp.

Schaller, H.J. (1989) Solid state galvanic cells for thermodynamic investigations. In H. Brodowsky, and H.J. Schaller, Eds. Thermochemistry of Alloys, p. 329-358. Kluwer Academic Publishers.

Schwerdtfeger, K. and Zwell, L. (1968) Activities in solid iridium-iron and rhodium-iron alloys at 1200°C. Transactions of the Metallurgical Society of AIME, 242, 631-633.

Spencer, P.J. and Kubaschewski, O. (1978) A thermodynamic assessment of the iron-oxygen system. CALPHAD, 2, 147-167.

Stern, C.R. and Wyllie, P.J. (1975) Effect of iron absorption by noble-metal capsules on phase boundaries in rock-melting experiments at 30 kilobars. American Mineralogist, 60, 681-689.

Taylor, R.W. and Muan, A. (1962) Activities of iron in iron-platinum alloys at 1300°C. Transactions of the Metallurgical Society of AIME, 224, 500-502.

Thompson, J.B. (1967) Thermodynamic properties of simple solutions. In P.H. Abelson, Ed. Researches in Geochemistry, 2, p. 340-361.

Van der Laan, S.R. and Koster van Groos, A.F. (1991) Pt-Fe alloys in experimental petrology applied to high-pressure research on Fe-bearing systems. American Mineralogist, 76, 1940-1949.

Wasylenki, L.E. (1998) Partial melting of depleted peridotite in the earth's upper mantle and implications for generation of mid-ocean-ridge basalts. Geological and Planetary Sciences, California Institute of Technology, Pasadena. p. 158.

Williams, R.J. and Mullins, O. (1981) JSC systems using solid ceramic oxygen electrolyte cells to measure oxygen fugacities in gas-mixing systems. NASA Technical Memoransum 58234, 37 p.

Table 1. Experimental conditions and results

Run	Temp (°C)	Fe-oxide phase†	$\log_{10} f_{O_2}$ (atm)	time (hr)	n*	X_{Fe}^{alloy}	1σ	$\ln \gamma_{Fe}^{alloy}$	1σ	starting alloy@
				forward experiments						
Pt/Fe 38	1200	Wüstite	-9.93	96	12	0.477	0.011	-1.77	0.08	Pt
Pt/Fe 39	1200	Magnetite	-8.63	97	16	0.352	0.003	-3.29	0.07	Pt
Pt/Fe 34	1200	Magnetite	-7.74	89	23	0.290	0.003	-4.47	0.07	Pt
Pt/Fe 35	1200	Magnetite	-7.05	161	15	0.254	0.003	-5.38	0.07	Pt
Pt/Fe 36	1200	Magnetite	-6.50	144	12	0.211	0.002	-6.04	0.07	Pt
Pt/Fe 28	1300	Wüstite	-9.14	46.5	23	0.524	0.009	-1.34	0.07	Pt
Pt/Fe 21	1300	Wüstite§	-9.05	47	19	0.539	0.004	-1.49	0.07	Pt
Pt/Fe 10	1300	Wüstite	-8.50	45	16	0.472	0.009	-2.08	0.08	Pt
Pt/Fe 30	1300	Wüstite§	-7.95	46	21	0.400	0.004	-2.63	0.07	Pt
Pt/Fe 33	1300	Magnetite§	-7.59	40.5	14	0.359	0.003	-3.02	0.07	Pt
Pt/Fe 9	1300	Magnetite§	-7.47	44	19	0.361	0.003	-3.22	0.07	Pt
Pt/Fe 14	1300	Magnetite	-6.90	46.5	28	0.314	0.003	-3.95	0.07	Pt
Pt/Fe 11	1300	Magnetite	-6.15	45.5	21	0.275	0.004	-4.96	0.07	Pt
Pt/Fe 13	1300	Magnetite	-5.64	44	9	0.220	0.001	-5.52	0.07	Pt
Pt/Fe 15	1300	Magnetite§	-5.10	47	26	0.204	0.002	-6.27	0.07	Pt
Pt/Fe 12	1300	Magnetite	-3.97	48	9	0.118	0.003	-7.46	0.08	Pt
Pt/Fe 17	1300	Magnetite§	-3.20	45.5	25	0.082	0.001	-8.28	0.14	Pt
Pt/Fe 31	1400	Magnetite	-5.81	21.5	14	0.292	0.004	-3.92	0.07	Pt
Pt/Fe 26	1400	Magnetite	-5.79	20	24	0.291	0.003	-3.88	0.07	Pt
Pt/Fe 32	1400	Magnetite	-5.40	22.5	12	0.254	0.005	-4.37	0.08	Pt
				reversal experiments						
Pt/Fe 36R	1200	Magnetite	-6.50	96	12	0.209	0.002	-6.03	0.07	Pt/Fe 34
Pt/Fe 33R	1300	Magnetite	-7.56	73	22	0.360	0.004	-3.08	0.07	Pt/Fe 28
Pt/Fe 37R	1300	Magnetite	-5.38	73	22	0.195	0.002	-5.79	0.07	Pt/Fe 11
Pt/Fe 17R	1300	Magnetite	-3.20	73	22	0.090	0.001	-8.37	0.14	Pt/Fe 30
Pt/Fe 32R	1400	Magnetite	-5.37	45.5	16	0.256	0.002	-4.44	0.07	Pt/Fe 31

Notes: X_{Fe}^{alloy} = mole fraction of Fe in Pt-Fe alloy, γ_{Fe}^{alloy} = activity coefficient of Fe in Pt-Fe alloy, 1σ values are standard deviations of the mean calculated by error propagation.

† Predicted Fe-oxide according to T- f_{O_2} conditions in the Fe-O system (Darken and Gurry 1945).

§ Phase identification confirmed by XRD analysis.

* Number of analyses. 3-4 analyses were obtained on each 4-5 wires.

@ "Pt" indicates that pure Pt wire was used as starting material. Otherwise, a Fe-bearing alloy taken from the run product of the indicated forward experiment was used.

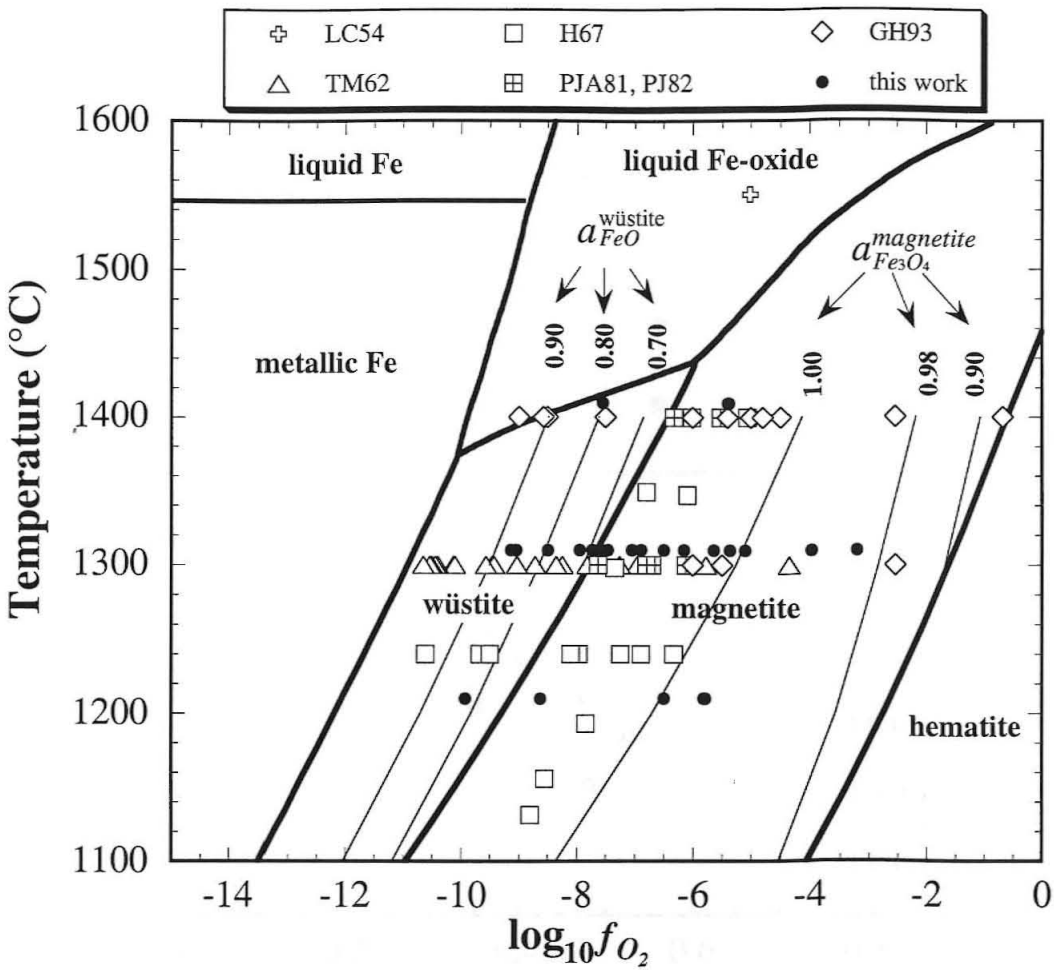

Figure 1. Run conditions for experiments in which the Pt-Fe alloys were equilibrated with Fe-oxides superimposed on the 1 atm phase diagram for the system Fe-O (Darken and Gurry 1946) as a function of temperature (°C) and $\log_{10} f_{O_2}$. Literature data are from: Larson and Chipman (1954), LC54, Taylor and Muan (1962), TM62, Heald (1967), H67, Petric et al. (1981) and Petric and Jacob (1982), PJA81 and PJ82, and Gudmundsson and Holloway (1993), GH93. Our data (filled circles) are shown as well, displaced 10°C above the actual run temperature for clarity. Curves of constant $a_{FeO}^{wüstite}$ in the wüstite (Darken and Gurry 1946) and constant $a_{Fe_3O_4}^{magnetite}$ in the magnetite field (see text) are also shown.

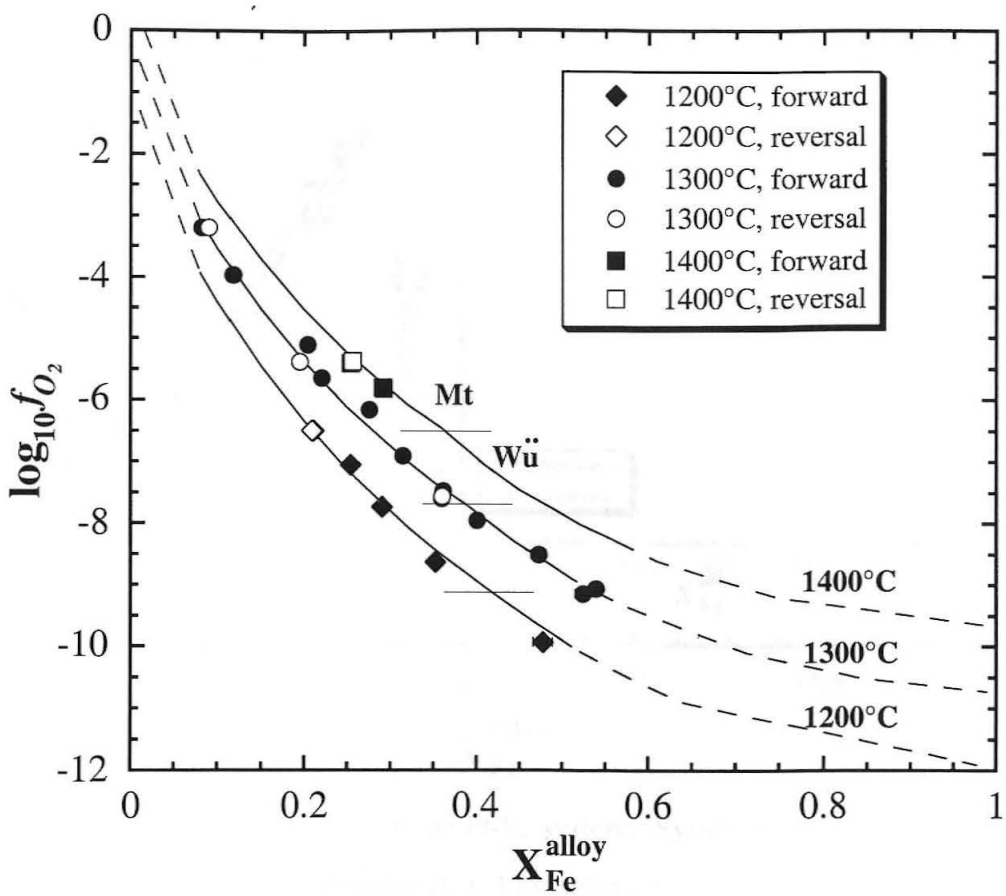

Figure 2. X_{Fe}^{alloy} vs. $\log_{10} f_{O_2}$ in the Pt-Fe system for data obtained in this study. Closed symbols reflect "forward" experiments in which pure Pt was used as starting material, and open symbols the results of reversals (the equilibrium composition of the alloy was approached from the high-Fe side). Where larger than the symbol size, individual error bars (1σ) are plotted. Also shown are predicted trends of $\log_{10} f_{O_2}$ as a function of X_{Fe}^{alloy} using the curve fit to our experimentally derived values (see text) with dashed curves extending outside our composition range. Positions of the wüstite-magnetite (WM) buffer at each temperature are indicated by horizontal lines segments cross-cutting the curves.

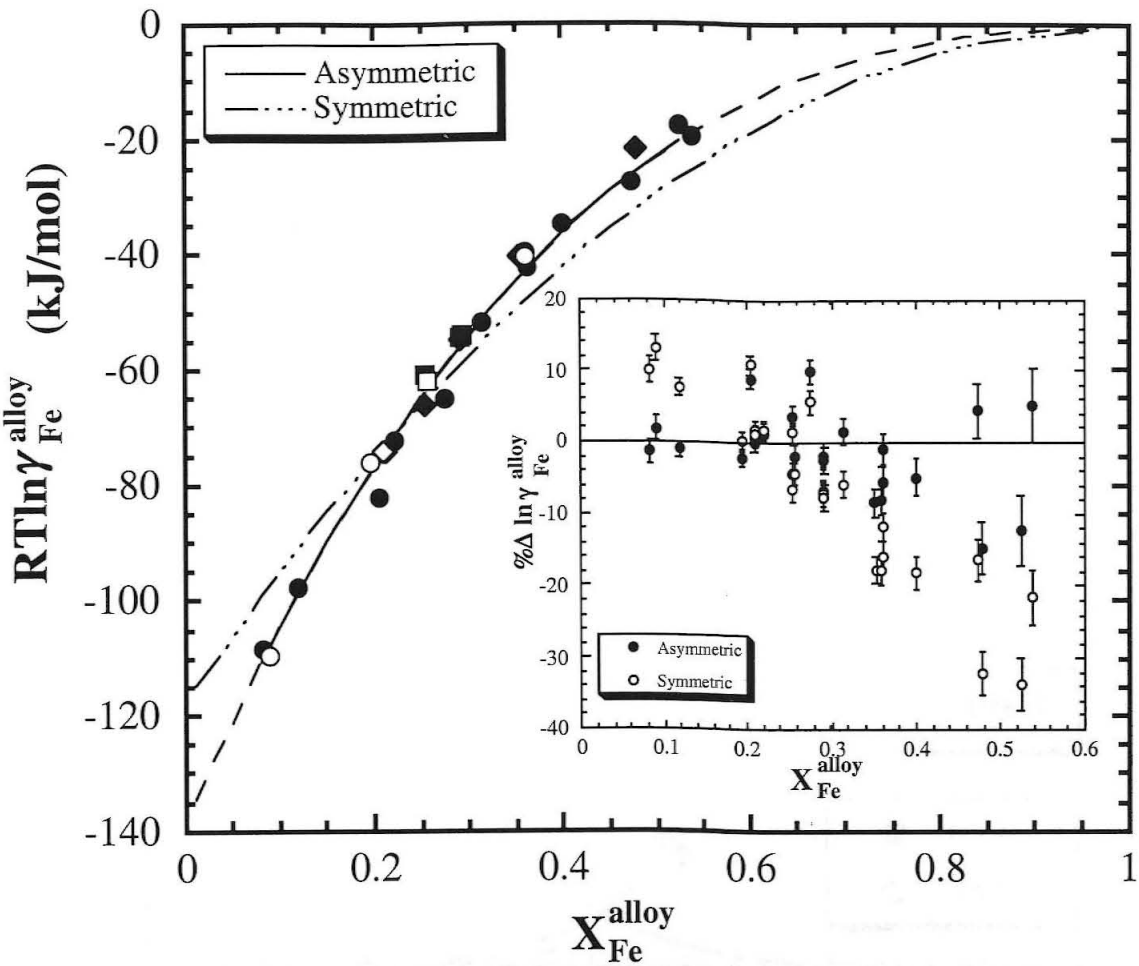

Figure 3. Values of $RT \ln \gamma_{Fe}^{alloy}$ vs. X_{Fe}^{alloy} in the Pt-Fe system. Symbols as in Figure 2. The best fits to our data assuming asymmetric (Eq. 11a, solid curve, dashed where extended beyond our data) and symmetric (dotted curve) regular solution behavior are shown. In the inset, % deviations of our data from fits to asymmetric (filled) and symmetric (open) regular solution models relative to the modeled $\ln \gamma_{Fe}^{alloy}$ are shown as a function of alloy composition.

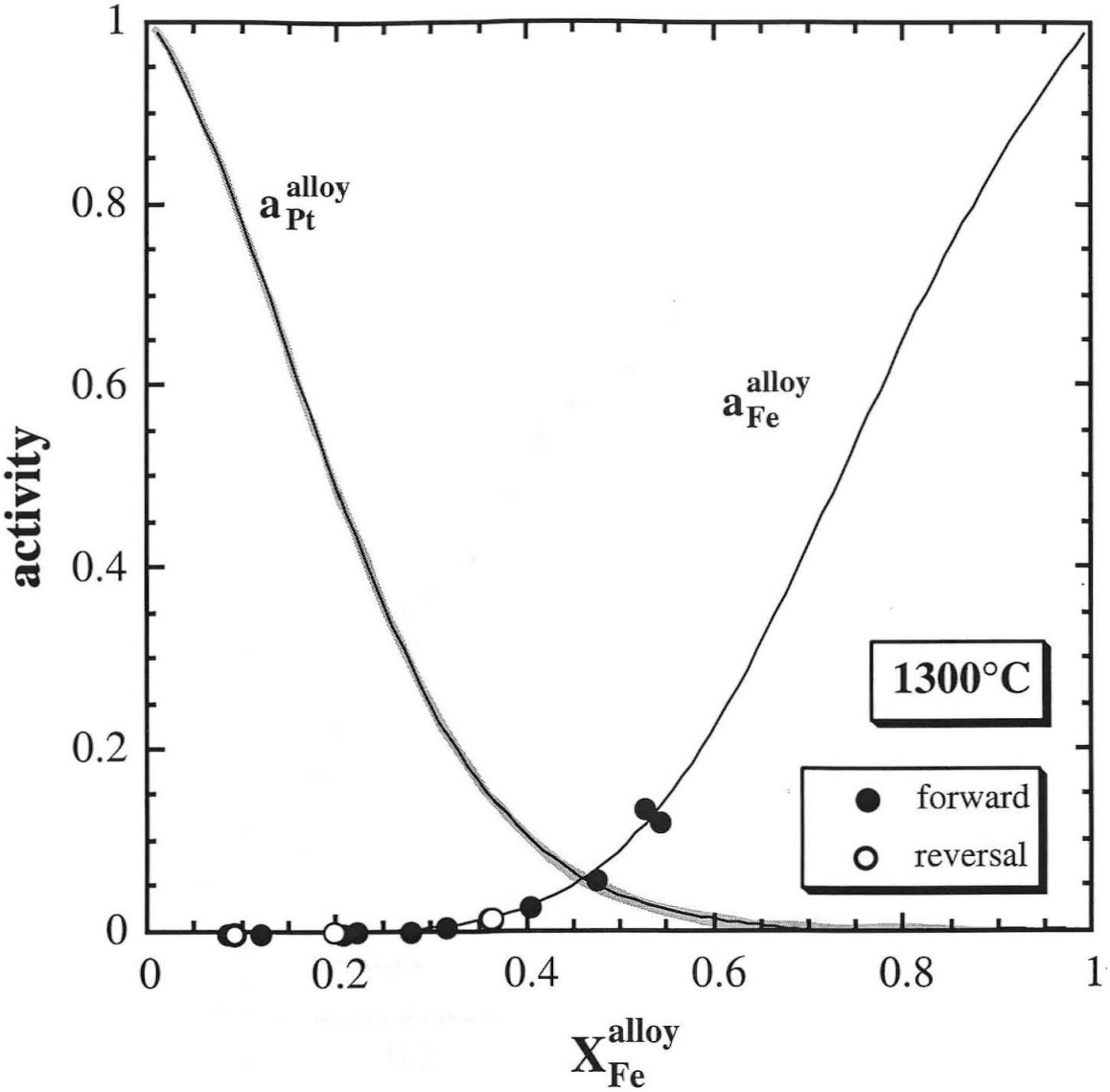
1
0.8
0.6
0.4
0.2
0
activity
a_{Pt}^{alloy}
a_{Fe}^{alloy}
1300°C
forward
reversal
0
0.2
0.4
0.6
0.8
1
X_{Fe}^{alloy}

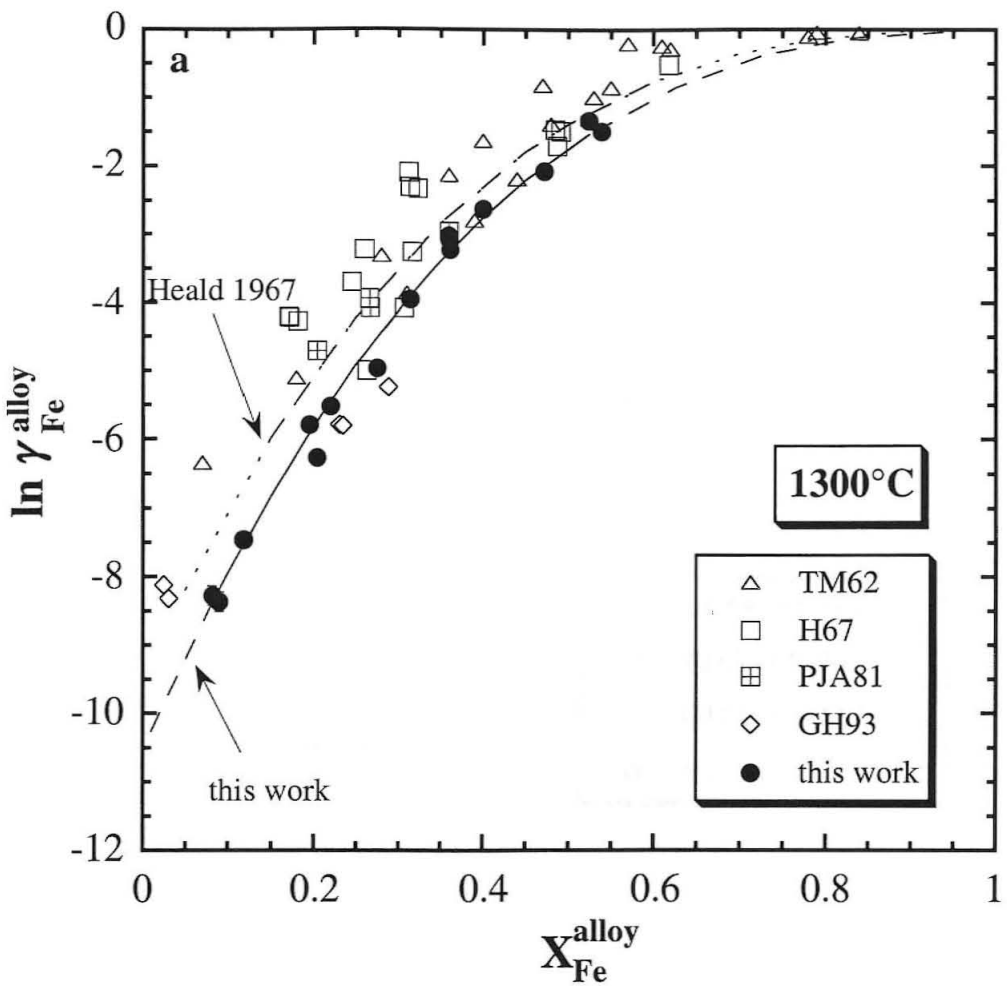

Figure 5. $\log_{10} f_{O_2}$ vs. X_{Fe}^{alloy} at 1300°C from previous experimental studies compared to this study. Data for both forward and reversal experiments from this study are shown by filled circles. The curves represent predicted trends calculated from our data using Equation 11a. Abbreviations for literature data are described in the caption to Figure 1. Positions of the WM and IW buffers are also indicated.

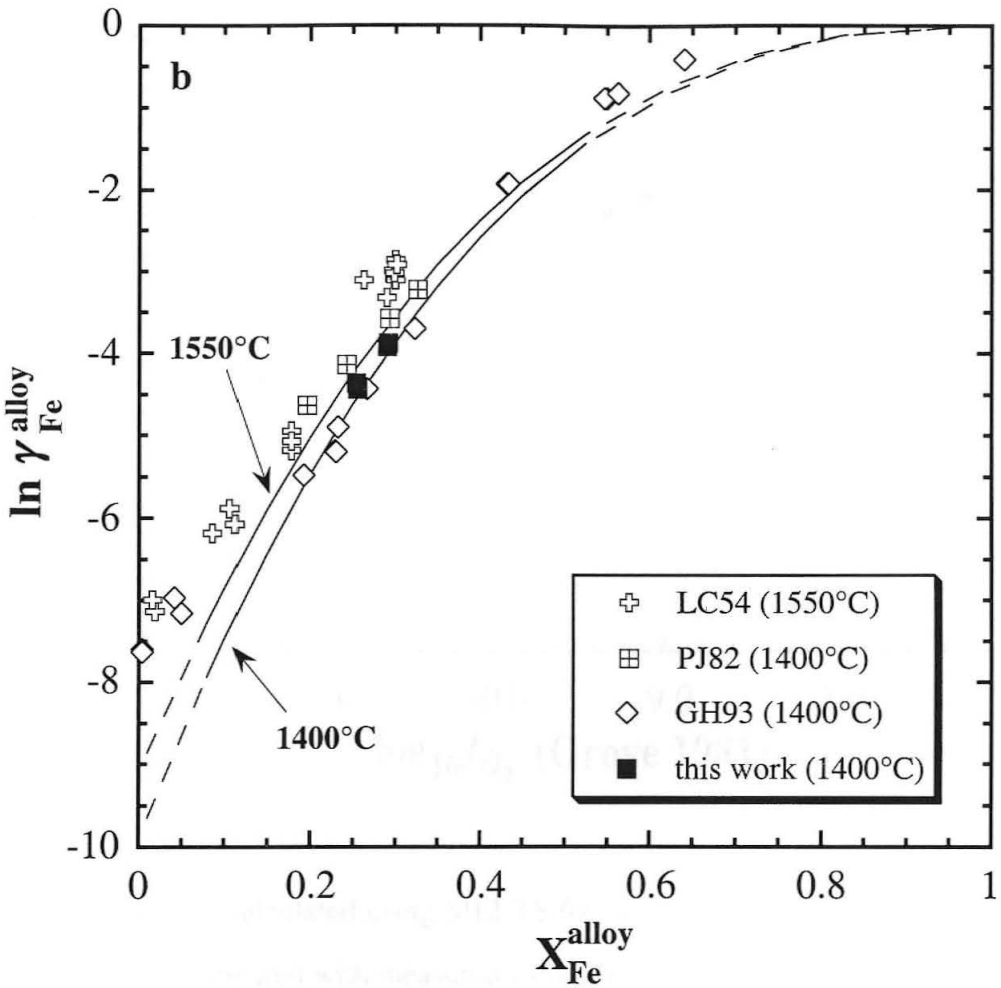

Figure 6. $\ln \gamma_{Fe}^{alloy}$ vs. X_{Fe}^{alloy} from previous experimental studies and our work, recalculated where necessary for magnetite-saturated experiments. Abbreviations and symbols are as given in the caption to Figure 1. The predicted curves for our data calculated using Equation 11a are also shown (solid curves with dashed extensions). (a) 1300°C. An asymmetric regular solution fit to Heald's (1967) data is also shown (dashed curve and dotted extensions). (b) 1400 and 1550°C.

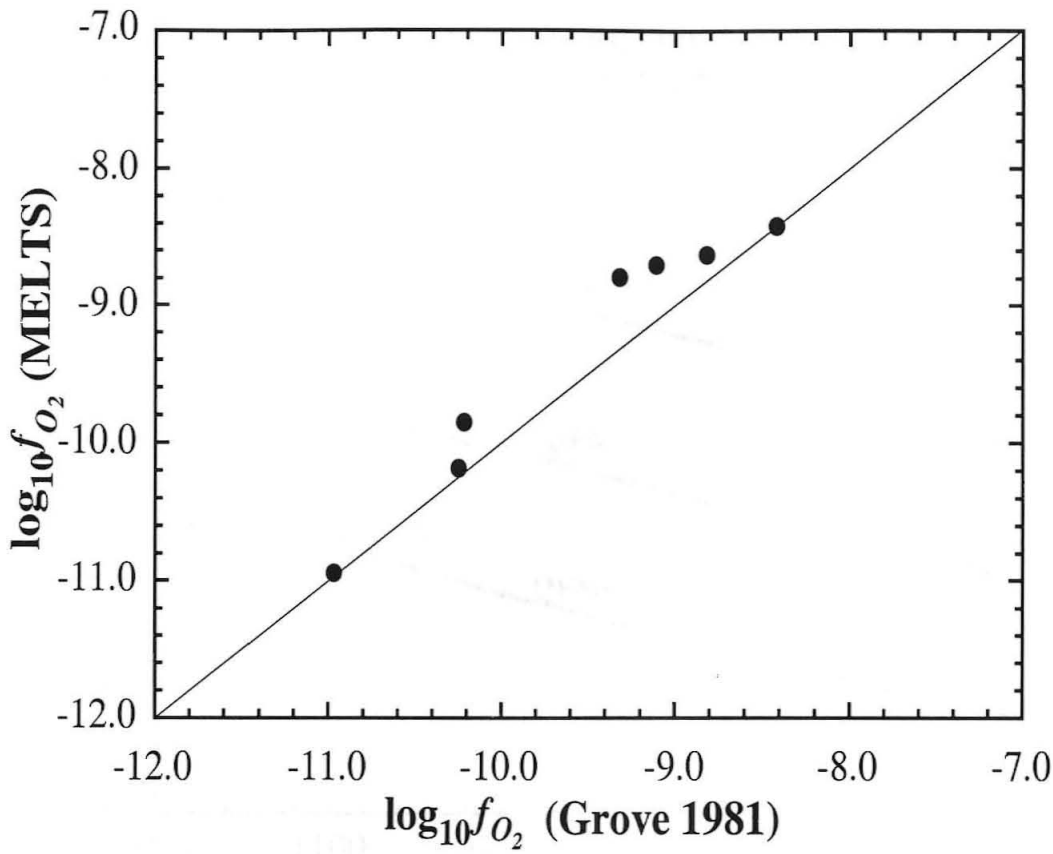

Figure 7. $\log_{10} f_{O_2}$ values calculated using MELTS for the liquid and alloy compositions given in Grove (1981) compared with measured values for selected experiments.

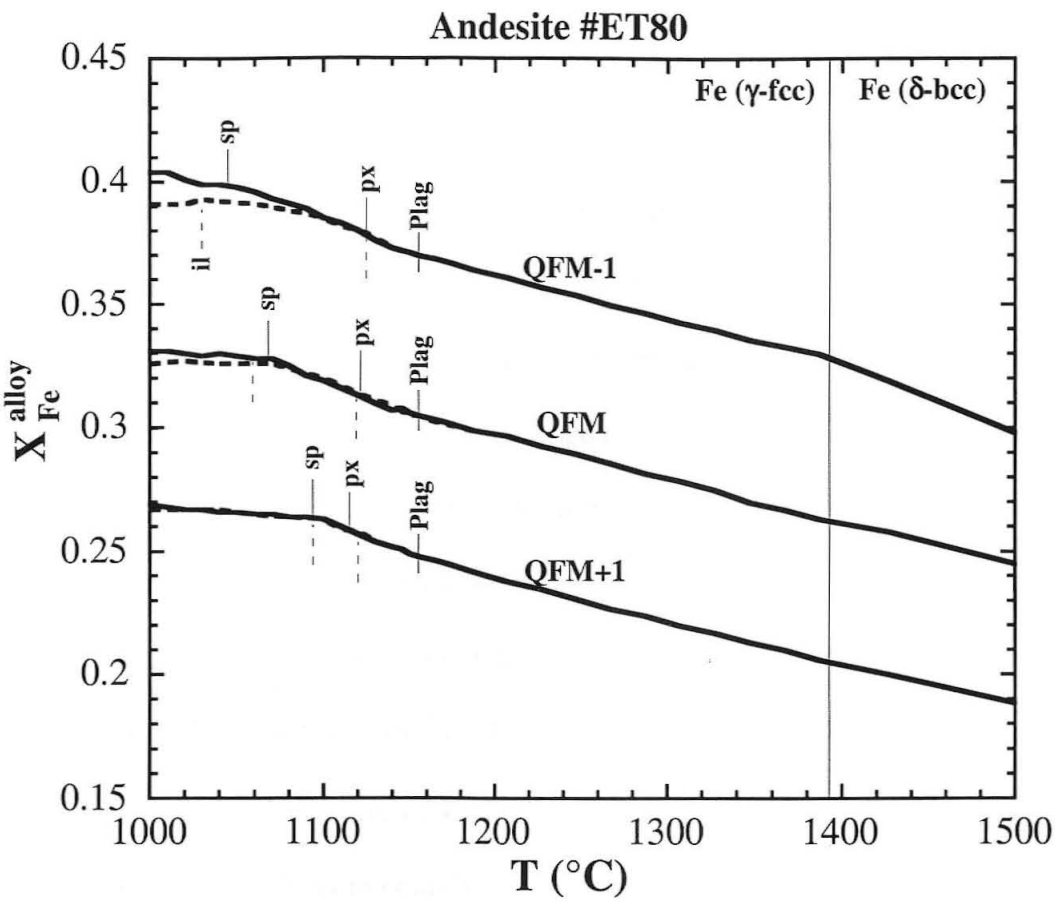

Figure 8. Pt-Fe alloy compositions in equilibrium with andesitic liquid during fractional (solid curves) and equilibrium (dashed curves) crystallization as a function of temperature and oxygen fugacity at 1 bar. Appearance temperatures of phases are indicated.

Chapter 2. The activity of chromite in multicomponent spinels. Part I: Experimental technique

Abstract—We determined activity-composition relationships in the Pt-Cr and Pt-Fe-Cr systems at 1300°C experimentally and used the results to constrain the thermodynamic properties of chromite-picrochromite spinels. The Pt-Cr binary is characterized by strong negative deviations from ideality throughout the investigated composition range; the activity-composition relationship can be fit by an asymmetric regular solution with three binary interaction parameters. The ternary alloy was modeled as a four-suffix asymmetric regular solution; the three ternary interaction parameters in this model were constrained by combining interaction parameters for the three bounding binaries taken from this and previous work with results for a set of experiments in which the activity of Cr in Pt-Fe-Cr-alloys was fixed by coexisting Cr_2O_3 at known f_{O_2}.

The free energy of formation of $FeCr_2O_4$ at 1300°C was determined using the activities of Fe and Cr in Pt-alloys in equilibrium with oxide mixes of $FeCr_2O_4$ and Cr_2O_3. The free energy of formation of chromite from $Fe+Cr_2O_3+O_2$ was found to be –202.7±0.4 kJ/mol (1σ), which is indistinguishable from literature values. The activity-composition relationships of chromites in $(Fe,Mg)Cr_2O_4$ were determined from a set of experiments in which Pt-alloys were equilibrated with spinel+Cr_2O_3. $(Fe,Mg)Cr_2O_4$ spinels are nearly ideal at 1300°C; modeling our data with a one-site symmetric regular solution yields an interaction parameter of +2.14±0.62 kJ/mol (1σ) similar within errors to literature evaluation.

1. INTRODUCTION

Although spinel is usually an accessory mineral, it occurs in wide variety of igneous and metamorphic rocks on Earth and other planets, making it a potentially valuable indicator of petrologic processes. For example, changes in the Cr or Ti contents of spinels are linked to the degree of partial melting during melting of planetary mantles and to crystallization differentiation of basaltic magmas (Arai, 1987; Dick and Bullen, 1984; El Goresy, 1976), to variations in metamorphic grade in terrestrial serpentinites (e.g., Evans and Frost, 1975), and to both igneous crystallization and subsolidus reduction processes in meteorites (Haggerty, 1972). Spinel is also commonly used in constructing geothermometers, geobarometers, and oxygen barometers: for example, cordierite ($Fe_2Al_2Si_5O_{18}$, Cd), corundum (Al_2O_3, Cor) and hercynitic spinel ($FeAl_2O_4$, Hc) are common in contact aureoles, so pertinent reactions include the geothermometer Cd = Hc + 5Q and the geobarometer Cd + Cor = 2Hc (e.g., Grant and Frost, 1990). Likewise, in mantle peridotites the phase assemblage olivine+orthopyroxene+spinel leads to an oxygen barometer based on the reaction $2Fe_3O_4$ (magnetite; Mt) + $FeSiO_3$ (ferrosilite) = Fe_2SiO_4 (fayalite) + O_2 (e.g., Mattioli et al., 1987; O'Neill and Wall, 1987); the coexistence of a magnetite-ulvöspinel (Fe_2TiO_4, Usp) solid solution with a hematite (Fe_2O_3, Hem)–ilmenite ($FeTiO_3$, Ilm) solid solution, a common occurrence in terrestrial igneous rocks (e.g., Carmichael, 1967), allows temperature and oxygen fugacity to be constrained simultaneously using the reactions 6Usp + O_2 = 2Mt + 6Ilm and Hem + Usp = Mt + Ilm (Buddington and Lindsley, 1964).

The wide range of rock types and phase assemblages in which spinel occurs makes it potentially versatile for constraining conditions of origin of rocks, the calculation of precise and accurate pressures, temperatures, and oxygen fugacities is possible only if the activity-composition relationships of all the phases in an assemblage are well constrained. Although structurally simple, this is problematic for spinels because natural spinels are compositionally complex (e.g., there are often significant concentrations of six or more different cations substituting into the two crystallographically distinct sites), ordering of cations between sites can be a strong function of composition and temperature (e.g., Sack and Ghiorso, 1991a,b), and the occurrence of Fe and sometimes other cations in multiple valence states can complicate matters even further.

Although petrologic applications of spinel thermochemistry almost always involve compositionally complex spinels, experimental studies designed to obtain the thermodynamic properties of spinel have been generally limited to binary and rarely ternary subsystems, and most involve magnetite as an end-member [e.g., Fe_3O_4-$FeAl_2O_4$, (Mason and Bowen, 1981); Fe_3O_4-$MgFe_2O_4$, Fe_3O_4-$FeAl_2O_4$, Fe_3O_4-$MgAl_2O_4$ (Nell et al., 1989; Nell and Wood, 1989); Fe_3O_4-Fe_2TiO_4 (Katsura et al., 1975; Woodland and Wood, 1994); Fe_3O_4-$FeCr_2O_4$ (Katsura et al., 1975, Petric and Jacob, 1982); $FeAl_2O_4$-$FeCr_2O_4$ (Petric and Jacob, 1982); $FeCr_2O_4$-$MgCr_2O_4$ (Hino et al., 1994; Jacob and Iyengar, 1999), $MgAl_2O_4$-Fe_3O_4-$\gamma Fe_{3/8}O_4$ (Mattioli et al., 1987)]. This lack of direct experimentation on multicomponent spinels lead to the development of activity-composition models for natural spinels that are extrapolated from simple subsystems. The models attempt to take into account observed miscibility gaps, dependence of cation ordering energies on composition, and the degree of long-range ordering of di- and trivalent cations between

tetrahedral and octahedral sites (e.g., Sack, 1982; Sack and Ghiorso, 1991a,b), but they are usually not well constrained in those regions of composition space that are of greatest interest for applications to natural systems.

Chromium is an essential constituent of many spinels in terrestrial crustal and mantle rocks and in extraterrestrial rocks, so the activity-composition relationships for Cr-bearing spinel components are key to full utilization of spinel-bearing assemblages for thermometry and barometry. One way to determine the activity of the chromite component, $FeCr_2O_4$, in multicomponent spinels is to equilibrate them with a Pt-alloy at known temperature and oxygen fugacity and then measure the Fe and Cr contents of the alloy. If the activity coefficients of Fe and Cr in the alloy are known, the activity of the chromite component can then be readily calculated. In this paper, we focus on determining the activity-composition relationships of ternary Pt-Fe-Cr alloys (a key ingredient for determining the thermodynamic properties of multicomponent Cr-, Fe-bearing spinels based on equilibrium with Pt-alloys) by equilibrating them with Cr_2O_3 and simple Cr-, Fe-bearing spinels at known temperature and oxygen fugacity. The results of these experiments also yield the free energy of formation of end-member $FeCr_2O_4$ and activity-composition relationships for binary chromite-picrochromite ($MgCr_2O_4$) spinels at 1300°C. In Part II, we apply our technique to experimentally determine chromite activities in spinels whose compositions approximate those in ordinary chondrites.

2. THEORETICAL APPROACH

During the approach to equilibrium between a Cr-, Fe-bearing spinel and initially pure Pt metal wire at a fixed temperature and oxygen fugacity, cations in the spinel are partially reduced and dissolved into the metal. Equilibrium between metal, a Pt-bearing

alloy in our case, and a chromite-bearing spinel in the presence of an oxygen-bearing vapor can be represented by the reaction:

$$Fe^{PtFeCr} + 2Cr^{PtFeCr} + 2O_2^{gas} = FeCr_2O_4^{spinel}, \quad (1a)$$

and its equilibrium constant

$$K_1 = \exp[-\Delta G_1^\circ / RT] = \frac{a_{FeCr_2O_4}^{\text{spinel}}}{(a_{Fe}^{PtFeCr})(a_{Cr}^{PtFeCr})^2 (f_{O_2})^2}, \quad (1b)$$

which can be rearranged such that the activity of chromite is expressed as

$$a_{FeCr_2O_4}^{\text{spinel}} = \exp[-\Delta G_1^\circ / RT](a_{Fe}^{PtFeCr})(a_{Cr}^{PtFeCr})^2 (f_{O_2})^2. \quad (1c)$$

In Eqns. 1b and 1c, a_i^j refers to the activity of component i in system j, K_1 is the temperature-dependent equilibrium constant, R is the gas constant, T is the temperature in Kelvin, ΔG_1° is the free energy of formation of $FeCr_2O_4$ from the elements, and f_{O_2} is the oxygen fugacity. Equation 1c is the basis for our experimental approach to evaluating the thermodynamic properties of multicomponent spinels. Given the temperature, f_{O_2}, and ΔG_1°, Eqn. 1c yields the activity of chromite provided the activities of Fe and Cr in the metal are known. The thermodynamic properties of ternary Pt-Fe-Cr alloys, which are necessary to evaluate a_{Fe}^{PtFeCr} and a_{Cr}^{PtFeCr} in our experiments, have not been previously investigated, so we first performed a set of experiments to constrain activity-composition relationships in the relevant portion of this system.

Many binary systems of interest to metallurgists and geochemists are adequately described by expressing the excess free energy of mixing (ΔG^{ex}) as a Taylor expansion in composition, truncated after a suitable number of terms (e.g., Wohl, 1946; Wohl, 1953). For many systems, a second or third order polynomial is adequate (e.g., Grover, 1976;

Saxena, 1973), but where the two components are characterized by highly differing atomic or molecular size and/or shape, a fourth-order polynomial in terms of composition (sometimes referred to as a four-suffix asymmetric subregular solution) may be required leading to

$$\frac{\Delta G^{ex}}{RT} = X_j^{\phi} X_i^{\phi} (X_j^{\phi} W_{ij} + X_i^{\phi} W_{ji} - X_j^{\phi} X_i^{\phi} D_{ji}). \quad (2)$$

In Eqn. 2, W_{ij} and D_{ij} are subregular interaction parameters [temperature- and composition-independent constants referred to as Margules parameters (Hildebrand, 1929)], and X_i^{ϕ} is the mole fraction of component i in the solid solution ϕ. The activity of a particular component i, a_i^{ϕ}, is derived by differentiating the sum $\sum_j n_j \Delta G^{ex}$ over all j with respect to the number of moles of component i, n_i. For a binary alloy, the activity coefficient, γ_i^{ϕ} (obtained through the identity $\gamma_i^{\phi} = a_i^{\phi} / X_i^{\phi}$) can be expressed as a function of composition according to

$$RT \ln \gamma_i^{\phi} = [W_{ji} + 2(W_{ij} - W_{ji} - D_{ji}) X_i^{\phi} + 3 D_{ji} (X_i^{\phi})^2] (X_j^{\phi})^2. \quad (3)$$

Polynomial functions can also be constructed to represent the excess free energy of mixing in ternary and higher solutions. For example, Wohl (1953) expressed ΔG^{ex} as a power series truncated after the fourth degree and obtained a formulation in which the binaries have a four-suffix subregular behavior:

$$\frac{\Delta G^{ex}}{RT} = \sum_{i \neq j} X_i^{\phi} X_j^{\phi} (X_i^{\phi} W_{ij} + X_j^{\phi} W_{ij} - X_i^{\phi} X_j^{\phi} D_{ij}) + X_i^{\phi} X_j^{\phi} X_k^{\phi} (\tfrac{1}{2} \sum_{i \neq j} W_{ij} - \sum_{i \neq j} X_i^{\phi} C_i). \quad (4a)$$

Most of the terms in this equation refer to binaries (cf. Eqn. 2); the effects of ternary interactions are incorporated via the ternary interaction parameters, C_i's. Letting

components 1=Pt, 2=Cr, and 3=Fe and differentiating Eqn. 4a for ΔG^{ex} for the ternary system with respect to the number of moles of Cr results in the following expression for the activity coefficient of Cr (after Wohl, 1953):

$$
\begin{aligned}
&RT\ln\gamma_{Cr}^{PtFeCr} = \\
&[W_{CrPt} + (W_{PtCr} - W_{CrPt} - D_{PtCr}) * X_{Cr}^{PtFeCr} + 3D_{PtCr}(X_{Cr}^{PtFeCr})^2](X_{Pt}^{PtFeCr})^2 + \\
&+[W_{CrFe} + (W_{FeCr} - W_{CrFe} - D_{CrFe}) * X_{Cr}^{PtFeCr} + 3D_{CrFe}(X_{Cr}^{PtFeCr})^2](X_{Fe}^{PtFeCr})^2 + \\
&+ X_{Fe}^{PtFeCr} X_{Pt}^{PtFeCr}[\tfrac{1}{2}(W_{PtCr} + W_{CrPt} + W_{FeCr} - W_{CrFe} - W_{PtFe} - W_{FePt}) + \\
&+ X_{Cr}^{PtFeCr}(W_{PtCr} - W_{CrPt} + W_{FeCr} - W_{CrFe}) + +(X_{Pt}^{PtFeCr} - X_{Fe}^{PtFeCr})(W_{PtFe} - W_{FePt}) + \\
&+3X_{Fe}^{PtFeCr} X_{Pt}^{PtFeCr} D_{PtFe} - X_{Cr}^{PtFeCr} C_{Cr} - \\
&-(1 - 3X_{Cr}^{alloy})(X_{Cr}^{PtFeCr} C_{Cr} + X_{Pt}^{PtFeCr} C_{Pt} + X_{Fe}^{PtFeCr} C_{Fe})].
\end{aligned}
\tag{4b}
$$

Expressions for the other components can be obtained by advancing the subscript of the parameters and variables of the equation in the order Pt→Cr, Cr→Fe, Fe→Pt. For Fe, this leads to

$$
\begin{aligned}
&RT\ln\gamma_{Fe}^{PtFeCr} = \\
&[W_{FeCr} + (W_{CrFe} - W_{FeCr} - D_{FeCr}) * X_{Fe}^{PtFeCr} + 3D_{FeCr}(X_{Fe}^{PtFeCr})^2](X_{Cr}^{PtFeCr})^2 + \\
&+[W_{FePt} + (W_{PtFe} - W_{FePt} - D_{FePt}) * X_{Fe}^{PtFeCr} + 3D_{FePt}(X_{Fe}^{PtFeCr})^2](X_{Pt}^{PtFeCr})^2 + \\
&+ X_{Pt}^{PtFeCr} X_{Cr}^{PtFeCr}[\tfrac{1}{2}(W_{CrFe} + W_{FeCr} + W_{PtFe} - W_{FePt} - W_{CrPt} - W_{PtCr}) + \\
&+ X_{Fe}^{PtFeCr}(W_{CrFe} - W_{FeCr} + W_{PtFe} - W_{FeCr}) + +(X_{Cr}^{PtFeCr} - X_{Pt}^{PtFeCr})(W_{CrPt} - W_{PtCr}) + \\
&+3X_{Pt}^{PtFeCr} X_{Cr}^{PtFeCr} D_{CrPt} - X_{Fe}^{PtFeCr} C_{Fe} - \\
&-(1 - 3X_{Fe}^{PtFeCr})(X_{Fe}^{PtFeCr} C_{Fe} + X_{Cr}^{PtFeCr} C_{Cr} + X_{Pt}^{PtFeCr} C_{Pt})].
\end{aligned}
\tag{4c}
$$

Equations 3, 4b, and 4c are the basic tools with which we develop a ternary composition model for Pt-Fe-Cr alloys and evaluate activities of components in coexisting phases. The ternary is developed stepwise by first characterizing the three binaries, Pt-Fe, Pt-Cr, and Fe-Cr using Eqn. 3, and then evaluating the ternary interaction parameters via Eqn. 4b.

3. EXPERIMENTAL PROCEDURES AND ANALYTICAL TECHNIQUES

3.1. Analytical procedures

Platinum-alloys were analyzed for Pt, Fe, Cr, and Mg using a JEOL733 Superprobe with an accelerating voltage of 20 keV. Pure metals were used as standards for Pt, Fe, and Cr, and $MgAl_2O_4$ was used for Mg. With a beam current of 25 nA, counts were collected for 30 seconds on peak and 15 seconds at each background position on the standards. For the metals from the run products, Pt (L_α) and Fe (K_α) were analyzed first using the same analytical conditions as for the standards (i.e., 25 nA); Cr (K_α) and Mg (K_α) were then analyzed with a beam current up to 400 nA and counting times between 10 and 30 minutes as needed to achieve detection limits $\leq$40 ppm for both Cr and Mg. Magnesium was found to be below detection limit in all alloys. Note that count rates on standards for Cr and Mg were much lower than on samples. This was necessary to prevent dead time corrections, which become nonlinear at very high count rates (J. Goldstein, written communication, 1998), from introducing spurious counts. A ZAF correction procedure (Armstrong, 1988) was applied to the results.

Oxides (the various spinels and Cr_2O_3) were analyzed using an accelerating voltage of 15 keV and a beam current of 10 nA. X-ray counts were collected for 30 seconds on peak and 15 seconds on each background using Fe_2O_3, Cr_2O_3 and $MgAl_2O_4$ as standards.

3.2. Starting materials

Chromite was prepared following the procedure of Petric and Jacob (1982): reagent grade powders of Fe (Alfa Products), Fe_2O_3 (JMC Puratronic), and Cr_2O_3 (JMC Puratronic) were ground in a molar ratio of 1:1:3 in an automated alumina mortar under

ethanol for ~7 hr. The mixture was pressed into 7 mm diameter pellets, placed inside loosely capped alumina ceramic cylinders, and sealed inside an evacuated quartz tube. The quartz tube was then heated at 1100°C for 4 days. Picrochromite was prepared following the procedure of O'Neill and Dollase (1994): reagent MgO (JMC Puratronic) was sintered in Al_2O_3 crucibles at 1000°C for 40 hr and then ground together with reagent grade Cr_2O_3 in the required molar ratio in an automated alumina mortar under ethanol for ~6 hr. The mixture was pressed into 13 mm diameter pellets, placed inside a Pt crucible, suspended from a sample holder at the hot spot of a vertical furnace, and held in a flowing H_2-CO_2 gas at 1100°C and $\log_{10} f_{O_2}$=–11.5 for 20 hr. Chromite and picrochromite were mixed in three different ratios corresponding to nominal mole fractions of chromite, $X_{FeCr_2O_4}^{(Fe,Mg)Cr_2O_4}$, of 0.13, 0.46, and 0.83. The three spinel binary mixes and a pure chromite powder were further mechanically mixed with 40 mole% Cr_2O_3 using an automated alumina mortar under ethanol for 2 hr to produce starting material for the experiments.

Homogeneity and the degree to which oxides were converted to chromite and picrochromite were determined using a Scintag Pad-V x-ray diffractometer and electron microprobe analyses. Usually one synthesis cycle was sufficient to produce chromite with average lattice parameter of a_o=8.3665±0.0201Å, consistent with a stoichiometric chromite standard, 8.3790Å (NBS 25,19,50). Two cycles were required to achieve pure picrochromite with a_o=8.3240±0.0088Å [reference standard taken as 8.3330Å (NBS 539,9,34)]. The compositions of the various spinels were further characterized using EPMA analyses and found to be homogeneous. Some alumina was probably incorporated into the spinels and Cr_2O_3 through contamination during grinding in the alumina mortar. We can only place upper limits on this effect due to our use of alumina polishing

compound but analyses of all run products [Cr_2O_3 (0.45±0.16 wt% Al_2O_3), $FeCr_2O_4$ (0.32±0.07 wt% Al_2O_3) and $(Fe,Mg)Cr_2O_4$ (0.68±0.16 wt% Al_2O_3 excluding one sample with up to 2 wt% Al_2O_3 that we attribute to alumina grit)] show that the amount of alumina in solid solution is small. Assuming that Raoult's law holds for the Cr-bearing oxides, these concentration levels introduce errors of 0.01-0.02% into Cr activity coefficients in alloys and 0.02-0.05% into calculated activity coefficients of $FeCr_2O_4$ spinels. Since the errors involved are small compared to other sources of error and we observed no correlation between apparent alumina content and the thermodynamic properties, we ignore the effect of alumina contamination on our results.

3.3. Experimental conditions

Kessel et al. (2001) present a detailed description of the furnace setup and calibration procedure. All of the experiments were conducted at 1 atm in a Deltech DT-31 furnace or a home-built $MoSi_2$ furnace with gas-mixing capability. The oxygen fugacity was set by mixing CO_2 and H_2 gases and measured using an yttria-doped-zirconia solid electrolyte oxygen sensor ($SIRO_2$®, Ceramic Oxide Fabricators, Ltd., Australia) with an uncertainty of ±0.05 log units. Temperatures were measured using a Pt-$Pt_{90}Rh_{10}$ (type S) thermocouple and are estimated to be accurate to within ±3°C. All experiments were conducted at 1300°C.

In each experiment, up to five crucibles, made from 0.625 cm diameter, 1 cm long Al_2O_3 rods (Vesuvius McDanel), were suspended using Pt wire from a sample holder in the vicinity of the furnace hot spot. Each crucible contained up to three horizontally stacked pellets (7 mm diameter, 1-2 mm thick) of identical oxide/s pressed around three pieces of Pt or Pt-Fe wire of known composition [see preparation and compositions in

Kessel et al. (2001)]. One crucible contained a pellet of Cr_2O_3 pressed around pure Pt wires [3-5 mm long, 75 μm diameter wires (99.9999%, Alfa® ÆSAR)]. A second crucible contained one or more pellets of $FeCr_2O_4$+Cr_2O_3, each pellet containing two wires of Pt-Fe alloy of known composition, above and below the expected equilibrium Fe concentration at the conditions of the experiment. Each of the remaining three crucibles contained pellets of one of the three spinel binary mixes [$(Fe,Mg)Cr_2O_4$ +Cr_2O_3] pressed around two Pt-Fe alloys.

Experiments were conducted for 8-14 days to ensure a close approach to equilibrium of the Pt-alloys with the surrounding oxides. These run durations were at least twice the characteristic time required to homogenize Fe in Pt wire based on the diffusion data of Berger and Schwartz (1978). We are not aware of any diffusion data on Cr in Pt, but concentrations of both Fe and Cr across the wires were homogeneous within analytical error. Also, the Pt-Fe wires of initially different compositions and in pellets at different positions in a stack converged in each crucible to the compositions that were indistinguishable. Run durations were also found to be sufficient for complete conversion of the binary spinel mixtures to the equilibrium solid-solution phase as shown by EPMA analyses.

Experiments were terminated by raising the crucibles into the cold region of the furnace under the flowing gas mixture. Once cooled, samples were removed from the furnace. A small piece of each pellet containing a Pt-alloy surrounded by oxides was mounted in epoxy within a brass cylinder for examination of the textures around the wire and analyses of the oxides. The second wire from each pellet was physically separated from the adjacent oxides, mounted using epoxy to a piece of quartz glass, and the

combination mounted in epoxy within a brass cylinder such that a vertical cross section of the wire was exposed. This sample was used to determine the alloy composition and to check for homogeneity across the wire. Alumina impregnated papers were used to expose the wires and oxides, and diamond powder (<0.25 μm) to achieve the final polished surfaces.

4. EXPERIMENTAL RESULTS

The experimental conditions and results for each set of experiments are listed in Tables 1-3. The experiments were conducted at 1300°C, with oxygen fugacities ranging from $\log_{10} f_{O_2}$=–11.63 to –7.90, corresponding to –0.86 log units below the iron–wüstite (IW) buffer to +2.83 above. Values of X_{Fe}^{PtFeCr} and X_{Cr}^{PtFeCr} were calculated from the measured wt% Fe and Cr, respectively, by averaging all analyses (3-10) made on each wire. The averages and their uncertainties (the standard deviation of the distribution of measured alloy compositions from each wire) are listed in the tables. Results for Pt-alloys equilibrated with Cr_2O_3 (Table 1) were used to constrain an activity-composition model for the Pt-Cr binary system. Compositions of Pt-alloys equilibrated with $FeCr_2O_4$+Cr_2O_3 (Table 2) and $(Fe,Mg)Cr_2O_4$+Cr_2O_3 (Table 3) were used to construct a ternary Pt-Fe-Cr model by taking advantage of the existence of Cr_2O_3 in the mixes, which fixed the activity of Cr in the alloy. Platinum-alloys equilibrated with $FeCr_2O_4$+Cr_2O_3 were also used to evaluate the free energy of formation of end-member chromite and those equilibrated with $(Fe,Mg)Cr_2O_4$+Cr_2O_3 to evaluate the thermodynamics of binary $(Fe,Mg)Cr_2O_4$ spinels.

4.1. Pt-Fe and Fe-Cr binaries

Activity-composition relationships of alloys in the Pt-Fe system at various temperatures were evaluated in Kessel et al. (2001) and only a brief summary is presented here. At 1300°C, the system is characterized by strong negative deviations from ideality that can be described by a three-suffix asymmetric subregular solution with two binary interaction parameters (i.e., Eqn. 3 with $D_{ji}=0$), values of which are listed in Table 4. The thermodynamic properties of alloys in the Fe-Cr system have little influence on our model for Pt-Fe-Cr alloys because this binary is much more ideal then either Pt-Fe or Pt-Cr joins, leading to a small contribution to the activity coefficient, at least for compositions of interest for this study (i.e., very low in Cr and relatively rich in Pt). For the Fe-Cr binary we used activity-composition relationships for Fe-Cr austenite (γ, fcc) alloys ($X_{Cr}^{FeCr} \leq 0.06$ at 1300°C) from Andersson and Sundman (1987). For consistency with Eqns. 3 and 4, we refit their model activities at 1300°C to a three-suffix asymmetric subregular solution with least-squares best-fit interaction parameters as given in Table 4. These alloys are characterized by a moderate positive deviation from ideality.

4.2. Pt-Cr binary

Activity-composition relationships in the Pt-Cr system were determined following the approach used by Kessel et al. (2001) for Pt-Fe alloys. Initially pure Pt wire was equilibrated with Cr_2O_3 at a fixed temperature and f_{O_2}. Under these conditions, if the reaction

$$2Cr^{PtCr} + \tfrac{3}{2}O_2^{gas} = Cr_2O_3 \qquad (5a)$$

reaches equilibrium, the corresponding expression for the equilibrium constant can be solved for a_{Cr}^{PtCr}:

$$a_{Cr}^{\mathrm{PtCr}} = \left(\frac{a_{Cr_2O_3}^{\mathrm{oxide}}}{K_5 (f_{O_2})^{3/2}} \right)^{1/2} . \qquad (5b)$$

The equilibrium constant, K_5, can be obtained from the free energy of formation of Cr_2O_3 from the elements, ΔG_5°, via $\Delta G_5^\circ = -RT \ln K_5$. We used ΔG_5° from Holzheid and O'Neill (1995). Since Cr_2O_3 is essentially a stoichiometric 2:3 oxide throughout the range of experimental conditions explored in this study [as expected from Kofstad (1983) and confirmed by EPMA analyses], its activity, $a_{Cr_2O_3}^{oxide}$, is taken as equal to 1, and a_{Cr}^{PtCr} can be readily calculated from Eqn. 5b. Iron was detected in the Pt-Cr wires (and presumed to be due to contamination by vapor transport from adjacent crucibles), but was always less than 0.4 wt% Fe. Such low Fe concentrations introduce only a small error in the calculation of $\ln \gamma_{Cr}^{PtCr}$ (less than 0.3% based on the ternary model developed below).

Experimental run conditions are presented in Table 1. Uncertainties in $\ln \gamma_{Cr}^{PtCr}$ were found by propagating errors on temperature, $\log_{10} f_{O_2}$, and X_{Cr}^{PtCr} (<5%) to be less than 1.5%. Alloys in the Pt-Cr system are characterized by strong negative deviations from ideality (i.e., $\gamma_{Cr}^{PtCr} << 1$) over the range of compositions explored in this study. Figure 1 shows our data for $RT \ln \gamma_{Cr}^{PtCr}$ plotted against X_{Cr}^{PtCr} compared to the best fits assuming three-suffix and four-suffix subregular solution behavior. Our data are clearly poorly fit by a three-suffix asymmetric subregular solution at the Cr-poor end of the binary but are well described by a four-suffix solution, parameters for which are given in Table 4. Uncertainties in the Margules parameters were calculated using a Monte Carlo simulation

taking into account uncertainties on the alloy composition and Cr activity. The required large D_{PtCr} value and the small uncertainty associated with it also indicate the necessity of using three binary interaction parameters.

The deviations of our data from best fits to both models are shown as an inset in Fig. 1 as a function of composition. Deviations from a four-suffix subregular solution model are independent of X_{Cr}^{PtCr} and most data plot within 1σ of the predicted curve. In contrast, absolute deviations from the best fit to a three-suffix subregular solution model show a systematic increase with decreasing X_{Cr}^{PtCr}. Since Cr contents of interest for the ternary system in this study are $X_{Cr}^{PtCr}<0.005$, we adopted the four-suffix subregular solution.

Results from previous studies at 1225 and 1500°C are also shown in Fig. 1. For the sake of consistency, all of these data were recalculated using ΔG_5^o from Holzheid and O'Neill (1995) based on the reported f_{O_2}, temperature, and alloy compositions. Schwerdtfeger and Muan (1965) equilibrated mixtures of Pt and Cr_2O_3 powders at 1225°C and known f_{O_2}'s and measured the Cr concentration in Pt by x-ray diffraction. Their results are scattered but generally consistent with our results at 1300°C. Pretorius and Muan (1992) and Garbers-Craig and Dippenar (1997) equilibrated Pt wires with Cr_2O_3 at 1500°C and known f_{O_2}'s and measured the Cr concentration in the Pt alloy using SEM-EDS and EPMA, respectively. These two studies complement each other in alloy compositions and result in a well-defined trend that is slightly different from ours. None of the available studies on the Pt-Cr system were done at 1300°C preventing a direct comparison, but all of the experiments in these latter two studies yield slightly Cr-poor

alloys at any given f_{O_2} compared to our predicted compositions based on the results we obtained at 1300°C and assuming subregular solution behavior (i.e., $RT\ln\gamma_{Cr}^{PtCr}$ is independent of temperature for a given alloy composition). Such deviations would be consistent with incompletely equilibrated alloys but both Pretorius and Muan (1992) and Garbers-Craig and Dippenar (1997) demonstrated equilibrium through time series and reversal experiments. Garbers-Craig and Dippenar (1997) published uncertainties on alloy compositions (2%) and, assuming that uncertainties in temperature (±3°C) and $\log_{10} f_{O_2}$ (±0.05) were the same as in our experiments, this leads to uncertainties in calculated $RT\ln\gamma_{Cr}^{PtCr}$ of ~5%. Their data deviate from our model by 4–18% (most of the data are consistent with our model within 2σ). We used the same error estimates for data of Pretorius and Muan (1992) although analytical uncertainties are likely to be larger by several % because they used SEM-EDS to determine alloy composition. All but one of the data points from Pretorius and Muan (1992) are consistent at the 2σ level with an extrapolation of our model to 1500°C.

4.3. Pt-Fe-Cr ternary model

If Cr_2O_3 and an Fe-bearing oxide are equilibrated with Pt, the equilibrium Pt-bearing alloy will contain Fe and Cr, and while the activity of Cr in the alloy at a given f_{O_2} is fixed by the presence of Cr_2O_3 (as in the Pt-Cr_2O_3 experiments described in the preceding section), the Cr concentration will in general be different due to the presence of Fe. Table 2 presents results of a set of experiments in which Pt-alloys were equilibrated with mixtures of $FeCr_2O_4$+Cr_2O_3. The equilibrium oxides were essentially end-member

$FeCr_2O_4$ and Cr_2O_3, as confirmed by microprobe analyses of oxide grains in the vicinity of the Pt-alloys extracted from run products (i.e., the solubility of $FeCr_2O_4$, FeO, or Fe_2O_3 in Cr_2O_3 and visa versa are negligible over the range of conditions explored in this study). Table 3 presents results for a set of experiments in which Pt-alloys were equilibrated with mixtures of $FeCr_2O_4$+$MgCr_2O_4$+Cr_2O_3. The addition of picrochromite to the spinel reduced the activity of FeO in the oxides relative to the $FeCr_2O_4$+Cr_2O_3 assemblage, so the activity of Fe in the alloy at any given f_{O_2} is also reduced. Values of X_{Fe}^{PtFeCr} in our ternary experiments were in the range 0.19-0.53.

The changes in alloy composition, X_{Fe}^{PtFeCr} and X_{Cr}^{PtFeCr}, with f_{O_2} for alloys in equilibrium with $FeCr_2O_4$+Cr_2O_3 are shown in Fig. 2. To test the approach to equilibrium, up to three pellets were placed in a crucible, each composed of the mixed oxides but pressed around Pt-Fe wires of different initial Fe content. Starting with Pt-Fe alloys initially higher and lower in Fe than the equilibrium alloy composition enabled us to "reverse" our experimental results. Also displayed in Fig. 2 are the initial X_{Fe}^{PtFeCr} values in each experiment. All Pt-alloys at a given f_{O_2} converge to the same Fe content within analytical errors. This convergence gives us considerable confidence that equilibrium was attained in these experiments.

The activity of Cr in the Pt-alloys in equilibrium with either $FeCr_2O_4$+Cr_2O_3 or $FeCr_2O_4$+$MgCr_2O_4$+Cr_2O_3 was calculated using Eqn. 5b assuming that end-member Cr_2O_3 was in equilibrium with the alloys (i.e., $a_{Cr_2O_3}^{oxide}$=1); corresponding values of $\ln\gamma_{Cr}^{PtFeCr}$ were obtained from the measured X_{Cr}^{PtFeCr}. For each of our 25 experiments, interaction parameters for the three bounding binaries (Table 4) and values of $\ln\gamma_{Cr}^{PtFeCr}$ were inserted

into Eqn. 4b to produce one equation in the three unknown ternary parameters C_{Cr}, C_{Fe}, and C_{Pt}. We then used an iterative least-squares technique to find best fit values of the three parameters. However, this resulted in a large and unrealistic value for C_{Cr} (on the order of 11,000 kJ/mol) and led to inconsistencies in the resulted binary spinel activity-composition relationships. The source of the problem is that C_{Cr} is multiplied by X_{Cr}^{PtFeCr} in Eqn. 4b, which has a very small value in our experiments, and therefore the value of C_{Cr} is poorly constrained. It was found that fixing the value of C_{Cr} anywhere in the range of –500 to +500 kJ/mol and solving for the other two parameters, C_{Fe}, and C_{Pt}, iteratively had virtually no effect on the sum of the squares of the residuals of the model in the composition range covered by our experiments. We therefore chose arbitrarily to set C_{Cr} to 0 and determined best-fit values for the other two ternary interaction parameters in the Pt-Fe-Cr system. This procedure yielded C_{Pt}=+115.7 kJ/mol, and C_{Fe}=–68.6 kJ/mol (Table 4). Values of $\ln\gamma_{Cr}^{PtFeCr}$ calculated using Eqn. 4b and the interaction parameters derived above are given in Tables 2 and 3. Uncertainties in the model $\ln\gamma_{Cr}^{PtFeCr}$ values calculated by propagating errors on temperature, and alloy composition [X_{Cr}^{PtFeCr} (1-3%) and X_{Fe}^{PtFeCr} (0.1-3%)] are less then 2.5% (1σ). Deviations of model from observed values calculated using Eqn. 5b are shown in Fig. 3 as a function of $\log_{10} f_{O_2}$ to be less than 0.2 log units (<5%). Deviations of model $\ln\gamma_{Cr}^{PtFeCr}$ that include ternary interactions are all within 2σ of observed values and are independent of $\log_{10} f_{O_2}$ as shown in Fig. 3. In contrast, as also shown in Fig. 3, model $\ln\gamma_{Cr}^{PtFeCr}$ values in which ternary interactions are ignored yield much larger deviations and show a systematic increase with $\log_{10} f_{O_2}$ indicating that the ternary interaction effect is significant and can not be ignored.

The effect of Fe on Cr activity coefficients is significant and our model quantifies this. Figure 4a shows model values of $\ln\gamma_{Cr}^{PtFeCr}$ calculated using Eqn. 4b with the parameters from Table 4 as a function of X_{Cr}^{PtFeCr}. At constant X_{Cr}^{PtFeCr}, $\ln\gamma_{Cr}^{PtFeCr}$ increases with increasing Fe by 6 ln units for X_{Fe}^{PtFeCr} ranging between zero (i.e., Pt-Cr alloys) and X_{Fe}^{PtFeCr}=0.4. Also shown in Fig. 4a are the model $\ln\gamma_{Cr}^{PtFeCr}$ calculated for our experiments from the measured X_{Cr}^{PtFeCr} and ternary model parameters. The corresponding X_{Fe}^{PtFeCr} values for each Pt-alloy is shown next to the symbol. Model $\ln\gamma_{Fe}^{PtFeCr}$ values calculated from Eqn. 4c, identical to values calculated using the Pt-Fe activity-composition model developed by Kessel et al. (2001) are given in Tables 2 and 3 together with calculated uncertainties. Uncertainties in model $\ln\gamma_{\mathrm{Fe}}^{\mathrm{PtFeCr}}$ calculated by propagating errors on temperature and alloy composition are less then 2.5% (1σ). The values of $\ln\gamma_{Fe}^{PtFeCr}$ are insensitive to whether or not ternary interactions are incorporated because $X_{Fe}^{PtFeCr} >> X_{Cr}^{PtFeCr}$ and using either the evaluated C_i's or setting them equal to zero yields essentially the same results. This conclusion is demonstrated in Fig. 4b showing model values of $\ln\gamma_{\mathrm{Fe}}^{\mathrm{PtFeCr}}$ calculated using Eqn. 4c as a function of X_{Fe}^{PtFeCr} for a range of X_{Cr}^{PtFeCr}. The model values of $\ln\gamma_{\mathrm{Fe}}^{\mathrm{PtFeCr}}$ calculated for our experiments are also shown and the corresponding X_{Cr}^{PtFeCr} value is given. We conclude that the activities of Cr and Fe in Pt-alloys can be obtained for a given alloy composition using the model developed above. Knowledge of a_{Cr}^{PtFeCr} and a_{Fe}^{PtFeCr} is the basis for obtaining activities of Cr-, Fe-bearing oxides or silicates using Pt-alloy equilibration. In Part II, activities of chromite in the spinels of ordinary chondrites will be evaluated using the alloy model developed here.

4.4. Free energy of formation of chromite

In the set of experiments in which Pt-alloys were equilibrated with mixtures of end-member $FeCr_2O_4$ and Cr_2O_3, equilibrium 1a holds, but the presence of Cr_2O_3 also allows an evaluation of the free energy of formation of chromite, ΔG_6°, from Cr_2O_3, Fe, and O_2 based on the equilibrium:

$$Fe^{PtFeCr} + Cr_2O_3 + \tfrac{1}{2}O_2^{gas} = FeCr_2O_4^{spinel}. \qquad (6a)$$

This yields an expression for ΔG_6°:

$$\Delta G_6^\circ = -RT\ln\left[\frac{a_{FeCr_2O_4}^{\text{spinel}}}{a_{Fe}^{PtFeCr}\,(a_{Cr_2O_3}^{\text{oxide}})\,(f_{O_2})^{1/2}}\right]. \qquad (6b)$$

Using our measured values of X_{Fe}^{PtFeCr} for each experiment calculating a_{Fe}^{PtFeCr} from our activity-composition model for ternary alloys and setting both $a_{FeCr_2O_4}^{spinel}$ and $a_{Cr_2O_3}^{oxide}$ equal to 1 allows ΔG_6° to be determined from Eqn. 6b. Calculated values of ΔG_6° are given in Table 2 and shown in Fig. 5a as a function of $\log_{10} f_{O_2}$. The uncertainties obtained by propagating errors on temperature, f_{O_2}, and a_{Fe}^{PtFeCr} are less than 1.5% (1σ). The average ΔG_6° and standard deviation of the mean at 1300°C is –202.7±0.4 kJ/mol with no observed dependency on $\log_{10} f_{O_2}$; this value is given in Table 4. Our results (Fig. 5a) are indistinguishable from the values of ΔG_6°=–202.5±6.8 and –202.5±0.6 kJ/mol obtained by Hino et al. (1994) and Jacob and Alcock (1975), respectively. Hino et al. (1994) equilibrated liquid silver with crucibles made of $FeCr_2O_4$ saturated with Cr_2O_3 at temperatures between 1150 and 1450°C and $\log_{10} f_{O_2}$ between –9.68 and –6.07 and the free energy of chromite was determined using their activity-composition model for Fe-Ag

liquids. Jacob and Alcock (1975) determined the free energy of formation of chromite at temperatures between 750 and 1600°C and $\log_{10} f_{O_2}$ corresponding to the equilibrium of $FeCr_2O_4$+Cr_2O_3+Fe using a bielectrolyte solid-state galvanic cell based on Eqn. 6a. The excellent agreement between our value and those in the literature determined using entirely independent techniques provides strong validation of the activity-composition relationship for binary Pt-Fe alloys we have developed (Kessel et al., 2001) and of our conclusion that at low Cr concentrations in the alloys, the effects of Cr on Fe activity coefficients can be neglected.

The free energy of formation of $FeCr_2O_4$ from the elements, ΔG_1°, at 1300°C and 1 bar can be calculated from our alloy compositions in two ways. First, measured values of X_{Fe}^{PtFeCr} and X_{Cr}^{PtFeCr} can be used given our activity-composition relationship for the ternary alloys to compute values of a_{Fe}^{PtFeCr} and a_{Cr}^{PtFeCr}, which can then be substituted into Eqn. 1b to calculate ΔG_1° directly. The observed values (Table 2) are independent of $\log_{10} f_{O_2}$ (Fig. 5b) and the average and standard deviation of the mean at 1300°C is –923.5±2.1 kJ/mol. Alternatively, our values of ΔG_6° (Fig. 5a) can be corrected to ΔG_1° via ΔG_5° from Holzheid and O'Neill (1995), yielding –924.0±0.4 kJ/mol. The same procedure, applied to ΔG_6° values of Hino et al. (1994) and Jacob and Alcock (1975), gives –923.8±6.8 and –923.8±0.6 kJ/mol, respectively. The four estimates of ΔG_6° at 1300°C are in excellent agreement. Note that in contrast to ΔG_6°, our error on a direct determination of ΔG_1° is larger than that of Jacob and Alcock (1975) or our own value obtained via ΔG_6° and ΔG_5° because the direct calculation of ΔG_1° requires an explicit evaluation of a_{Cr}^{PtFeCr}, which contributes uncertainty to the value of ΔG_1°. However, the fact that the determination of

ΔG_1° based on our measured values of X_{Fe}^{PtFeCr} and X_{Cr}^{PtFeCr} is indistinguishable from values based on independent measurements and/or calculations from the literature provides strong validation of the activity-composition relationship for ternary Fe-Pt-Cr alloys we have developed.

5. ACTIVITY OF CHROMITE IN (Fe,Mg)Cr_2O_4 SPINELS

In section 4, we presented a ternary model for Pt-Fe-Cr alloys using experiments in which $FeCr_2O_4$+$MgCr_2O_4$+Cr_2O_3 were equilibrated with Pt-Fe-Cr alloys. We used the binary spinels primarily as a vehicle to extend the range of alloy compositions explored in this study by decreasing the activity of $FeCr_2O_4$ in the spinels (and that of Fe in the metal relative to coexistence with $FeCr_2O_4$+Cr_2O_3 at a given f_{O_2}). However, these experiments also constrain the thermodynamic properties of binary (Fe,Mg)Cr_2O_4 spinels, and we examine these constraints in this section. As described above, three different mixes of $FeCr_2O_4$+$MgCr_2O_4$ were studied experimentally (nominal mixes, expressed as mole fractions of $FeCr_2O_4$ in $Fe_XMg_{1-X}Cr_2O_4$ were $X_{FeCr_2O_4}^{(Fe,Mg)Cr_2O_4}$=0.13, 0.46, 0.83), each mixed together with 40 mole% of Cr_2O_3. Up to three pellets of a given binary spinel mix were pressed around Pt-Fe wires, each with a different initial Fe content so that the equilibrium alloy composition could be approached from both Fe-poor and Fe-rich compositions. Homogeneous spinel and Cr_2O_3 were present in all run products as confirmed, with particular attention to the vicinity of the Pt-Fe alloys, by electron probe analyses. Analyzed values of $X_{FeCr_2O_4}^{(Fe,Mg)Cr_2O_4}$ in Cr_2O_3-saturated run products (calculated on an Al_2O_3-free basis) were 0.12±0.01 (n=12), 0.44±0.05 (n=18), and 0.81±0.02 (n=18), in agreement within uncertainties with the nominal values. The standard deviations refer to the

distribution of measured spinel compositions and arise primarily from contamination from overlap of the beam on adjacent Cr_2O_3 grains during the analyses of individual spinel grains. The fraction of Fe^{3+} in the spinel run products, calculated assuming mass and charge balance, was found to be less than 0.001, and the coexisting Cr_2O_3 was found to be stoichiometric, indicating that the solubilities of Fe_3O_4 in $Fe_XMg_{1-X}Cr_2O_4$ and of FeO or Fe_2O_3 in Cr_2O_3 are negligible under the experimental conditions used in this study.

The activity of $FeCr_2O_4$ in $Fe_XMg_{1-X}Cr_2O_4$, $a_{FeCr_2O_4}^{(Fe,Mg)Cr_2O_4}$, can be calculated based on Eqn. 6b given the Fe content of the coexisting alloy at a given f_{O_2}. For each experiment, we substituted ΔG_6^o from Table 4 and a_{Fe}^{PtFeCr} calculated using Eqn. 4c into Eqn. 6b to obtain $a_{FeCr_2O_4}^{(Fe,Mg)Cr_2O_4}$. The calculated activities are given in Table 3 and shown in Fig. 6 as a function of composition. Errors (1σ) on $a_{FeCr_2O_4}^{(Fe,Mg)Cr_2O_4}$ calculated using Eqn. 6a are 6-7% based on propagating the errors on temperature, f_{O_2}, and alloy composition. $(Fe,Mg)Cr_2O_4$ spinels are essentially ideal at 1300°C (Fig. 6). Our activities can be reasonably fit to a one-site symmetric regular solution of the form:

$$RT\ln\gamma_{FeCr_2O_4}^{(Fe,Mg)Cr_2O_4} = W_{(Fe,Mg)Cr_2O_4}\left(X_{MgCr_2O_4}^{(Fe,Mg)Cr_2O_4}\right)^2, \quad (7)$$

and a best fit of our data yields $W_{(Fe,Mg)Cr_2O_4}$=+2.14±0.62 kJ/mol (1σ) taking into account the uncertainties on $RT\ln\gamma_{FeCr_2O_4}^{(Fe,Mg)Cr_2O_4}$. The activities derived at $\log_{10} f_{O_2}$=–9.83 are systematically higher than the activities derived at either $\log_{10} f_{O_2}$=–11.07 or –8.69 for reasons that are unclear, but all results agree within 2σ and a best fit excluding data obtained at $\log_{10} f_{O_2}$=–9.83 yields essentially ideal behavior ($W_{(Fe,Mg)Cr_2O_4}$=+0.29±0.75 kJ/mol). Also shown in Fig. 6 are results at 1300°C from previous studies (Hino et al.,

1994; Jacob and Iyengar, 1999). For consistency, previous results were recalculated based on the reported f_{O_2}, temperature, and spinel composition, using our ΔG^{o}_{6}. Previous results for $(Fe,Mg)Cr_2O_4$ range from nearly ideal (Jacob and Iyengar, 1999) to systematic negative deviations from ideality (Hino et al., 1994). Hino et al. (1994) equilibrated liquid silver with crucibles made of $(Fe,Mg)Cr_2O_4$ saturated with Cr_2O_3 at temperatures between 1150 and 1450°C and $\log_{10} f_{O_2}$ between –7.73 and –6.20. Values of $a_{FeCr_2O_4}^{(Fe,Mg)Cr_2O_4}$ were then calculated using Eqn. 6b based on their experimentally determined activity-composition relationships for Fe-Ag liquids and their derived free energy of formation of $FeCr_2O_4$ from Fe and Cr_2O_3. Jacob and Iyengar (1999) determined $a_{FeCr_2O_4}^{(Fe,Mg)Cr_2O_4}$ at temperatures between 777 and 1077°C and $\log_{10} f_{O_2}$ corresponding to the equilibrium of $FeCr_2O_4$+Cr_2O_3+Fe using a bielectrolyte solid-state galvanic cell based on Eqn. 6a. Since both Fe and Cr_2O_3 exist as end-member phases in the cell, the activity of chromite is a function of the oxygen fugacity and the equilibrium constant at each temperature. They found no temperature dependence for the mixing properties of spinel and the activity of $FeCr_2O_4$ from their study presented in Fig. 6 is an extrapolation of their data to 1300°C. Both data sets imply small negative deviations from ideality with the data of HINO et al. (1994) displaying greater deviations (recalculated using our ΔG^{o}_{6} to $W_{(Fe,Mg)Cr_2O_4}$=–5.14±2.22 kJ/mol) than those of Jacob and Iyengar (1999) (recalculated $W_{(Fe,Mg)Cr_2O_4}$=–1.96±0.09 kJ/mol). We conclude based on our own data and those from the literature that the absolute value of $W_{(Fe,Mg)Cr_2O_4}$ is not more than a few kilojoules and that spinels in the $(Fe,Mg)Cr_2O_4$ system are essentially ideal at 1300°C.

Chromite and picrochromite are two end-member spinels with a common trivalent cation, Cr^{3+}. Both spinels are completely normal even at high temperature due to a very large octahedral site preference energy for Cr^{3+} (–158 kJ, Dunitz and Orgel, 1957) compared to those of Mg^{2+} and Fe^{2+} (~-17 kJ), leading to exclusive occupation of the octahedral sites by Cr^{3+}. In the absence of redox reactions, a large size mismatch between cations on the same site, or substitution of cations on multiple crystallographically distinct sites, the thermodynamic behavior of $(Fe,Mg)Cr_2O_4$ is influenced primarily by simple mixing of divalent cations on the tetrahedral site. The free energy of mixing in such simple spinel systems has been shown previously to approximate closely statistically ideal mixing (O'Neill and Navrotsky, 1984). Essentially ideal behavior or slightly positive deviations from ideality such as that we and others have observed for $FeCr_2O_4$-$MgCr_2O_4$ solid solutions is also typical of other systems such as $FeSiO_3$-$MgSiO_3$ (e.g., Nafziger, 1973) where changes in composition involve only mixing of Fe^{2+} and Mg^{2+} on one site.

An alternative approach to calculating the activity of $FeCr_2O_4$ in $Fe_XMg_{1-X}Cr_2O_4$ solutions is based on the equilibrium between the spinel of interest and the Pt alloy (Eqn. 1a): that is, a_{Cr}^{PtFeCr} is not assumed to be fixed by f_{O_2} and the presence of Cr_2O_3 in the equilibrium assemblage; it is instead calculated from the measured X_{Cr}^{PtFeCr} and our activity-composition model (Eqn. 4b and the parameters listed in Table 4) for ternary alloys. The activity of $FeCr_2O_4$ in the three binary spinels in each experiment is then calculated according to Eqn. 1c using the above determined ΔG_1^o. Activities of chromite in $(Fe,Mg)Cr_2O_4$ calculated in this way and associated uncertainties (14-20%) obtained through propagation of errors on temperature, f_{O_2}, and alloy composition, are given in Table 3. Note that uncertainties on $a_{FeCr_2O_4}^{(Fe,Mg)Cr_2O_4}$ calculated using this approach are much

larger than activities calculated via Eqn. 6a due to relatively large uncertainties in a_{Cr}^{PtFeCr}; nevertheless, the approach of using Eqn. 1a is very valuable in that it does not require the presence of Cr_2O_3, and thus extends the range of conditions under which spinel activities can be determined using our techniques. Figure 7 compares $a_{FeCr_2O_4}^{(Fe,Mg)Cr_2O_4}$ values calculated by the two methods. Differences in $a_{FeCr_2O_4}^{(Fe,Mg)Cr_2O_4}$ determined with these two methods are in all cases less than 30% and average 12%, relative to the values obtained using reaction 6a, and all determinations agree within 2σ. We conclude that Eqn. 1a provides a viable method for obtaining chromite activities where end-member Cr_2O_3 is not stable, and in Part II we demonstrate the use of this approach for natural spinels in ordinary chondrites.

6. CONCLUSIONS

The experimental technique developed in this study provides a method for obtaining chromite activities in multicomponent spinels by equilibrating the spinel of interest with Pt-alloy at a known temperature and oxygen fugacity. Given the temperature and f_{O_2} of the experiment, and free energy of formation of chromite from the elements, the activity of chromite in any given spinel can be determined if the activities of Fe and Cr in the Pt-alloy are known. The activity-composition relationships in the ternary Pt-Fe-Cr system, modeled as a four-suffix asymmetric regular solution, were constrained by combining interaction parameters for the three bounding binaries with three ternary interaction parameters. The Pt-Cr binary is characterized by an asymmetric regular solution with three binary interaction parameters of W_{PtCr}=–129.1±1.2 kJ/mol, W_{CrPt}=–80.9±4.4 kJ/mol, and D_{PtCr}=+94.4±2.5 kJ/mol (1σ). Combining the thermodynamic properties of the Pt-Cr system with those of Pt-Fe (Kessel et al., 2001)

and Fe-Cr (Andersson and Sundman, 1987), the ternary interaction parameters were found to be C_{Cr}=0, C_{Pt}=+115.7 kJ/mol, and C_{Fe}=–68.6 kJ/mol.

The activities of Fe and Cr in a set of Pt-alloys equilibrated with $FeCr_2O_4$ and Cr_2O_3 were calculated using the ternary Pt-Fe-Cr model and the free energy of formation of chromite from the elements was found to be –923.5±2.1 kJ/mol (1σ). The free energy of formation of chromite from $Fe+Cr_2O_3+O_2$ was found to be –202.7±0.4 kJ/mol (1σ). These values are in excellent agreement with literature, providing a measure of the internal consistency of our ternary alloy model. The activities of chromite in $(Fe,Mg)Cr_2O_4$ are compatible with a one-site symmetric regular solution yields an interaction parameter of +2.14±0.62 kJ/mol (1σ) similar within errors to literature evaluation. The experimental method developed above provides a method for obtaining chromite activities in multicomponent spinels.

Acknowledgements. This work was supported by NASA grant NAG–10423. Discussions with Mike Baker and a written communication with Joe Goldstein led to significant improvements in the quality of this study. Ma Chi is thanked for his help with the analytical work.

REFERENCES

Andersson J. O. and Sundman B. (1987) Thermodynamic properties of the Cr-Fe system. *CALPHAD* 11, 83-92.

Arai S. (1987) An estimation of the least depleted spinel peridotite on the basis of olivine-spinel mantle array. *Neues Jahrb. Mineral. Mh.* 1987, 347-357.

Armstrong J. T. (1988) Quantitative analysis of silicate and oxide materials: Comparison of Monte Carlo, ZAF, and $\phi(\rho Z)$ procedures. In *MicroBeam Analysis* (ed. D. E. Newbury), pp. 239-246. San Francisco Press, Inc.

Berger D. and Schwartz K. (1978) Zur Fremddiffusion in Platin. *Neue Huette* 23, 210-212.

Buddington A. F. and Lindsley D. H. (1964) Iron-titanium oxide minerals and synthetic equivalents. *Journal of Petrology* 5, 310-357.

Carmichael I. S. E. (1967) The iron-titanium oxides of salic volcanic rocks and their associated ferromagnesian silicates. *Contributions to Mineralogy and Petrology* 14, 36-64.

Dick H. J. B. and Bullen T. (1984) Chromian spinel as a petrogenetic indicator in abyssal and alpine-type peridotites and spatially associated lavas. *Contributions to Mineralogy and Petrology* 86, 54-76.

Dieckmann R. (1982) Defects and cation diffusion in magnetite (IV): Nonstoichiometry and point defect structure of magnetite ($Fe_{3-\delta}O_4$). *Berichte der Bunsen Gesellschaft für Physikalische Chemie* 86, 112-118.

Dunitz J. and Orgel L. (1957) Electronic properties of transition metal oxides II. *Journal of the Physical and Chemistry of Solids* 3, 318-323.

El Goresy A. (1976) Oxide minerals in lunar rocks. In *Oxide Minerals*, Vol. 3 (ed. D. Rumble). Southern Printing Company.

Evans B. W. and Frost B. R. (1975) Chrome-spinel in progressive metamorphism - a preliminary analysis. *Geochimica et Cosmochimica Acta* 39, 959-972.

Garbers-Craig A. M. and Dippenar R. J. (1997) Thermodynamic properties of solid Pt-Mn, Pt-Cr, and Pt-Mn-Cr alloys at 1500°C. *Metallurgical and Material Transactions* 28B, 547-552.

Grant J. A. and Frost B. R. (1990) Contact metamorphism and partial melting of pelitic rocks in the aureole of the Laramie anorthosite complex Morton Pass, Wyoming. *American Journal of Science* 290, 425-472.

Grover J. (1976) Chemical mixing in multicomponent solutions: An introduction to the use of Margules and other thermodynamic excess functions to represent non-ideal behaviour. In *Thermodynamics in Geology* (ed. D. G. Fraser), pp. 410. D. Reidel Publishing Company.

Haggerty S. E. (1972) Solid solution, subsolidus reduction and compositional characteristics of spinels in some Apollo 15 basalts. *Meteoritics* 7, 353-370.

Hildebrand J. H. (1929) Solubility XII, Regular solutions. *Journal of American Chemical Society* 51, 66-80.

Hino M., Higuchi K-I., Nagasaka T., and Ban-ya S. (1994) Phase equilibria and activities of the constituents in $FeO{\cdot}Cr_2O_3$-$MgO{\cdot}Cr_2O_3$ spinel structure solid solution saturated with Cr_2O_3. *ISIJ International* 34, 739-745.

Holzheid A. and O'Neill H. S. C. (1995) The Cr-Cr_2O_3 oxygen buffer and the free energy of formation of Cr_2O_3 from high-temperature electrochemical measurements. *Geochimica et Cosmochimica Acta* 59, 475-479.

Jacob K. T. and Alcock C. B. (1975) The oxygen potential of the systems Fe+$FeCr_2O_4$-Cr_2O_3 and Fe+FeV_2O_4+V_2O_3 in the temperature range 750-1600°C. *Metallurgical Transactions* 6B, 215-221.

Jacob K. T. and Iyengar G. N. K. (1999) Thermodynamics and phase equilibria involving the spinel solid solution $Fe_xMg_{1-x}Cr_2O_4$. *Metallurgical and Materials Transactions B* 30, 865-871.

Jamieson H. E., Roeder P. L., and Grant A. H. (1992) Olivine-pyroxene-PtFe alloy as an oxygen geobarometer. *Journal of Geology* 100, 138-145.

Katsura T., Wakihara M., Hara S., and Sugihara T. (1975) Some thermodynamic properties in spinel solid solutions with the Fe_3O_4 component. *Journal of Solid State Chemistry* 13, 107-113.

Kessel R., Beckett J. R., and Stolper E. M. (2001) Thermodynamic properties of the Pt-Fe system. *American Mineralogist*. 86, 1003-1014.

Kofstad P. (1983) *Nonstoichiometry, Diffusion, and Electrical Conductivity in Binary Metal Oxides*. Robert E. Krieger Publishing company.

Mason T. O. and Bowen H. K. (1981) Electric conduction and thermopower of magnetite and iron-aluminate spinels. *Journal of American Ceramic Society* 64, 237-242.

Mattioli G. S., Wood B. J., and Carmichael I. S. E. (1987) Ternary-spinel volume in the system $MgAl_2O_4$-Fe_3O_4-$\gamma Fe_{3/8}O_4$: Implications for the effect of P on intrinsic f_{O2} measurements of mantle-xenolith spinels. *American Mineralogist* 72, 468-480.

Nafziger R. H. (1973) High-temperature activity-composition relations of equilibrium spinels, olivines, and pyroxenes in the system Mg-Fe-O-SiO_2. *American Mineralogist* 58, 457-465.

Nell J. and Wood B. J. (1989) Thermodynamic properties in a multicomponent solid solution involving cation disorder: Fe_3O_4-$MgFe_2O_4$-$MgAl_2O_4$ spinels. *American Mineralogist* 74, 1000-1015.

Nell J., Wood B. J., and Mason T. O. (1989) High-temperature cation distributions in Fe_3O_4-$MgAl_2O_4$-$MgFe_2O_4$-$FeAl_2O_4$ spinels from thermopower and conductivity measurements. *American Mineralogist* 74, 339-351.

O'Neill H. St. C. and Dollase W. A. (1994) Crystal structure and cation distributions in simple spinels from powder XRD structural refinements: $MgCr_2O_4$, $ZnCr_2O_4$, Fe_3O_4 and the temperature dependence of the cation distribution in $ZnAl_2O_4$. *Journal of Physics and Chemistry of Minerals* 20, 541-555.

O'Neill H. St. C. and Navrotsky A. (1984) Cation distributions and thermodynamic properties of binary spinel solid solutions. *American Mineralogist* 69, 733-753.

O'Neill H. St. C. and Wall V. J. (1987) The olivine-orthopyroxene-spinel oxygen geobarometer, the nickel precipitation curve, and the oxygen fugacity of the earth's mantle. *Journal of Petrology* 28, 1169-1191.

Petric A. and Jacob K. T. (1982) Thermodynamic properties of Fe_3O_4-FeV_2O_4 and Fe_3O_4-$FeCr_2O_4$ spinel solid solutions. *Journal of the American Ceramic Society* 65, 117-122.

Pretorius E. B. and Muan A. (1992) Activity-composition relations in platinum-chromium and platinum-vanadium alloys at 1500°C. *Journal of the American Ceramic Society* 75, 1361-1363.

Sack R. O. (1982) Spinels as petrogenetic indicators: Activity-composition relations at low pressures. *Contribution to Mineralogy and Petrology* 79, 169-180.

Sack R. O. and Ghiorso M. S. (1991a) Chromium spinels as petrogenetic indicators: thermodynamics and petrological applications. *American Mineralogist* 76, 827-847.

Sack R. O. and Ghiorso M. S. (1991b) An internally consistent model for the thermodynamic properties of Fe-Mg titanomagnetite-aluminate spinels. *Contribution to Mineralogy and Petrology* 106, 474-505.

Saxena S. K. (1973) Thermodynamics of rock-forming crystalline solid solutions. In *Minerals, Rocks and Inorganic Materials*, Vol. 8 (ed. S. K. Saxena), pp. 188. Springer.

Schwerdtfeger K. and Muan A. (1965) Activity measurements in Pt-Cr and Pd-Cr solid alloys at 1225°C. *Transactions of the Metallurgical Society of AIME* 233, 1904-1906.

Topfer J., Aggarwal S., and Dieckmann R. (1995) Point defect and cation tracer diffusion in $(Cr_xFe_{1-x})_{3-\delta}O_4$ spinels. *Solid State Ionics* 81, 251-266.

Wohl K. (1946) Thermodynamic evaluation of binary and ternary liquid systems. *Transactions of the American Institute of Chemical Engineers* 42, 215-249.

Wohl K. (1953) Thermodynamic evaluation of binary and ternary liquid systems. *Chemical Engineering Progress* 49, 218-219.

Woodland A. B. and Wood B. J. (1994) Fe_3O_4 activities in Fe-Ti spinel solid solutions. *European Journal of Mineralogy* 6, 23-37.

Table 1. Experimental conditions and results for Pt/Cr+Cr_2O_3 at 1300°C

Run	$\log_{10} f_{O_2}$ (atm)	Time (hr)	N[a]	X_{Cr}^{PtCr}[b]	$\ln \gamma_{Cr}^{PtCr}$[c]
RK281	-11.63	402	10	0.2386(29)[d]	-6.06(9)
RK191	-11.36	212.5	3	0.2130(23)	-6.41(9)
RK150	-11.07	284	7	0.1943(10)	-6.82(9)
RK135	-10.83	214	6	0.1639(12)	-7.06(9)
RK291	-10.68	236	3	0.1570(20)	-7.29(9)
RK255	-10.61	313	5	0.1610(16)	-7.42(9)
RK212	-10.17	211	5	0.1309(28)	-7.98(9)
RK286	-9.83	256	5	0.1040(14)	-8.34(9)
RK248	-9.67	216	10	0.0936(35)	-8.50(10)
RK137	-9.50	191	3	0.0799(6)	-8.64(9)
RK156	-9.25	189.5	3	0.0689(9)	-8.94(9)
RK267	-9.22	309.5	5	0.0679(8)	-8.97(9)
RK218	-8.73	330	10	0.0433(22)	-9.36(10)
RK296	-8.69	221.5	3	0.0396(3)	-9.34(9)
RK180	-7.90	188	4	0.0131(3)	-9.60(9)

[a]N=Number of analyses.

[b] X_i^j = mole fraction of *i* in *j*.

[c] γ_i^j = activity coefficient of *i* in *j*.

[d]Numbers enclosed in parentheses indicate one standard deviation of the mean calculated by error propagation.

Table 2. Experimental conditions and results for $Pt/Fe+FeCr_2O_4+Cr_2O_3$ at 1300°C

Run[a]	$\log_{10} f_{O_2}$	Time	X_{Cr}^{PtFeCr}[b]	X_{Fe}^{PtFeCr}	X_{Fe}^{PtFeCr}	$\ln\gamma_{Cr}^{PtFeCr}$[c]	$\ln\gamma_{Cr}^{PtFeCr}$	$\ln\gamma_{Fe}^{PtFeCr}$	ΔG_6^{o}[e]	ΔG_1^{o}[f]
	(atm)	(hr)		(initial)	(final)	(observed)	(model)	(model)	(kJ/mol)	(kJ/mol)
RK280-43	-11.63	402	0.00462(5)[d]	0.539	0.527(3)	-2.12(9)	-2.08(3)	-1.47(2)	-202.6(8)	-922.8(3.5)
RK190-38	-11.36	212.5	0.00427(14)	0.477	0.499(3)	-2.50(10)	-2.41(3)	-1.70(3)	-202.4(9)	-921.3(3.6)
RK274-43	-11.20	431	0.00388(8)	0.447	0.483(4)	-2.68(9)	-2.60(5)	-1.85(4)	-202.4(9)	-921.8(3.7)
RK205-28	-11.07	190	0.00347(3)	0.524	0.467(3)	-2.79(9)	-2.81(4)	-2.00(3)	-202.8(9)	-924.4(3.5)
RK134-10	-10.83	214	0.00299(12)	0.472	0.445(3)	-3.05(10)	-3.09(4)	-2.22(2)	-202.8(9)	-924.9(3.7)
RK134-21	-10.83	214	0.00298(6)	0.539	0.444(9)	-3.05(9)	-3.11(12)	-2.24(6)	-203.1(1.1)	-925.8(4.5)
RK199-38	-10.73	189.5	0.00285(11)	0.400	0.435(4)	-3.19(10)	-3.22(5)	-2.33(6)	-202.9(1.1)	-924.9(3.8)
RK290-28	-10.68	236	0.00244(4)	0.524	0.431(1)	-3.12(9)	-3.27(2)	-2.37(3)	-202.8(9)	-928.0(3.4)
RK254-44	-10.61	313	0.00274(4)	0.371	0.428(6)	-3.35(9)	-3.31(7)	-2.40(5)	-202.3(1.0)	-922.4(3.9)
RK211-30	-10.17	211	0.00209(8)	0.400	0.389(2)	-3.85(10)	-3.85(3)	-2.87(4)	-203.0(1.0)	-924.4(3.6)
RK237-33	-10.00	642.5	0.00213(21)	0.359	0.376(2)	-4.16(13)	-4.03(4)	-3.02(5)	-202.8(1.0)	-920.6(4.3)
RK285-33	-9.83	256	0.00150(4)	0.359	0.369(2)	-4.10(9)	-4.14(3)	-3.12(4)	-201.9(1.0)	-924.2(3.6)
RK247-30	-9.67	216	0.00143(3)	0.400	0.352(2)	-4.32(9)	-4.37(3)	-3.34(5)	-203.0(1.1)	-925.7(3.6)
RK136-9	-9.50	191	0.00127(5)	0.361	0.343(4)	-4.49(10)	-4.51(5)	-3.47(7)	-202.5(1.3)	-924.3(3.9)
RK136-10	-9.50	191	0.00135(7)	0.472	0.342(2)	-4.56(11)	-4.52(4)		-202.7(9)	-923.1(3.8)
RK136-11	-9.50	191	0.00133(8)	0.275	0.343(2)	-4.54(11)	-4.51(3)	-3.47(3)	-202.5(9)	-923.0(3.8)
RK266-33	-9.22	309.5	0.00107(7)	0.359	0.321(1)	-4.82(11)	-4.83(2)	-3.78(2)	-203.1(9)	-924.7(3.8)
RK232-39	-9.01	644	0.00111(3)	0.352	0.309(2)	-5.21(10)	-5.01(3)	-3.96(3)	-202.9(9)	-918.9(3.6)
RK295-11	-8.69	221.5	0.00070(3)	0.275	0.293(3)	-5.31(10)	-5.25(4)	-4.20(10)	-201.9(1.6)	-921.5(3.9)

[a]RKx-y: experiment #x with initial Pt-Fe alloy #y, y refers to the run in Kessel et al. (2001) in which the initial alloy was produced.

[b] X_i^j=mole fraction of i in j based on three analyses for Cr and five for Fe.

[c] γ_i^j= activity coefficient of i in j, model values calculated based on f_{O_2}, final X_{Fe}^{PtFeCr}, and $\Delta G^{o}_{f,\,Cr_2O_3}$ from Holzheid and O'Neill (1995).

[d]Numbers enclosed in parentheses indicate one standard deviation of the mean calculated by error propagation.

[e] ΔG_i^o=free energy of formation of chromite for reaction i.

[f]Calculated directly from Eqn. 1.

Table 3. Experimental conditions and results for Pt/Fe+(Fe,Mg)Cr_2O_4+Cr_2O_3 at 1300°C

Run[a]	$\log_{10} f_{O_2}$	Time	$X^{(Fe,Mg)Cr_2O_4}_{FeCr_2O_4}$	X^{PtFeCr}_{Cr}[b]	X^{PtFeCr}_{Fe}	X^{PtFeCr}_{Fe}	$\ln\gamma^{PtFeCr}_{Cr}$[c]	$\ln\gamma^{PtFeCr}_{Cr}$	$\ln\gamma^{PtFeCr}_{Fe}$	$a^{(Fe,Mg)Cr_2O_4}_{FeCr_2O_4}$[c]	$a^{(Fe,Mg)Cr_2O_4}_{FeCr_2O_4}$
	(atm)	(hr)			(initial)	(final)	(observed)	(model)	(model)	(6a)	(1a)
RK147-9	-11.07	284	0.13	0.02395(25)[d]	0.361	0.312(3)	-4.72(9)	-4.60(4)	-3.58(2)	0.14(1)	0.17(3)
RK147-11	-11.07	284	0.13	0.02571(70)	0.275	0.307(2)	-4.80(9)	-4.64(3)	-3.62(2)	0.13(1)	0.17(3)
RK148-9	-11.07	284	0.46	0.00772(3)	0.361	0.398(1)	-3.59(9)	-3.65(2)	-2.69(2)	0.43(3)	0.37(5)
RK148-11	-11.07	284	0.46	0.00748(12)	0.275	0.403(1)	-3.56(9)	-3.58(2)	-2.63(2)	0.46(3)	0.43(6)
RK148-13	-11.07	284	0.46	0.00720(4)	0.220	0.405(2)	-3.52(9)	-3.56(3)	-2.61(1)	0.47(3)	0.42(6)
RK149-9	-11.07	284	0.83	0.00423(5)	0.361	0.455(4)	-2.99(9)	-2.94(5)	-2.11(3)	0.87(6)	0.92(16)
RK149-11	-11.07	284	0.83	0.00424(1)	0.275	0.451(3)	-2.99(9)	-3.00(3)	-2.15(2)	0.82(5)	0.79(12)
RK149-13	-11.07	284	0.83	0.00432(4)	0.220	0.452(6)	-3.01(9)	-2.98(7)	-2.14(4)	0.83(6)	0.85(17)
RK282-13	-9.83	256	0.13	0.00292(1)	0.220	0.321(1)	-5.41(9)	-5.55(2)	-4.53(3)	0.19(1)	0.14(2)
RK282-44	-9.83	256	0.13	0.00252(7)	0.371	0.329(2)	-5.41(9)	-5.57(2)	-4.56(2)	0.18(1)	0.13(2)
RK283-13	-9.83	256	0.46	0.00180(4)	0.220	0.356(2)	-4.77(9)	-4.80(2)	-3.75(2)	0.49(3)	0.45(6)
RK283-44	-9.83	256	0.46	0.00179(4)	0.371	0.357(2)	-4.62(9)	-4.69(4)	-3.65(3)	0.56(4)	0.47(8)
RK284-13	-9.83	256	0.83	0.00345(10)	0.220	0.215(2)	-4.28(9)	-4.31(3)	-3.28(3)	0.88(6)	0.81(13)
RK284-44	-9.83	256	0.83	0.00407(6)	0.371	0.206(1)	-4.27(9)	-4.29(2)	-3.27(3)	0.89(6)	0.83(13)
RK292-11	-8.69	221.5	0.13	0.00310(3)	0.275	0.197(2)	-6.79(9)	-6.69(3)	-5.84(3)	0.14(1)	0.17(3)
RK292-36	-8.69	221.5	0.13	0.00309(10)	0.211	0.194(2)	-6.79(10)	-6.72(3)	-5.89(4)	0.13(1)	0.15(2)
RK293-11	-8.69	221.5	0.46	0.00123(3)	0.275	0.255(1)	-5.87(9)	-5.82(2)	-4.82(3)	0.50(3)	0.53(8)
RK293-36	-8.69	221.5	0.46	0.00122(6)	0.352	0.253(1)	-5.86(10)	-5.84(2)	-4.84(4)	0.49(3)	0.49(9)
RK294-11	-8.69	221.5	0.83	0.00077(2)	0.275	0.283(2)	-5.41(9)	-5.39(3)	-4.36(4)	0.88(6)	0.88(14)

[a]RKx-y: experiment # x with initial Pt-Fe alloy #y; y refers to the run in Kessel et al. (2001) in which the initial alloy was produced.

[b] X_i^j =mole fraction of *i* in *j* based on three analyses for Cr and five for Fe.

[c] γ_i^j = activity coefficient of *i* in *j*, model values calculated based on f_{O_2}, final X_{Fe}^{PtFeCr}, and $\Delta G^{o}_{f,\,Cr_2O_3}$ from Holzheid and O'Neill (1995).

[d]Numbers enclosed in parentheses indicate one standard deviation of the mean calculated by error propagation.

[e] $a_{FeCr_2O_4}^{(Fe,Mg)Cr_2O_4}$ =Activity of chromite as calculated from reaction 6a or 1a.

Table 4. Recommended values of thermodynamic parameters

Interaction parameter[a]	Value (kJ/mol)	1σ	Source[e]
	Alloys		
W_{PtFe}	-138.0	3.3	1
W_{FePt}	-90.8	23.9	1
D_{PtFe}	0.0		1
W_{PtCr}	-129.1	1.2	2
W_{CrPt}	-80.9	4.4	2
D_{PtCr}	+94.4	2.5	2
W_{CrFe}	+5.3		3
W_{FeCr}	+15.0		3
D_{FeCr}	0.0		3
C_{Cr}	0.0		2
C_{Pt}	+115.7		2
C_{Fe}	-68.6		2
	Oxides		
ΔG_1°[b]	–923.5	2.1	2
ΔG_1°[c]	–924.0	0.4	2+4
ΔG_6°	–202.7	0.4	2
$W_{(Fe,Mg)Cr_2O_4}$[d]	+2.14	0.62	2

[a] W_{ij}, W_{ji}, and D_{ij} are binary interaction parameters for the system *i-j* (c.f. Eqn. 2) and C_k are ternary interaction parameters for the system Pt-Fe-Cr.

[b] ΔG_i°=free energy of formation of chromite from reaction *i* calculated directly (Eqn. 1).

[c] ΔG_i°=free energy of formation of chromite from reaction *i* calculated (Eqn. 6).

[d] $W_{(Fe,Mg)Cr_2O_4}$=interaction parameter for the chromite-picrochromite spinel binary.

[d] 1=Kessel et al. (2001), 2=this work,
3=Andersson and Sundman (1987), 4=Holzheid and O'Neill (1995).

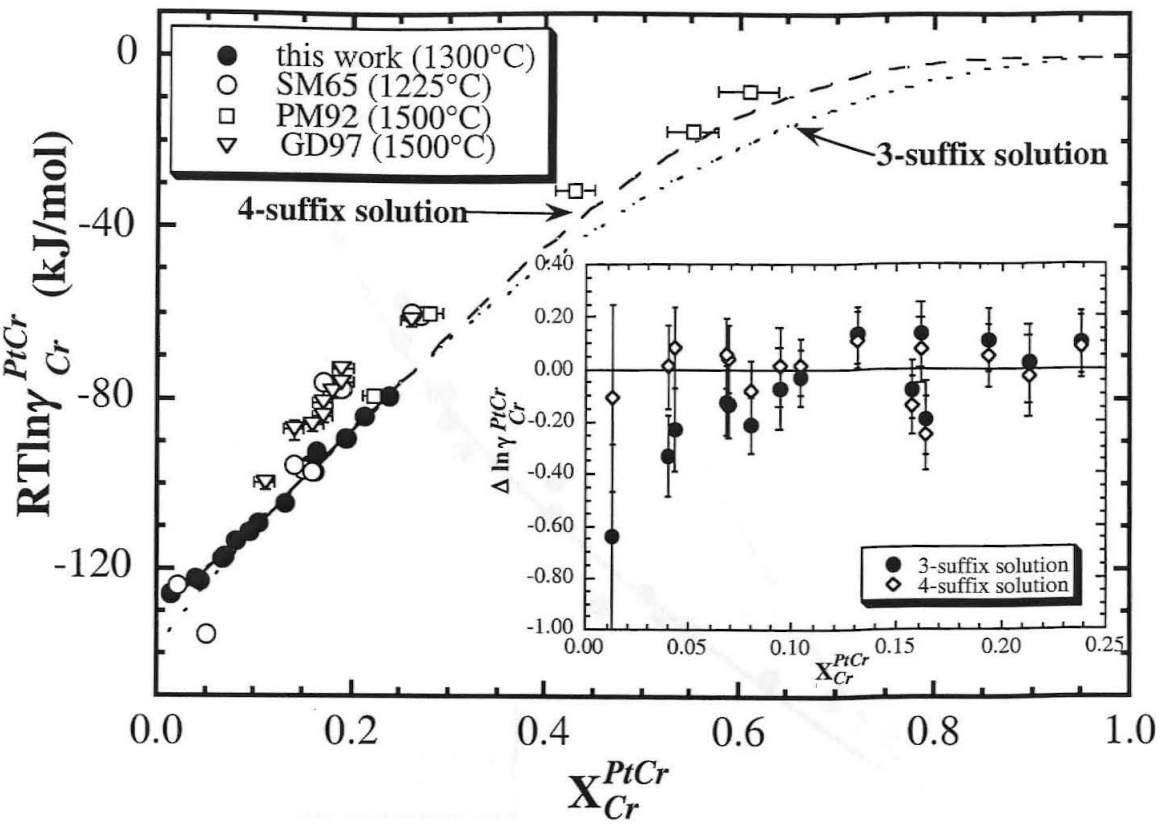

Figure 1. Values of $RT\ln\gamma_{Cr}^{PtCr}$ vs. X_{Cr}^{PtCr} in the Pt-Cr system. The best fits to our data assuming four-suffix (solid curve, dashed where extended beyond our data) and three-suffix (dotted curve) asymmetric subregular solution behavior are shown. Literature data are from Schwedtfeger and Muan (1965)–SM65; Pretorius and Muan (1992)–PM92, and Garbers-Craig and Dippenar (1997)–GD97. Uncertainties (1σ) for both Pretorius and Muan (1992) and and Garbers-Craig and Dippenar (1997) were calculated by propagating reported uncertainties on alloy composition given by Garbers-Craig and Dippenar (1997). The inset shows deviations of our data from best fits to three-suffix and four-suffix subregular solution models relative to the modeled $\ln\gamma_{Cr}^{PtCr}$ as a function of alloy composition.

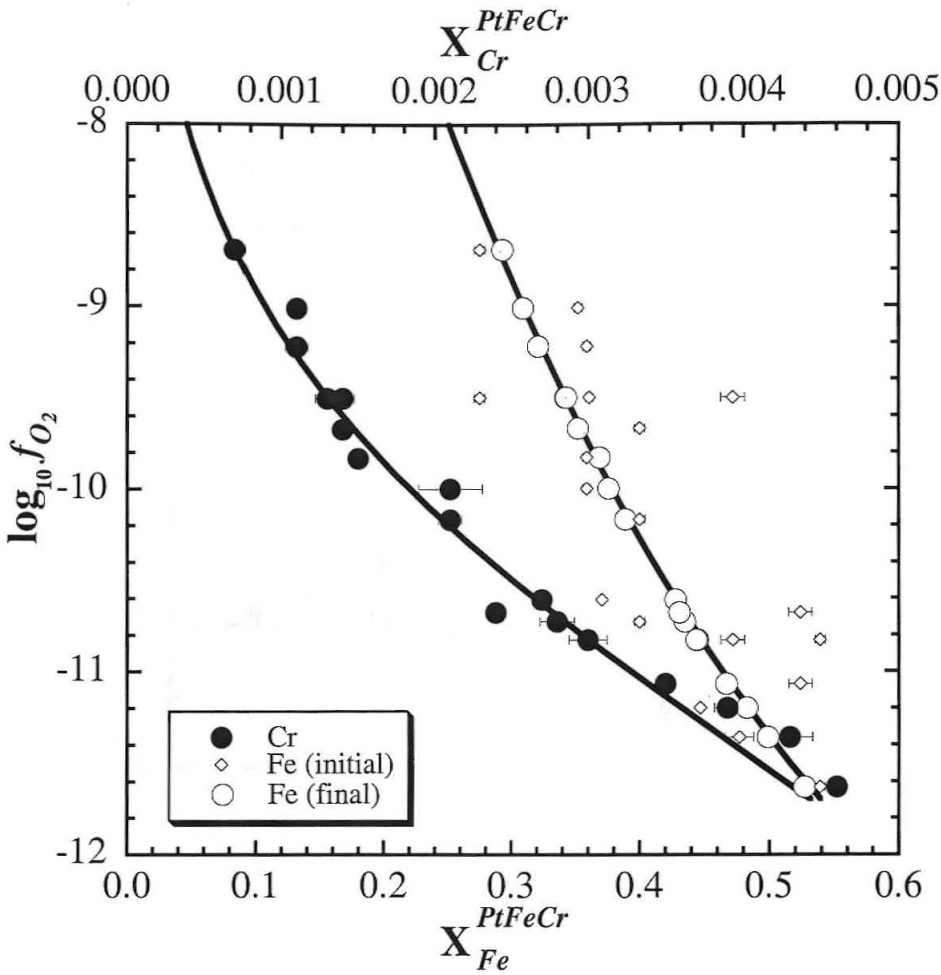

Figure 2. X_{Fe}^{PtFeCr} (plotted along the lower x-axis) and X_{Cr}^{PtFeCr} (plotted along the upper x-axis) vs. $\log_{10} f_{O_2}$ in the Pt-Fe-Cr system for data obtained in this study. Small open diamonds are initial values of X_{Fe}^{PtFeCr} (Cr-free) of Pt-alloys in each pellet in a given experiment, and large circles represent the equilibrium alloy composition. Individual error bars (1σ) are plotted where larger than the symbol size. Also shown are predicted trends of $\log_{10} f_{O_2}$ as a function of X_{Fe}^{PtFeCr} and X_{Cr}^{PtFeCr} using the curve fit of our experimentally derived activities to a four-suffix Margules expansion (see text).

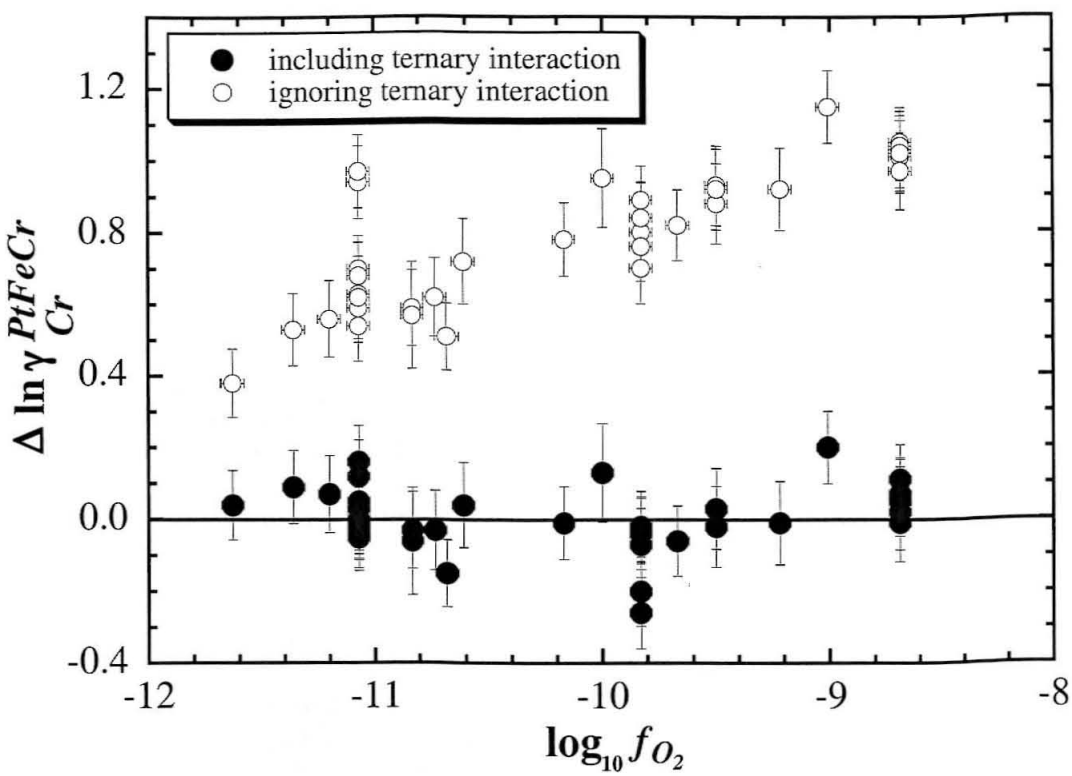

Figure 3. Deviations between model values of $\ln\gamma_{Cr}^{PtFeCr}$ calculated using Eqn. 4b and experimentally observed values calculated via Eqn. 5b as a function of $\log_{10} f_{O_2}$. Filled symbols refer to values that include ternary interactions while open symbols refer to values in which ternary interactions are ignored. Error bars (1σ) are shown.

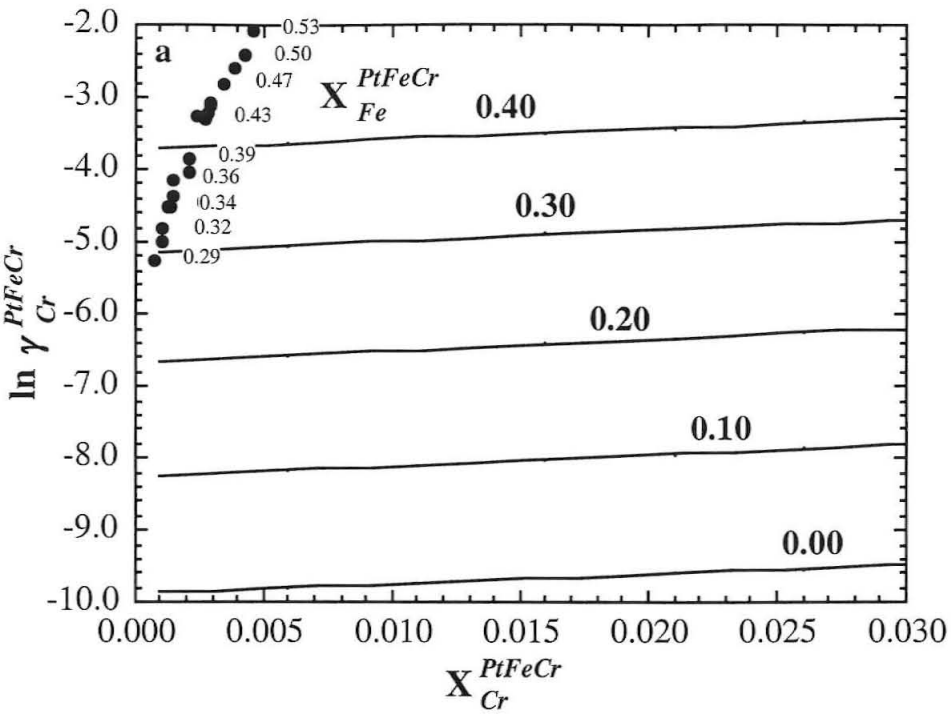
a
X_{Fe}^{PtFeCr}
0.53
0.50
0.47
0.43
0.40
0.39
0.36
0.34
0.32
0.30
0.29
0.20
0.10
0.00
$\ln \gamma_{Cr}^{PtFeCr}$
X_{Cr}^{PtFeCr}

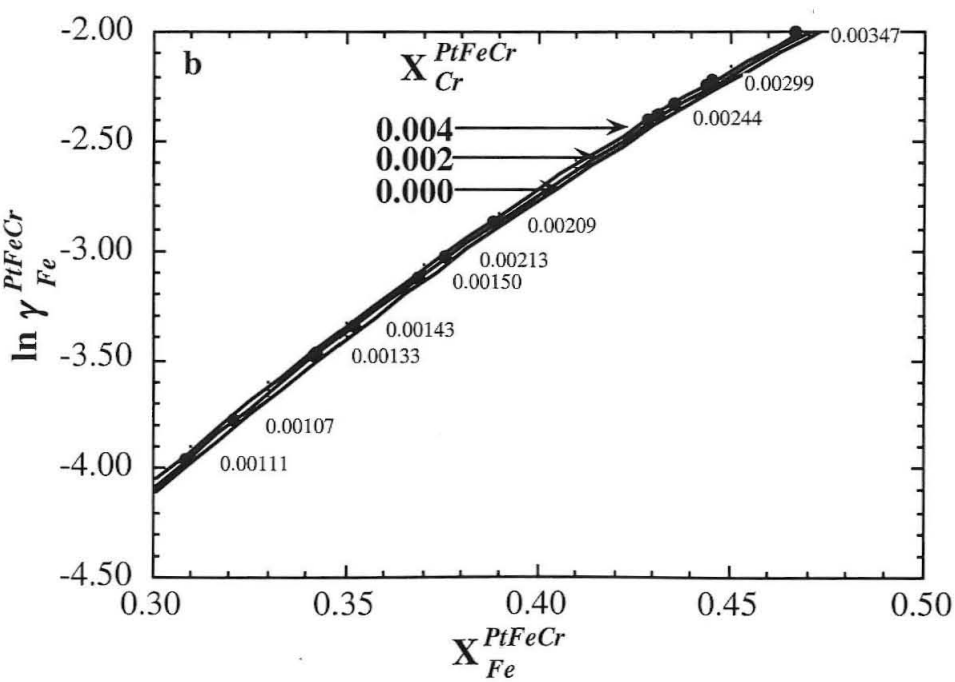
b
X_{Cr}^{PtFeCr}
0.004
0.002
0.000
0.00347
0.00299
0.00244
0.00209
0.00213
0.00150
0.00143
0.00133
0.00107
0.00111
$\ln \gamma_{Fe}^{PtFeCr}$
X_{Fe}^{PtFeCr}

Figure 4. (a) Model values of $\ln\gamma_{Cr}^{PtFeCr}$ as a function of X_{Cr}^{PtFeCr} calculated for various values of X_{Fe}^{PtFeCr}. Solid circles represent the model $\ln\gamma_{Cr}^{PtFeCr}$ values obtained in our experiments from the measured X_{Cr}^{PtFeCr}. Numbers adjacent to the symbols represent the corresponding X_{Fe}^{PtFeCr} values. (b) Model values of $\ln\gamma_{Fe}^{PtFeCr}$ as a function of X_{Fe}^{PtFeCr} calculated for various values of X_{Cr}^{PtFeCr}. Solid circles represent the model $\ln\gamma_{Fe}^{PtFeCr}$ values obtained in our experiments from the measured X_{Fe}^{PtFeCr}. Numbers adjacent to the symbols represent the corresponding X_{Cr}^{PtFeCr} values.

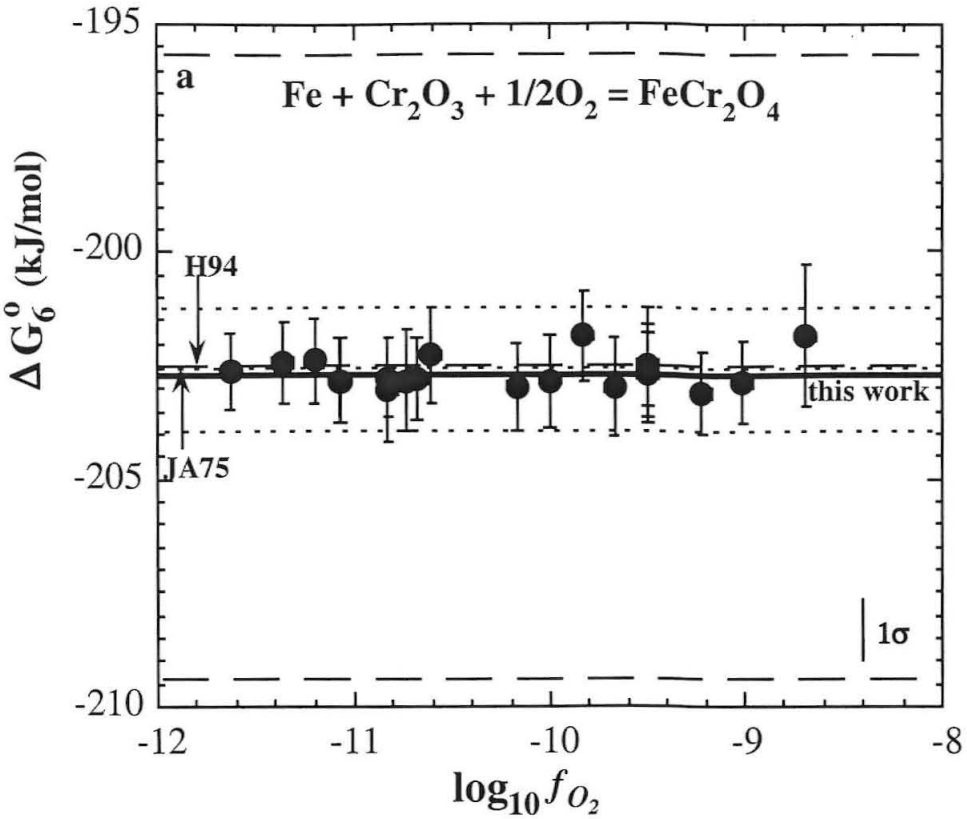
a
Fe + Cr2O3 + 1/2O2 = FeCr2O4
H94
JA75
this work
1σ
ΔG°6 (kJ/mol)
log10 fO2
-195
-200
-205
-210
-12
-11
-10
-9
-8

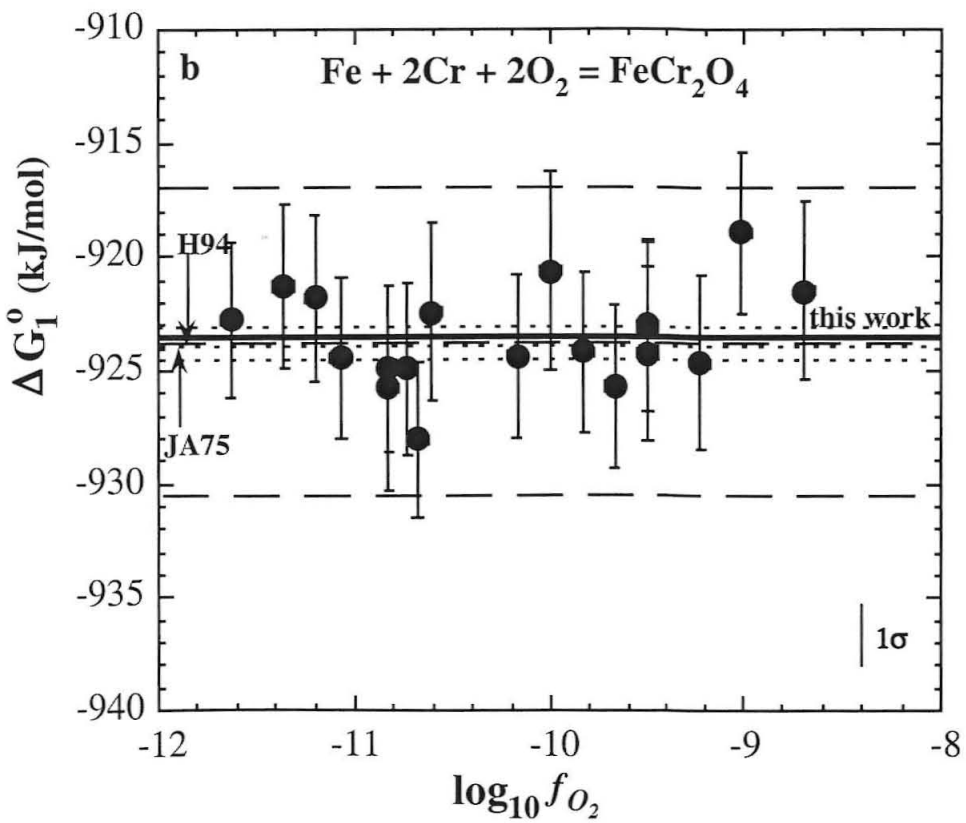
b
Fe + 2Cr + 2O2 = FeCr2O4
H94
JA75
this work
1σ
ΔG°1 (kJ/mol)
log10 fO2
-910
-915
-920
-925
-930
-935
-940
-12
-11
-10
-9
-8

Figure 5. Free energy of formation of $FeCr_2O_4$ at 1300°C as a function of $\log_{10} f_{O_2}$. Error bars (1σ) are shown. (a) Formation of $FeCr_2O_4$ from Cr_2O_3 and Fe and O_2 (Eqn. 6a) calculated using the model values of a_{Fe}^{alloy}. (b) Formation of $FeCr_2O_4$ from the elements (Eqn. 1a) calculated using the model values of a_{Cr}^{alloy} and a_{Fe}^{alloy}. Averages and 1σ bounds for Hino et al. (1994)–H94 and Jacob and Alcock (1975)–JA75 are also shown in both panels (dashed and dotted lines, respectively).

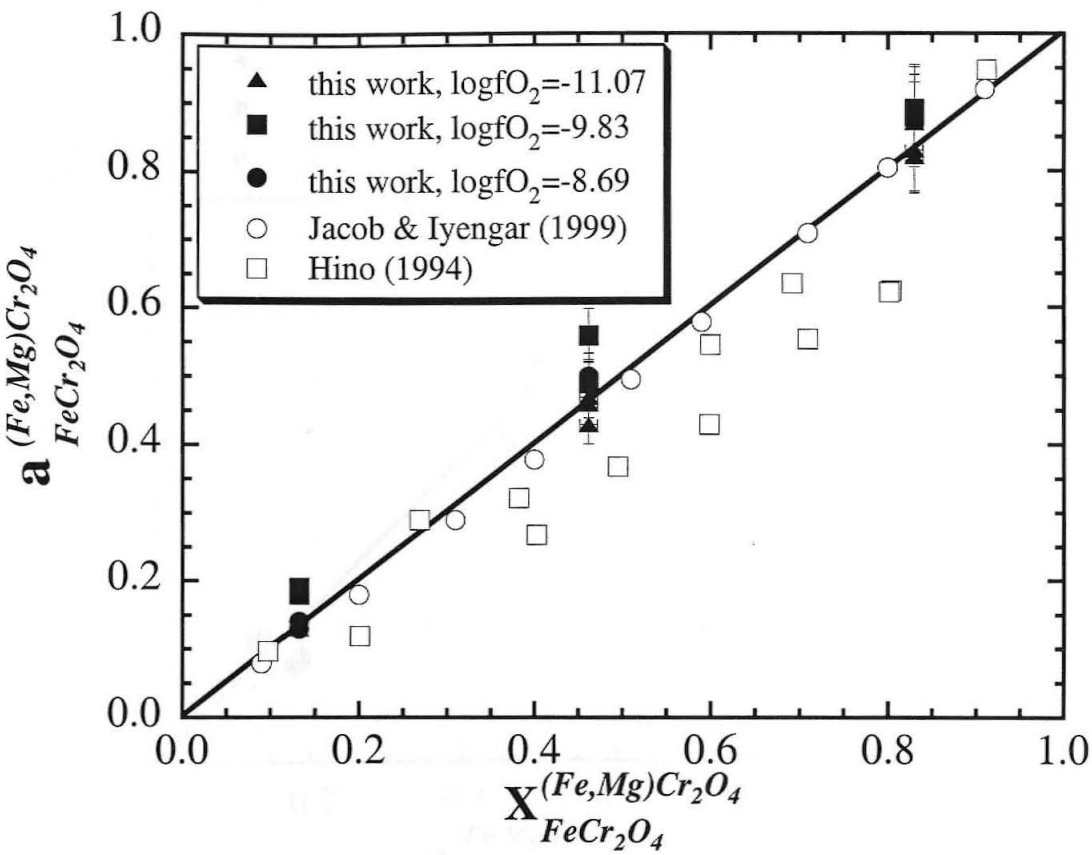

Figure 6. $a_{FeCr_2O_4}^{(Fe,Mg)Cr_2O_4}$ at 1300°C as a function of $X_{FeCr_2O_4}^{(Fe,Mg)Cr_2O_4}$. Activities of chromite were calculated from reaction 6a based on the model a_{Fe}^{alloy}. Also shown are results from Hino et al. (1994) and Jacob and Iyengar (1999). Ideal solution behavior is indicated by the solid line.

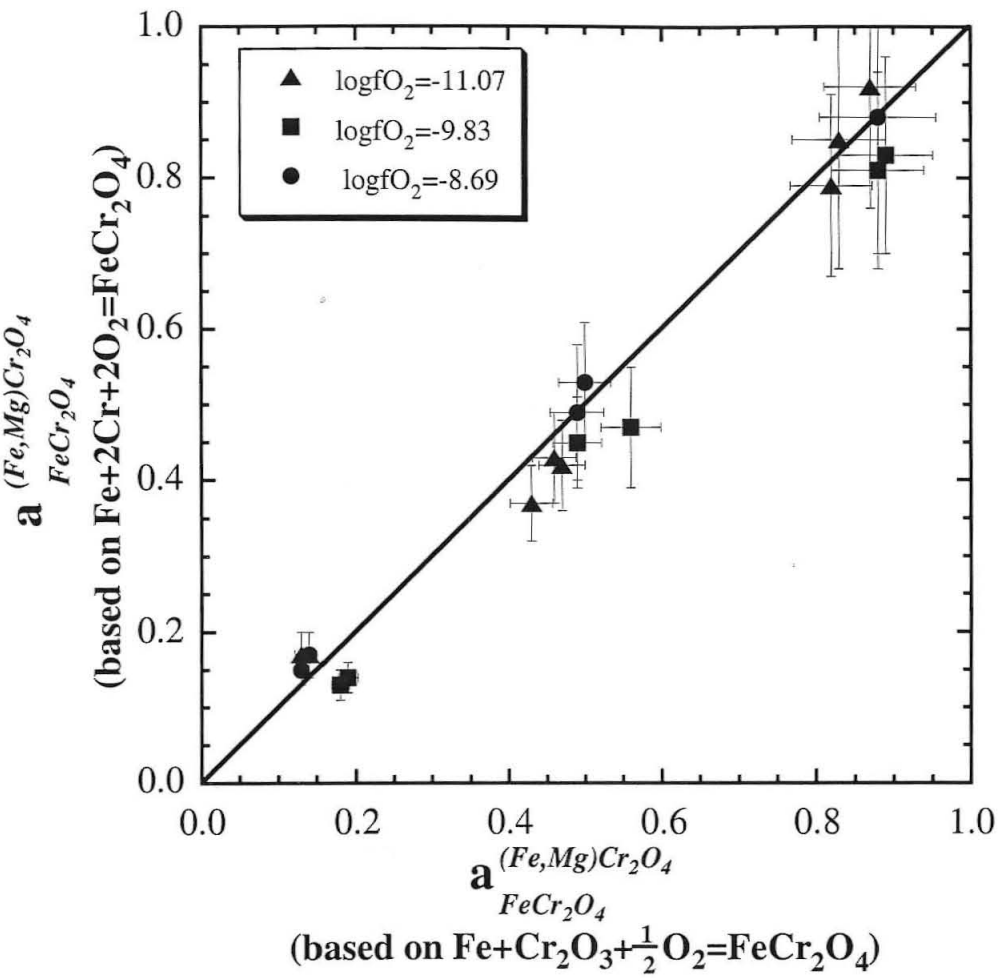

Figure 7. $a_{FeCr_2O_4}^{(Fe,Mg)Cr_2O_4}$ calculated via Eqn. 1a plotted against calculated via Eqn. 6a. Error bars (1σ) are shown.

Chapter 3. The thermal history of equilibrated ordinary chondrites and the relationship between textural maturity and temperature

Abstract—The compositions and textures of phases in equilibrated ordinary chondrites from H, L, and LL groups spanning petrographic types 4 to 6 were studied and used to constrain the thermal histories of the parent bodies. Based on Fe-Mg exchange between olivine and spinel, equilibration temperatures for all equilibrated chondrites are in the range 680-796°C. This is much smaller than the range of peak temperatures commonly assumed for equilibrated ordinary chondrites (600-950°C), especially if olivine-spinel thermometry records retrograde temperatures. Equilibration temperatures for the H chondrites are similar, 778±26°C. Maximum olivine-spinel temperatures recorded in L and LL chondrites are lower than in H chondrites and the type 4 chondrites record significantly lower temperatures than do types 5-6. Our data combined with olivine-spinel equilibration temperatures calculated for other equilibrated ordinary chondrites using mineral compositions from the literature demonstrate that, in general, type 4 chondrites record temperatures that are lower than or equal to those of types 5-6 chondrites. This implies a decoupling of metamorphic temperature from petrographic type and that the classification used to assign a type, which is based on textural maturation and chemical homogeneity is not a direct indication of peak metamorphic temperature.

Flat composition profiles in spinel in contact with olivine grains constrain cooling rates for ~650-800°C to a few degrees per million years. For H chondrites, the closure temperature is a function of the spinel grain size, such that larger grains, abundant in

types 5-6 chondrites, record temperatures of ~800°C while smaller grains, rare in types 5-6 but abundant in type 4 chondrites, record lower temperatures. For L and LL chondrites, we did not observe a well-defined relationship between grain size and olivine-spinel equilibration temperature but the similarity of temperatures for types 5-6 and lower than but overlapping values for type 4 chondrites suggest a similar behavior. Cooling rates of a few degrees per million years are in the range inferred across lower temperatures based on metallographic, fission tracks, and intra-site partitioning in pyroxene. These results suggest similar thermal history at high temperatures for types 5-6 and at least some type 4 chondrites within each chondrite group. The lack of correlation between petrographic type and cooling rate can not be used as an argument in favor of a rubble-pile model because chondrite type and temperature are largely decoupled. By the same token, increasing degree of metamorphism does not necessarily correspond to increasing depth within the parent body.

1. INTRODUCTION

Ordinary chondrites are primitive meteorites showing variable degrees of metamorphism ranging from negligible to intensities sufficient to completely obliterate the original phases. The variation in textural and chemical maturation from rock to rock is reflected in the commonly accepted classification scheme (Sears et al., 1980; Van Schmus and Wood, 1967), which combines a group designation (H, L, LL) based primarily on reduced to oxidized iron in the bulk with a number corresponding to the degree of metamorphism. The "unequilibrated" ordinary chondrites are labeled type 3 and subdivided into 3.0-3.9 with increasing number referring to increasing degree of metamorphism and "equilibrated" ordinary chondrites range in type from 4 to 7. The rare

type 7 chondrites have undergone partial melting but are generally regarded as a special class of impact related or reheated material (e.g., Taylor et al., 1987; Yamaguchi et al., 1998).

A fundamental issue in the study of ordinary chondrites is how the thermal history is related to the textures and chemical homogeneity that are used to define type. At present, there is a general assumption that increasing type corresponds to progressively increasing temperature, especially among the equilibrated chondrites (e.g., Dodd, 1981). Certainly, at the extremes there are substantial differences. Partial melting of type 7 chondrites requires temperatures of ~1000°C or more and geothermometry of type 6 chondrites frequently yields temperatures exceeding 900°C (e.g., Bunch and Olsen, 1974; Ishii et al., 1979; McSween and Patchen, 1989; Saxena, 1976). This contrasts with type 3 chondrites for which metal compositions (Wood, 1967), zoning in matrix olivine (Brearley et al., 1989), and the structural state of carbon aggregates (Brearley, 1990) suggest maximum temperatures not exceeding ~400°C (Wood, 1967; Dodd, 1969). On the other hand, the assertion that there is a systematic increase in peak metamorphic temperature from type 4 to 5 to 6 rests almost entirely on a semi-quantitative interpretation of pyroxene chemistry and feldspar grain size in LL chondrites (Heyse, 1978).

Relative equilibration temperatures among ordinary chondrites find an important resonance in thermal models of the parent bodies (e.g., McSween and Labotka, 1993; Miyamoto et al., 1981; Scott and Rajan, 1981). Two end-member scenarios are envisioned. An onion shell model, which was advocated by Dodd (1969) and Miyamoto et al. (1981) among others, postulates that ordinary chondrites of increasing petrographic

type were excavated from progressively deeper portions of an undifferentiated parent body. In this scenario, the most metamorphosed rocks (type 6) are from the center or deep interior and the least metamorphosed (type 3) from near surface environments. Such a model is consistent with possible heat source mechanisms (Miyamoto et al., 1981) and inferred peak temperatures for the different petrographic types (Dodd, 1969; Heyse, 1978). It also predicts that peak metamorphic temperatures should be correlated and cooling rates inversely correlated with petrographic type (i.e., deeper, hotter rocks cool more slowly). Cooling rates based on the retention of fission tracks in different minerals in several H chondrites (Pellas and Storzer, 1981) appear to agree with such a model but metallographic cooling rates derived from Ni zoning in alloys (Scott and Rajan, 1981; Taylor et al., 1987) do not. Based on the metallographic data, Scott and Rajan (1981) suggested that the parent bodies of ordinary chondrites were disrupted and reassembled leading to a rubble-pile structure. In this model, cooling below 500°C occurs after previously metamorphosed fragments are assembled to form the parent body from which ordinary chondrites were later extracted. This leads to a decoupling of cooling rates above and below 500°C.

Both onion shell and rubble-pile models draw from various geobarometers, geothermometers, and oxygen barometers as applied to ordinary chondrites in order to infer peak metamorphic conditions, and the metamorphic processes that took place within the parent bodies or small fragments prior to reassembly (e.g., Bunch and Olsen, 1974; Clayton, 1993; Colucci and Hewins, 1984; Heyse, 1978; Ishii et al., 1979; McSween and Patchen, 1989; Onuma et al., 1972; Saxena, 1976; Van Schmus and Koffman, 1967). Since results of these studies are often inconsistent, the thermal modeling based on them

(e.g., Bennett and McSween, 1996; Miyamoto et al., 1981) must also be regarded with some care.

In this paper, we apply olivine-spinel thermometry to a suite of equilibrated H, L, and LL ordinary chondrites spanning petrographic types 4-6 and constrain the temperatures that prevailed near peak metamorphic conditions. Our objective is to characterize the relationship between homogeneity of phase compositions and textures, which are the primary indicators of chondrite type, and the corresponding metamorphic conditions as reflected in peak metamorphic temperatures and cooling rates during retrograde metamorphism.

2. SAMPLES AND ANALYTICAL METHODS

We studied 11 meteorites (Table 1) representing H, L, and LL chondrites from petrographic types 4, 5, and 6. Except for Greenwell Springs, all of the selected representatives are falls and all are characterized by low shock intensity and relatively unbrecciated character. Six of the thin sections (three Hs and three LLs) are identical to samples studied by Gastineau and McSween (2001) and McSween (private communication, 2001).

Each thin section was examined by SEM and compositions of spinels, olivines, pyroxenes, and feldspars were obtained using a JEOL733 Superprobe. Operating conditions included an accelerating voltage of 15 keV and a beam current of 10 nA with counting times of 30 seconds on peak and 15 seconds at each background position. A ZAF correction procedure (Armstrong, 1988) was applied to the results. Spinels were analyzed for Fe, Cr, Mg, Al, Ti, Mn, Si, Ca, V, and Ni using Fe_2O_3, Cr_2O_3, $MgAl_2O_4$ (for both Mg and Al), TiO_2, Mn-olivine, anorthite (both for Si and Ca), V_2O_3, and NiO as

standards. Silicon, Ca, and Ni were always below the detection limit (0.008, 0.012, 0.043 elemental wt%, respectively). Olivines were analyzed for the same elements using fayalite, Cr_2O_3, forsterite (for both Mg and Si), anorthite, TiO_2, Mn-olivine, V_2O_3, and Ni-olivine as standards. Chromium, Al, Ti, Ca, V, and Ni were always below detection limit (0.020, 0.007. 0.026, 0.012, 0.027, 0.043 elemental wt%, respectively). The same standards were used for pyroxene except that diopside was used for Si. Nickel and V were invariably below detection. Feldspars were analyzed for Fe, Mg, Al, Ca, Ti, Si, Na, and K using fayalite, forsterite, anorthite (for both Al and Ca), TiO_2, albite (both for Si and Na), and microcline as standards. Magnesium and Fe were always below the detection limit (0.011, 0.031 elemental wt%, respectively).

3. MINERAL COMPOSITIONS

Average major element compositions and end-member mole fractions determined for olivines, spinels, pyroxenes, and feldspars in each meteorite are given in Tables 2a-d. Cations in olivines, pyroxenes, and feldspars were calculated for the appropriate number of oxygens assuming that all Fe is Fe^{2+}. The cation sums for individual analyses were 2.995±0.005 per 4 oxygens in olivine, 4.000±0.001 per 6 oxygens in pyroxene and 5.024±0.112 per 8 oxygens in feldspar. Cations in spinels were calculated using mass and charge balance constraints assuming that the spinel is stoichiometric with exactly three cations for every four oxygens. The end-member mole fractions were calculated for each mineral from the cations per formula unit. Also shown in the tables are ranges of mineral compositions found in the literature for these meteorites. All analyzed minerals are located in the matrix material outside chondrules and the spinel grains were always in contact with metal in order to support work on redox conditions, which will be reported

elsewhere. Olivine, pyroxene, and feldspar were always in the vicinity of the spinel grains (<200 μm) but not necessarily in contact in the plane of the thin section.

Olivine in all of the meteorites is Mg-rich and the dominant pyroxene is a low-Ca enstatite (the mole fraction of wollastonite ranges from 0.010 to 0.017). Fayalite (Fe_2SiO_4, Fa) and ferrosilite ($Fe_2Si_2O_6$, Fs) contents of olivine and pyroxene in type 4-6 ordinary chondrites analyzed in this work are shown in Fig. 1a. Also shown are fields representing each group of ordinary chondrites as defined originally by Keil and Fredriksson (1964) and revised by Fredriksson et al. (1968). The olivines and pyroxenes are equilibrated in that standard deviations on Fa and Fs contents are typically <1 mole% (Table 2a and 2c). Compositions for both phases are generally in good agreement with the literature. We found significantly lower ferrosilite content in Saratov pyroxenes than Folco et al. (1997). We also obtained more magnesian olivine in Siena than reported by Kurat et al. (1969) although the wide range of olivine, pyroxene, and spinel compositions noted by these authors for different portions of Siena suggests that our results for this meteorite may actually be consistent with their results.

Spinels in ordinary chondrites are Cr-rich (Table 2b, Bunch et al., 1967). The chromite ($FeCr_2O_4$, Chr) contents of spinel of type 4-6 ordinary chondrites analyzed in this work are shown in Fig. 1b as a function of Fayalite in olivine. All of the H chondrites have similar spinel compositions. The results for Allegan (H5) are similar to those of Bunch et al. (1967) though they obtained slightly higher chromite contents than we did. Type 5 and 6 L and LL chondrites have similar ranges in spinel composition and are generally more Cr-rich than in the H chondrites. The results for Siena (LL5) are in the range of compositions found by Kurat et al. (1969). Spinels in both L4 and LL4

chondrites exhibit even higher chromite contents than in types 5-6 leading to a much broader range of spinel compositions in L and LL chondrites than in H chondrites. Overall, our results are consistent with the findings of Bunch et al. (1967) based on a much larger database. To evaluate possible textural responses to metamorphism and their relationships to peak metamorphic conditions, we also determined the minimum dimension in the plane of the thin section for each spinel grain analyzed in each meteorite. Averages and standard deviations are given in Table 2b. The average spinel is coarser in types 5-6 chondrites than in type 4 for all groups and the largest grains (>100 μm) are restricted to types 5-6.

Feldspars in equilibrated ordinary chondrites are sodic (e.g., Brearley and Jones, 1998; Rubin, 1992; Van Schmus and Ribbe, 1968; Table 2d). For H and LL chondrites, the compositions we determined ($Ab_{84}An_{10}Or_6$, and $Ab_{87}An_9Or_6$, respectively) are identical within error for all meteorites in a group regardless of petrographic type. On the other hand, feldspar compositions in the L chondrites vary considerably with standard deviations on the mole fraction of Ab an order of magnitude higher than observed in H or LL chondrites (Table 2d). Neither the variability nor the composition appears to be related to the assigned petrographic type. The feldspar in Saratov (L4) is alkali-rich with less than 0.5% CaO whereas feldspars in Ausson (L5) are more Ca-rich than those in either H or LL chondrites. Since it has been suggested that the mean feldspar grain size is correlated with temperature (Heyse, 1978), we also determined maximum dimensions in the plane of the thin sections of 15 grains in the vicinity (<200 μm) of the analyzed

spinels in each meteorite. Feldspar grains increase in length with increasing petrographic type as noted by Van Schmus and Wood (1967) and Heyse (1978).

4. THERMAL HISTORY OF EQUILIBRATED ORDINARY CHONDRITES

4.1. Olivine-spinel equilibration temperatures

We used olivine-spinel thermometry in this study as our principle tool for probing the metamorphic history of equilibrated ordinary chondrites. The basic idea is that core compositions of coexisting olivine and spinel record peak or near peak metamorphic conditions. By inserting observed phase compositions into a thermodynamically based model for the partitioning of Fe and Mg between olivine and spinel, it is possible to extract an equilibration temperature. A necessary but insufficient condition for preservation of peak metamorphic conditions is that central regions of coexisting grains be homogeneous (i.e., unzoned) and retain initial composition. As a test for this condition, we obtained traverses in the vicinity of one or two olivine-spinel contacts in each of the meteorites studied. Traverses extended from the olivine core across the interface to the spinel core at intervals of 1-2 μm were taken. Mineral stoichiometry along the traverse was within the accepted range except within 5 μm of the interface where systematic deviations from stoichiometry were observed due to x-ray generation of atoms from the adjacent phase and secondary fluorescence effects. A representative traverse for each meteorite is shown in Figs. 2a–c with $Y_{Mg}^{mineral} = Mg/(Mg + Fe^{2+})$, where Mg and Fe^{2+} are the cation mole fractions in the minerals, plotted as a function of distance from the interface. A slight increase in $Y_{Mg}^{olivine}$ of ~0.5 mole% is observed in

many of the olivine grains towards the interface with the spinel. Values of Y_{Mg}^{spinel} for all spinel analyses in a given traverse are identical within analytical uncertainties with a standard deviation of less than 1 mole%. Values of Y_{Cr}^{spinel} $[Cr^{3+}/(Cr^{3+}+Al^{3+}+Fe^{3+})]$ and Y_{Al}^{spinel} $[Al^{3+}/(Cr^{3+}+Al^{3+}+Fe^{3+})]$ from core to rim are also constant within error.

We used the thermodynamic models of Sack and Ghiorso (1989) for olivine and Sack and Ghiorso (1991a,b) for multicomponent spinels to estimate metamorphic temperatures experienced by equilibrated ordinary chondrites. Sack and Ghiorso (1989) describe olivine as a symmetric regular solution with negative deviations from ideality. The thermodynamic behavior of spinel is more complicated and was modeled by Sack and Ghiorso (1991a,b) using a second degree Taylor expansion in composition and ordering parameters. The model parameters were calibrated to reproduce experimental data on miscibility gaps and order-disorder phenomena. Sack and Ghiorso (1991a,b) expressed the equilibrium between olivine and spinel by equating Fe-Mg exchange potentials of the two phases, $\mu^{ol}_{Mg(Fe)-1} = \mu^{sp}_{Mg(Fe)-1}$, and showed good agreement between calculated and experimentally observed equilibrium temperatures.

Following Sack and Ghiorso (1991a,b), we calculated olivine-spinel equilibration temperatures for ordinary chondrites by equating Fe-Mg exchange potentials. We used the average compositions of coexisting olivine and spinel to estimate temperatures for three to eight olivine-spinel pairs in each meteorite (averages for all pairs in each meteorite are given in Tables 2a and 2c; individual results are available upon request from the authors). Most spinels and olivines are in contact with each other. A few are separated by as much as 60 μm in the plane of the thin section but we observed no

relationship between calculated temperature and distance between the minerals. The temperatures are shown in Fig. 3 and the averages are given in Table 3. The individual temperatures for all four H chondrites are equal within error to the H average (778±26°C). The data are suggestive of a subtle increase in temperature with increasing petrographic type in that lowest, mean, and highest temperatures increase with type, and we discuss this below. Calculated temperatures for the L chondrites extend to significantly lower values than observed in the H chondrites. The lowest temperatures (680±15°C) in our suite of ordinary chondrites are recorded by Saratov (L4) reflecting its unusually chromite-rich spinels. Ausson (L5) exhibits a wide range of spinel compositions resulting in a correspondingly wide range in temperatures (691-823°C) although the average (756°C) is essentially equivalent to that of Glatton (L6; 749°C). A similar behavior is observed for the LL chondrites. Mean temperatures for Greenwell Springs (LL4) are at the low end of the range for the group. Temperature ranges for the LL5-6 chondrites are broad and extend down into the LL4 range.

There are two key features to our data. First, the total range of our average temperatures for equilibrated ordinary chondrites (659-829°C) is much smaller than commonly assumed (e.g., 600-950°C, Dodd, 1969, Heyse, 1978) and the maximum temperatures (~830°C) much lower. If the maximum temperatures correspond to or close to peak metamorphic conditions, then this result has important implications for thermal models of the ordinary chondrite parent bodies because they attempt to match peak temperature. Second, only for type 4 versus types 5-6 in L and perhaps LL chondrites are there significant temperature differences plausibly tied to petrographic type. This suggests that the systematic variations in textural maturation and degree of homogeneity

of phases, which are the basis for classifying ordinary chondrites (Van Schmus and Wood, 1967), are not strongly correlated with temperature.

To test the idea that type 4 chondrites record temperatures lower than or equal to types 5-6, we took olivine (Johnson and Prinz, 1997; Mason, 1963; Rubin, 1990) and spinel (Bunch et al., 1967; Christophe Michel-Levy and Deneise, 1992; Hutchison et al., 1981; Johnson and Prinz, 1997; Kleinschrot and Okrusch, 1999; Snetsinger et al., 1967) compositions for types 4-6 chondrites available in the literature and calculated equilibration temperatures. We avoided meteorites that are strongly shocked (>S3) or show evidence of impact melting. We also restricted consideration of spinel analyses to those containing less than 2.5 wt% Fe_2O_3, which corresponds to a mole fraction of magnetite of ~0.03. Equilibrated ordinary chondrites were metamorphosed under very reducing, metal-saturated conditions (e.g., Brett and Sato, 1984; McSween and Labotka, 1993; Mueller, 1964; Williams, 1971). A significant amount of Fe^{3+} is not expected and all of our analyses (Table 2b) are consistent with less than 2 mole% magnetite. Even with these constraints, the exercise is not entirely satisfying in the sense that "coexisting" phases are not from adjacent grains or even from the same thin section and compositions were taken from different studies. Some equilibrated ordinary chondrites exhibit substantial differences in phase compositions in different portions of the meteorite (e.g., Kurat et al., 1969) and there is, therefore, a possibility that some of the olivine-spinel pairs we selected effectively come from different rock fragments. The gross features of such calculations should, nevertheless, provide insight into whether the results for our suite are generally applicable to equilibrated ordinary chondrites.

For olivine-spinel pairs of H chondrites constructed from literature data, the models of Sack and Ghiorso (1989, 1991a,b) yield 705–793°C for four H4 chondrites, consistent with our data for Avanhandava (728-791°C) and Phum-Sambo (735-800°C). These temperatures are within the range of the calculated values for six H5 chondrites (668–820°C) and overlap ranges for three H6 chondrites (750–803°C), and our results for Allegan (H5, 747-806°C) and Guareña (H6, 768-820°C). A similar result is obtained for the L chondrites. Calculated temperatures of four L4 chondrites range from 618–690°C, in agreement with our result for Saratov (L4, 659-694°C) and lower than the range of temperatures calculated for two L5 (739–765°C) and four L6 chondrites (691–764°C) and the L5-6 chondrites analyzed in this study (691-823°C). There is a hint in the L chondrite data that L4s record slightly lower temperatures than do L5-6. Unfortunately, our survey of the literature yielded no accepted spinel compositions from LL4 chondrites. The calculated temperature of one LL5 chondrite is 663°C and a range of 644–756°C was obtained for six LL6 chondrites. These values are generally lower than but overlap our data for LL5-6 chondrites (734-829°C).

Two common themes run through all of these calculated temperatures. First, the range in olivine-spinel temperatures is only 160°C (659-829°C). This is substantially smaller than commonly assumed for types 4-6 chondrites (~350°C) and the temperatures are quite a bit higher than those experienced by type 3 chondrites (<400°C). If types 4-6 sampled progressively greater depths in the parent bodies, then there is a significant gap in coverage between type 3 and 4 chondrites. Second, spinel and olivine in type 4 chondrites record temperatures that are lower than or equal to those of types 5-6

chondrites and the results for the latter are, virtually, indistinguishable. The general implication here is one of decoupling metamorphic temperature from petrographic type.

We noted above in discussing Fig. 3 that there may be a subtle increase in olivine-spinel equilibration temperature for the H chondrites in going from type 4 to 5 to 6 as minimum, mean, and maximum temperatures for our samples all increase progressively. In principle, this could reflect differences in either prograde or retrograde temperatures. Since spinels are far smaller and less abundant than olivine we might for the latter case expect a correlation between spinel grain size and calculated temperature. Figure 4a shows calculated temperatures as a function of the minimum dimension of the spinels in the plane of the thin section for the H chondrites. For each meteorite, the highest temperatures are associated with the largest spinel grains and the lowest temperatures with the smallest spinel grains. In types 5 and 6 chondrites, the larger grains (50-170 μm) record similarly high temperatures of ~800°C while many of the smaller grains (<70 μm) yield lower temperatures extending down to 750°C. Spinels in type 4 chondrite are all smaller than 70 μm and record lower temperatures, similar to those recorded by the smaller grains in types 5 and 6. The solid curves envelop the change in temperature as a function of spinel grain size in H chondrites. One interpretation of this result is that all H chondrites were subject to essentially the same peak temperatures of ~800°C. The larger grains in H5 and H6 chondrites preserve this temperature but smaller grains in H5-6 and most grains in H4s yield a range of temperatures that correlates with grain size because the smaller grains partially re-equilibrated during cooling. Alternatively, the maximum temperature was higher than 800°C and all grains re-equilibrated. If so, olivine-spinel

pairs in equilibrated ordinary chondrites record conditions during retrograde metamorphism. The relationships are slightly different for L (Fig. 4b) and LL (Fig. 4c) chondrites. Spinels in the type 5 and 6 chondrites are generally larger than and record generally higher temperatures than type 4 spinels. The only overlap in size and/or temperature between spinels in type 4 versus spinels in types 5 and 6 is obtained from two small grains in Siena (LL5). The lack of a plateau analogous to that observed in Fig. 4a may reflect in part the absence of spinel grains larger than 100 μm in our analyzed sections of these meteorites. We return to the issue of whether olivine-spinel pairs record peak or retrograde temperatures in section 4.3.

4.2. Comparison with previous thermometry work

4.2.1. Cation partitioning thermometers

Most approaches to determining the metamorphic temperatures experienced by ordinary chondrites of different petrographic type including the present study are based on the temperature-dependent partitioning of two cations between two coexisting phases. Craig (1964) was the first to calculate temperatures for the equilibrated ordinary chondrites using this approach. He modeled the distribution of Fe and Mg between olivine and orthopyroxene, two commonly coexisting phases in equilibrated ordinary chondrites, and concluded that peak temperatures were roughly ~1250°C regardless of group or type. Later, experimental data (e.g., Larimer, 1968) showed that this particular exchange is relatively insensitive to temperature. Although Williams (1971) was able to obtain an approximate equilibration temperature of 880±150°C for type 5 and 6 chondrites, Fe-Mg partitioning between olivine and pyroxene is unsuitable for accurate

thermometry. The underlying approach of Craig's (1964) work is, nevertheless, shared by most subsequent studies.

Type 6 chondrites contain coexisting pyroxenes that are common and readily analyzed. This motivates the use of the temperature dependence of cation partitioning between them to infer equilibration temperatures. The thermometer was initially calibrated using existing solution models for the two phases [e.g., Kretz, 1961 (Ca/Mg); Kretz, 1963 (Fe/Mg)] or phase diagrams [Lindsley, 1983; Lindsley and Anderson, 1983 (Ca/Mg)] and all workers have used the same framework with periodic updatings of thermodynamic formulations (e.g., Bunch and Olsen, 1974; Olsen and Bunch, 1984; Saxena, 1976; Van Schmus and Koffman, 1967). Van Schmus and Koffman (1967) calculated that type 6 equilibrated ordinary chondrites experienced a maximum metamorphic temperature of ~820°C regardless of petrographic type or group. Bunch and Olsen (1974) found modest differences in metamorphic temperatures among type 6 chondrites from 900°C for H, to 940°C for L, and 980°C for LL chondrites and were re-evaluated by Olsen and Bunch (1984) to 830°C for H, and 860-930°C for L and LL chondrites. Saxena (1976) improved the thermodynamic treatment and revised the Bunch and Olsen (1974) equilibration temperatures downward to 875°C for H, 900°C for L and 920°C for LL chondrites. Ishii et al. (1979) used the coexistence of three pyroxene assemblages to infer temperatures in the range 940-990°C for type 6 H, L, and LL chondrites. Colucci and Hewins (1984) calculated equilibration temperatures of 867°C for H6, 907°C for L6 and 905°C for LL6 chondrites.

Application of two pyroxene thermometry to ordinary chondrites less equilibrated than type 6 is difficult because the clinopyroxene is rare and/or extremely fine-grained

and much of what is observed constitutes relic igneous grains that are only partially re-equilibrated. Thus, two-pyroxene thermometry provides little direct insight into possible correlations between temperature and type. Kleinschrot and Okrusch (1999) were able to obtain a two-pyroxene equilibrium temperature for Carcote (H5) of 750-840°C. McSween and Patchen (1989) and Harvey et al. (1993) examined the pyroxenes in H, L, and LL chondrites of types 3 to 7 but noted that equilibrium during metamorphism between the two phases pertained only in type 6 chondrites and a few type 5 chondrites. Clinopyroxenes were only partly overprinted by metamorphism in type 4-5 chondrites. Assuming equilibrium between orthopyroxene and clinopyroxene, they estimated equilibration temperatures in chondrites based on the composition of each pyroxene separately. The temperatures recorded by type 5-6 chondrites of 900-960°C based on the clinopyroxene compositions are 100-200°C higher than those based on the orthopyroxene compositions, which they attributed to partially annealed chemical variations caused by polymorphic inversions in the latter. The complications associated with structural changes, demonstrable lack of equilibrium in many meteorites, and inconsistency of temperatures inferred from the low and high calcium limbs of the solvus make two-pyroxene thermometry difficult to apply quantitatively to equilibrated ordinary chondrites. It is, however, probably fair to say that pyroxene in type 6 chondrites suggests that peak metamorphic temperatures were higher than the ~800°C implied by maximum values we obtained from olivine-spinel thermometry.

Olivine-spinel thermometry has been applied previously to ordinary chondrites by Bunch and Olsen (1974), Johnson and Prinz (1997) and Kleinschrot and Okrusch (1999). Bunch and Olsen (1974) reported temperatures in the range 867-972°C for ten chondrites

based on the geothermometer of Jackson (1969) and literature data for phase compositions (Bunch et al., 1970; Keil and Fredriksson, 1964). The relatively small temperature range is consistent with our results described above for the same meteorites. The absolute temperatures are significantly higher than we calculated but the agreement is actually very good given the major revisions in our knowledge of spinel thermochemistry since the publication of Jackson (1969).

Johnson and Prinz (1997) studied spinels and olivines from chondrules. Most of their data concerns carbonaceous chondrites and unequilibrated ordinary chondrites but they also considered Bjurböle (L/LL4), Aldsworth (LL5) and Appley Bridge (LL6). They used the formulation of Engi (1983), who modeled spinels as an ideal reciprocal system. Although they did not report specific temperatures, all of their data fall well below the 600°C isotherm, substantially lower than olivine-spinel temperatures of 660-670°C we obtained for these meteorites using their compositions and the formulation of Sack and Ghiorso (1989, 1991a,b). Figure 5 compares olivine-spinel temperatures for the suite of equilibrated ordinary chondrites studied here calculated using Engi's (1983) formulation and the calibration of Sack and Ghiorso (1989, 1991a,b). Engi's (1983) equations lead to systematic offsets of ~200°C relative to values calculated using the formulation of Sack and Ghiorso (1989, 1991a,b). The basic source of the discrepancy lies in the spinel models. Although we did not attempt to isolate the specific causes, compositions of spinel in equilibrated ordinary chondrites lie outside the calibration region provided by Engi (1983) and his model should, therefore, not be used.

Kleinschrot and Okrusch (1999) used spinel solution models of Fabriès (1979), and Ballhaus et al. (1991). Use of the Ballhaus et al. (1991) formulation, which was

designed for high-pressure assemblages in the earth's mantle, is inappropriate for ordinary chondrites. Fabriès (1979) calibrated the dependence of the olivine-spinel distribution coefficient on spinel composition and temperature by modeling spinels as ideal and empirically fitting existing phase equilibria data. Based on the Fabriès (1979) model, Kleinschrot and Okrusch (1999) obtained a temperature of equilibrium for Carcote (H5) of 650-720°C, which is much lower than the 820±33°C for the same olivine-spinel pairs using the formulation of Sack and Ghiorso (1989, 1991a,b).

4.2.2. Oxygen isotopes

Onuma et al. (1972) determined metamorphic temperatures for equilibrated ordinary chondrites, mostly of petrographic type 6, by examining the ^{18}O content of olivine, plagioclase, and orthopyroxene. Minerals in each meteorite were separated using heavy liquids and analyzed for $\delta^{18}O$. Clayton (1993) updated the temperatures by applying the calibration of Clayton and Kieffer (1991) to the isotopic compositions of Onuma et al. (1972). Plagioclase-based thermometry was rejected due to the poorly constrained dependence of isotope fractionation on composition (O'Neill and Taylor, 1967), but the average olivine-pyroxene isotopic temperatures, excluding Bjurböle (L4), was found to be 794°±57°C with no observed systematic variation between groups or petrographic types, which is in good agreement with our results. The isotopic temperature recorded by Bjurböle, 490°C, is much lower than any of the other values obtained by Clayton (1993) and significantly lower than the olivine-spinel temperature of 660-680°C derived for Bjurböle in this study from phase compositions given by Johnson and Prinz (1997). The latter is consistent with our results for Saratov (Table 3) and is in the range of temperatures we derived for L4 chondrites (659-694°C). Bjurböle is highly

friable (e.g., Grady, 2000), containing unequilibrated clasts and chondrules (Scott et al., 1985), and the clinopyroxene compositions are highly variable, indicating lack of equilibration (Bunch and Olsen, 1974). It is possible that the oxygen isotopic temperature reflects contributions from exotic material or that retrograde isotopic exchange among matrix minerals continued to an unusually low temperature in Bjurböle relative to other equilibrated ordinary chondrites. With the possible exception of Bjurböle, oxygen isotope thermometry yields temperatures that are consistent with results from cation partitioning, both in general range of temperatures and in demonstrating a lack of correlation between temperature and petrographic type.

4.2.3. Structural state of feldspar

MacKenzie (1957) related the separation of two x-ray diffraction peaks in feldspars to the temperature of formation. Miyashiro (1962) noted the high temperature structure in ordinary chondrites and suggested peak metamorphic temperatures higher than 700°C. Van Schmus and Ribbe (1968) estimated metamorphic temperatures for type 6 H, L, and LL chondrites by examining the structural state of feldspars using the calibration of MacKenzie (1957). Although they did not report specific temperatures, they suggested that the high temperature structure of feldspars in type 6 chondrites indicates peak temperatures for these meteorites in the range 750-850°C, which is consistent with our results for olivine-spinel thermometry.

4.2.4. Ca content in low-Ca pyroxene

There is little basis from thermometry described in this or previous work to suggest that temperature in equilibrated ordinary chondrites is correlated with type. In this study, we found a systematic increase in average olivine-spinel temperatures for H

chondrites but the effect is subtle and probably reflects variations in re-equilibration during metamorphism due to differences in grain size (see discussion in section 4.3). Although the idea that increasing petrographic type reflects increasing peak metamorphic temperatures appears to be entrenched (e.g., Dodd, 1981; McSween et al., 1988), the only quantitative support for this lies in the work of Heyse (1978) who proposed, based on the Ca content of low-Ca pyroxenes, that maximum temperatures experienced by LL chondrites increased systematically from <600°C for type 4 to 600-650°C for type 5 to 650-800°C for type 6. This led to the wide spread use of these and similar peak metamorphic temperatures for types 4, 5, and 6 chondrites not only in LLs but in every equilibrated ordinary chondrite group (e.g., Dodd, 1969; Miyamoto et al., 1981). The selected temperatures form the foundation of models to constrain the thermal evolution of ordinary chondrite parent bodies (e.g., Bennett and McSween, 1996; Miyamoto et al., 1981) and estimates of f_{O_2} during metamorphism (McSween and Labotka, 1993).

The source of Heyse's (1978) analysis of equilibrium temperatures in equilibrated ordinary chondrites lies in a beautiful linear correlation between feldspar grain size and Ca in orthopyroxene, expressed in terms of the wollastonite (Wo) content. Heyse (1978) established this relationship for a series of clasts in LL meteorites spanning petrographic types 4 through 7 and then proceeded to connect this relationship to corresponding variations in temperatures using a sketched version of the low-Ca line of the two-pyroxene solvus. Thus, the sequence in logic was to connect feldspar grain size, which is directly related to type, to pyroxene chemistry and to then connect pyroxene chemistry to temperature, thereby creating a linkage between type and temperature. The basic flaw in this logic lies in the second link. In essence, Heyse (1978) used an approximate version

of the two-pyroxene solvus to all equilibrated ordinary chondrites but applied it solely to orthopyroxene compositions. This approach can work if the second saturating phase is known to be present and in equilibrium. Heyse (1978) attempted to demonstrate that this assumption holds by comparing Fe-Mg distribution coefficients in coexisting orthopyroxenes and clinopyroxenes in type 6 chondrites to the range of experimental values reported by Lindsley et al. (1974) at 810°C and 15 kbar. He found comparable pyroxene compositions within the very loose constraints of the experimental data and concluded that equilibrium between orthopyroxene and clinopyroxene must, therefore, hold in all of the chondrites of his study. However, Heyse (1978) reports no clinopyroxene compositions in type 4 chondrites and the distribution coefficients in type 5 chondrites that he did analyze are outside the range of values given by Lindsley et al. (1974) which would suggest that orthopyroxene and clinopyroxene were not in equilibrium. Moreover, there is good evidence (McSween and Patchen, 1989) that many of the clinopyroxenes in type 4-5 chondrites bear relict igneous signatures only partly overprinted by metamorphism. Thus, Heyse's (1978) argument fails for types 4 and 5 chondrites and, therefore, the inferred relationship between texture and temperature, which rests upon this argument, is not sound.

Although we believe there is no direct tie between feldspar grain size and temperature, at least based on the arguments of Heyse (1978), our data and those of Scott et al. (1986) support the idea that Ca contents of orthopyroxene generally increases with increasing type for LL chondrites. We therefore consider whether Heyse's (1978) correlation between feldspar grain size and Wo contents of orthopyroxene, which was only demonstrated for LL chondrites, also holds for H or L chondrites. We then evaluate

possible controls on orthopyroxene composition in equilibrated ordinary chondrites and discuss how this may interface with Heyse's observations.

Average Wo contents of low-Ca pyroxenes analyzed in our study are shown in Fig. 6 as a function of average feldspar grain size (maximum dimension in the plane of the thin section) together with the data of Heyse (1978) for clasts in LL chondrites. Our data are generally consistent with coarsening of feldspar grains with increasing petrographic type (Table 2d) and the Wo data for low-Ca pyroxenes in LL chondrites are consistent with those of Heyse (1978). For the H chondrites, there is no correlation of grain size with Wo content of the pyroxene, in agreement with observations of Hutchison et al. (1980) and Scott et al. (1986). Our data for pyroxenes and feldspars in L chondrites are insufficient to preclude an LL-type correlation, but if it is present the slope is much lower than for LL chondrites. It is possible to construct a correlation between olivine-spinel temperatures (Table 3, Fig. 3) and feldspar grain sizes or Wo contents of low-Ca pyroxenes for L chondrites, but these would essentially be two point lines (type 4 versus types 5-6). The key point here is that most of the temperature variations we obtained through olivine-spinel thermometry is in type 4 chondrites for any given group, but the variation in feldspar grain size is a systematic function of type (e.g., Table 2d). Thus, temperature and textural maturation as exemplified by feldspar grain size are decoupled and the temperature estimates of Heyse (1978) which depend on such a correlation are incorrect.

To understand the evolution of Ca contents of pyroxenes in ordinary chondrites, we need to consider the Ca budget for the whole rock and the influence of other phases on pyroxene composition. Consider the balanced reaction:

$$\underset{An}{CaAl_2Si_2O_8}^{feldspar} + 2\underset{Fa}{Fe_2SiO_4}^{olivine} = \underset{Wo}{CaSiO_3}^{pyroxene} + \underset{Her}{FeAl_2O_4}^{spinel} + 3\underset{Fs}{FeSiO_3}^{orthopyroxene} \quad (1a)$$

(abbreviations given in Tables 2a-d). This reaction implies that as the composition of olivine, feldspar, and spinel shift with changing metamorphic conditions or time at temperature, the pyroxene composition and in particular the Ca content of the pyroxene will also shift. Note that reaction 1a does not involve clinopyroxene, which is rare to absent in type 4 and 5 chondrites, but does involve four phases, olivine, orthopyroxene, spinel, and feldspar that are present in all equilibrated ordinary chondrites. Reaction 1a has an equilibrium constant

$$K_1 = \frac{\left(a_{CaAl_2Si_2O_8}^{feldspar}\right)\left(a_{Fe_2SiO_4}^{olivine}\right)^2}{\left(a_{CaSiO_3}^{pyroxene}\right)\left(a_{FeAl_2O_4}^{spinel}\right)\left(a_{FeSiO_3}^{pyroxene}\right)^3} \quad . \quad (1b)$$

In Eqn. 1b, a_i^j refers to the activity of component i in phase j, and K_1 is the temperature-dependent equilibrium constant of reaction 1a. As shown above, olivine, pyroxene, and spinel are relatively homogeneous within each meteorite but differ from meteorite to meteorite. Provided the equilibrium encapsulated by reaction 1a holds, the compositions of phases will be controlled by the mineral with the slowest diffusion rate (feldspar), especially if growth occurs during metamorphism. Provided type 4-6 chondrites are metamorphosed rocks after material similar to type 3 chondrites (e.g., McSween et al. 1988), the feldspar is metamorphic because macroscopic feldspar grains are very rare in type 3 ordinary chondrites, and based on catholuminescence of chondrule mesostases (e.g., Sears et al., 1995), microcrystalline feldspar becomes progressively more common with increasing type in unequilibrated ordinary chondrites. Thus, if Eqn. 1a holds and the

composition of the feldspar changes with time or remains fixed by slow diffusion rates as temperature rises or falls, the compositions of the other phases adjust to compensate.

The variation of $\ln K_1$ with temperature is shown in Fig. 7 together with calculated values at the olivine-spinel equilibration temperatures for each ordinary chondrite. Also shown are calculated curves for L4, L5, and L6 chondrites as a function of temperature assuming constant compositions of phases (Tables 2a-d). The end-member chemical potentials used to calculate the free energy of reaction 1a and activities of components in the phases were obtained using the MELTS supplemental calculator (Ghiorso and Sack, 1995). Taking an average uncertainty of 2 kJ/mol for each end-member chemical potential (Berman, 1988), the equilibrium constant is known within 8 kJ/mol (1σ, shaded region). Although the precise location of the equilibrium is uncertain, if the olivine, orthopyroxene, and spinel all equilibrated with the feldspar, they should be consistent with a single curve within the gray region. Most of the meteoritic values of $\ln K_1$ are but values for Saratov (L4) and Ausson (L5) are well off the trend formed by the other meteorites, although error envelopes overlap at the 2σ level. These deviations reflect the anomalous feldspar compositions in these meteorites (An_1 in Saratov and An_{21} in Ausson) relative to other equilibrated ordinary chondrites (~An_{10}) and may indicate that feldspar in these meteorites is not in equilibrium with spinel and the ferromagnesian silicates. Lack of equilibrium is also consistent with the fact that standard deviations on both feldspar (Table 2d) and pyroxene (Table 2c) oxide wt%, in Ausson and especially Saratov, are generally at the high end for our suite of chondrites. We conclude that feldspar and pyroxene were probably not in equilibrium in Ausson and Saratov on a thin

section scale although a metastable equilibrium may have held for the other meteorites. The observation that Ausson is not in equilibrium is in agreement with the suggestion that Ausson is a breccia (Taylor et al., 1987).

4.3. Implications for cooling rates of equilibrated ordinary chondrites

Cooling rates in equilibrated ordinary chondrites have been estimated by metallography (Scott and Rajan, 1981; Taylor et al., 1987; Wood, 1967), fission track annealing (Pellas and Fiéni, 1988; Pellas and Storzer, 1981) and intra-crystalline site occupancy studies (Folco et al., 1996, 1997). All of these techniques yield information on cooling rates near or below ~500°C. Except for some severely reheated meteorites (Taylor et al., 1987), inferred cooling rates are in the order of 1-100°C/Ma for temperatures in the range 100-500°C. There may be some differences in cooling rates below 500°C for chondrites of different petrographic types (Pellas and Storzer, 1981) but this issue is not resolved, at least not in a compelling manner, and none of the methods directly constrains cooling rates during peak metamorphic conditions above 600°C. Given that Fe-Mg closure temperatures obtained above for olivine-spinel are 659-829°C for our data and both phases exhibit nearly flat composition profile (Figs. 2a-c), it may be possible to place some useful constraints on cooling rates during this critical portion of the thermal history. Lasaga (1983) developed a set of equations describing the kinetic response of ion exchange to a thermal history depending on diffusion coefficients of the cations of interest in the two phases, the enthalpy of the exchange reaction, grain sizes, and thermal history. The rate of change of composition in the olivine grains adjacent to a spinel is very slow due to relatively fast interdiffusion of Fe-Mg and the large grains regardless of the cooling rate. Only a slight zoning close to the interface with spinel is

expected at slow cooling rates. Due to a slower Fe-Mg interdiffusion in spinel compared to that in olivine, lack of zoning close to the interface with olivine implies either that the compositions correspond to the highest temperature at which both phases were held long enough to equilibrate or to complete re-equilibration during slow cooling.

We used interdiffusion coefficients for Fe-Mg in olivine and Cr-rich spinel from Ozawa (1984). The diffusion coefficient for olivine given in Ozawa (1984) is similar to that given in Buening and Buseck (1973) and used by Lasaga (1983). Ozawa's (1984) spinel diffusion coefficient is more appropriate for spinels from ordinary chondrites than the intrinsic diffusion of Mg in $MgAl_2O_4$ used by Lasaga (1983). The enthalpy of the olivine-spinel exchange reaction was taken from Lehmann (1983). Based on these parameters a flat equilibrium profile is expected in olivines with slight increase in $Y_{Mg}^{olivine}$ towards the interface with the spinel during slow cooling rates as observed in some of the olivine grains analyzed in this work and in the composition profiles of Ozawa (1984). In principle, it should be possible to extract kinetic information from this slight modification of the olivine composition close to the interface, but the errors in our analyses are significantly larger than desirable for such quantitative evaluation, especially given that the interface concentrations are weakly constrained. All spinel grains we analyzed exhibit flat profiles. Given the range of olivine-spinel equilibration temperatures and the correlation of temperature with spinel grain size for H chondrites, it is highly likely that most if not all spinel grains re-equilibrated to some extent and record retrograde temperatures. The flat profiles in the spinel grains were therefore generated during continuously re-equilibration to a closure temperature, $T_{ol\text{-}sp}$, below T_{max}, at which the flat profile was frozen in.

Figure 8 shows cooling rates as a function of olivine-spinel equilibration temperature indicating conditions under which a re-equilibrated flat profile is generated. If a grain is cooled faster than the rate indicated on the curve, the profile will be frozen in at a higher temperature. If the cooling rate is slower than indicated for a given grain, zoning will begin to develop. Superimposed on the set of curves in Fig. 8a are the curves shown in Fig. 4a enveloping the observed change in equilibration temperature as a function of spinel grain size for H chondrites. Due to sectioning effects (small sections of large grains will yield higher temperatures than expected for the given size), the curve corresponding to the maximum grain size at a given temperature (solid curve) is our best estimate of cooling rate experienced by H chondrites. Cooling rates of ~1-4°/Ma are indicated for temperatures between 730°C-820°C. These cooling rates indicate that the meteorites cooled from 900°C to 800°C in 25-100 Ma, in agreement with suggested duration of metamorphism of ~60 Ma (e.g., Göpel et al., 1994). There are, however, substantial errors associated with these calculations, leading to uncertainties in cooling rates of up to an order of magnitude (Ozawa, 1984). The inferred cooling rates are at the lower end of values obtained from metallographic and other techniques sensitive to cooling rates below ~500°C. A literal interpretation of our results would suggest that cooling rates at low temperatures actually exceeded those near peak metamorphic conditions in many cases thereby supporting a rubble-pile model. This would, however, be an overinterpretation. Although refinements in diffusivities - more sophisticated modeling of diffusive interaction between adjacent phases and analyses and geometric characteristics of grains in three dimensions – could well lead to a quantitative assessment of this issue, we view the current calculations as no better than semi-

quantitative. There are nevertheless two fundamentally important consequences for H chondrites: (1) olivine-spinel equilibrium is consistent with a simple single-stage thermal history in which smaller spinel grains equilibrated to lower temperatures than did larger grains. (2) H4-6 chondrites in our study are all consistent with essentially the same thermal history, at least for temperatures at and below ~800°C. If differences in type reflect differences in thermal history or peak temperature, then these variations occurred above 800°C over less than and probably much less than 200°C.

A clear relationship between grain size and olivine-spinel equilibration temperature is not present in our data for L and LL chondrites (Figs. 4b,c). Spinel grains analyzed in L and LL chondrites are much smaller (20-80 μm, Figs. 4b,c) and record lower olivine-spinel equilibration temperatures (Fig. 3) than observed in H chondrites. Spinels in the type 5 and 6 chondrites are generally larger than and record generally higher temperatures than type 4 spinels in L and LL chondrites with little overlap between type 4 and types 5,6. Correspondingly, lower cooling rates are indicated for L and LL chondrites, 0.08-1°/Ma and 0.1-3°/Ma for, respectively (Fig. 8b). The larger spinel grains and higher equilibration temperatures correspond to faster cooling rates for types 5,6 while slower cooling rates are indicated for type 4 chondrites in these two groups. However, due to the large uncertainties associated with these calculations, the cooling rates estimated for L and LL chondrites are considered here to be similar to those assigned to H chondrites.

The assignment of an ordinary chondrite to type 4, 5, or 6 is, in general, a trivial matter because the differences between types are very distinctive. These differences are often attributed to variations in peak metamorphic temperatures (e.g., Dodd, 1981) but

the overlap in olivine-spinel equilibration temperatures and at least for H chondrites, the systematics of grain size and temperature suggest that variations in temperature are not the root cause of different types. This of course begs the question of what processes or physical conditions lead to different types. The classification scheme of Van Schmus and Wood (1967) has two basic motifs, homogeneity of ferromagnesian silicates and textural maturation as exemplified by recrystallization of the matrix, degradation of chondrules outlines, and growth of crystals such as albitic plagioclase. Both of these motifs reflect the state of the precursor, extent of reaction, or some form of integrated time and temperature. We argue above that differences in type do not translate directly into differences in temperature and that many types 4-6 chondrites experienced very similar thermal histories. This suggests that time at high temperature is not a likely source of variation, except perhaps among the type 4 chondrites where ferromagnesian silicates can still display substantial heterogeneity on a thin section scale (i.e., type 4 chondrites were exposed to variable peak temperatures and/or cooling rates up to and including those experienced by types 5-6). Differences in fluid pressures, especially of H_2O, can have a profound influence on crystal growth rates (e.g., Lofgren, 1980; and references therein). There is considerable speculation regarding fluids in chondrites parent bodies (e.g., McSween and Labotka, 1993). The partial pressures are poorly constrained though probably quite low (Mendybaev et al., 1996). We can therefore not reject the possibility that differences in type reflect in part differences in fluid pressures during metamorphism. Another similar possibility is that chondrites were hydrothermally altered and that some of the observed differences in type reflect this pretreatment. A

resolution of these issues lies beyond the scope of this study but our results suggest that a simple appeal to thermal metamorphism is insufficient.

Acknowledgements – This work was supported by NASA grant NAG–10423. Discussions with Mike Baker and Hap McSween inspired part of this work and led to significant improvements in the quality of this study. Ma Chi is thanked for his help with the analytical work and Paul Asimow for his help with the MELTS calculations. Thin sections were generously provided by the Smithsonian Institution, the Field Museum, and D. S. Burnett, Caltech.

REFERENCES

Armstrong J. T. (1988) Quantitative analysis of silicate and oxide materials: Comparison of Monte Carlo, ZAF, and $\phi(\rho Z)$ procedures. In *MicroBeam Analysis* (ed. D. E. Newbury), pp. 239-246. San Francisco Press, Inc.

Ballhaus C., Berry R. F., and Green D. H. (1991) High pressure experimental calibration of the olivine-orthopyroxene-spinel oxygen geobarometer: implications for the oxidation state of the upper mantle. *Contributions to Mineralogy and Petrology* **107**, 27-40.

Bennett M. E. and McSween H. Y. (1996) Revised model calculations for the thermal histories of ordinary chondrite parent bodies. *Meteoritics and Planetary Science* **31**, 783-792.

Berman R. G. (1988) Internally consistent thermodynamic data for minerals in the system Na_2O-K_2O-CaO-MgO-FeO-Fe_2O_3-Al_2O_3-SiO_2-TiO_2-H_2O-CO_2. *Journal of Petrology* **29**, 445-522.

Brearley A. J. and Jones R. H. (1998) Chondritic meteorites. In *Planetary materials*, Vol. 36 (ed. J. J. Papike), pp. 3-1 - 3-398. Mineralogical Society of America.

Brearley A. J., Scott E. R. D., Keil K., Clayton R. N., Mayeda T. K., Boynton W. V., and Hill D. H. (1989) Chemical, isotopic and mineralogical evidence for the origin of matrix in ordinary chondrites. *Geochimica et Cosmochimica Acta* **53**, 2081-2093.

Brearley A. J. (1990) Carbon-rich aggregates in type 3 ordinary chondrites: characterization, origin, and thermal history. *Geochimica et Cosmochimica Acta* **54**, 831-850.

Brett R. and Sato M. (1984) Intrinsic oxygen fugacity measurements on seven chondrites, a pallasite, and a tektite and the redox state of meteorite parent bodies. *Geochimica et Cosmochimica Acta* **48**, 111-120.

Buening D. K. and Buseck P. R. (1973) Fe-Mg lattice diffusion in olivine. *Journal of Geophysical Research* **78**, 6852-6862.

Bunch T. E., Keil K., and Snetsinger K. G. (1967) Chromite composition in relation to chemistry and texture of ordinary chondrites. *Geochimica et Cosmochimica Acta* **31**, 1569-1582.

Bunch T. E., Keil K., and Olsen E. (1970) Mineralogy and petrology of silicate inclusions in iron meteorites. *Contribution to Mineralogy and Petrology* **25**, 297-340.

Bunch T. E. and Olsen E. (1974) Restudy of pyroxene-pyroxene equilibration temperatures for ordinary chondrite meteorites. *Contributions to Mineralogy and Petrology* **43**, 83-90.

Byerly G. R., Jarosewich E., Mason B., and Clarke R. S. (1988) The Greenwell Springs LL4 chondrite: A new fall from Louisiana, USA. *Meteoritics* **23**, 359-360.

Christophe Michel-Levy M. and Deneise A. B. (1992) Dahmani, a highly oxidized LL6 chondrite bearing Ni-rich taenite. *Meteoritic and Planetary Sciences* **27**, 184-185.

Clayton R. N. (1993) Oxygen isotopes in meteorites. *Annual Review of Earth and Planetary Science* **21**, 115-149.

Clayton R. N. and Kieffer S. W. (1991) Oxygen isotopic thermometer calibrations. In *Stable Isotopic Geochemistry*, Vol. 3 (ed. H. P. Taylor Jr., J. R. O'Neill, and R. Kaplan). Geochemical Society Special Publication.

Colucci M. T. and Hewins R. H. (1984) Ordinary chondrite pyroxene thermometry - one more time (abstract). *Lunar and Planetary Science Conference,* **15**, 180-181.

Craig H. (1964) Petrological and compositional relationships in meteorites. In *Isotopic and Cosmic Chemistry* (eds. H. Craig, S. L. Miller, and G. J. Wasserburg), pp. 401-451. North-Holland.

Dodd R. T. (1969) Metamorphism of the ordinary chondrites: A review. *Geochimica et Cosmochimica Acta* **33**, 161-203.

Dodd R. T. (1981) *Meteorites, A petrologic-chemical synthesis*. Cambridge University Press.

Engi M. (1983) Equilibria involving Al-Cr spinel: Mg-Fe exchange with olivine. Experiments, thermodynamic analysis, and consequences for geothermometry. *American Journal of Science* **283A**, 29-71.

Fabriès J. (1979) Spinel-olivine geothermometry in peridotites from ultramafic complexes. *Contributions to Mineralogy and Petrology* **69**, 329-336.

Folco L., Mellini M., and Pillinger C. T. (1996) Unshocked equilibrated H-chondrites: A common low-temperature record from orthopyroxene iron-magnesium ordering. *Meteoritics and Planetary Science* **31**, 388-393.

Folco L., Mellini M., and Pillinger C. T. (1997) Equilibrated ordinary chondrites: Constraints for thermal history from iron-magnesium ordering in orthopyroxene. *Meteoritics and Planetary Science* **32**, 567-575.

Fredriksson K., Nelen J., and Fredriksson B. J. (1968) The LL-group chondrites. In *Origin and Distribution of the Elements* (ed. L. H. Ahrens), pp. 457-466. Pergamon Press.

Gastineau H. K. and McSween H. Y. (2001) A test for oxidation during metamorphism of L and LL group chondrites, and implications for asteroid spectroscopy (submitted to *Meteoritics*).

Ghiorso M. S. and Sack R. O. (1995) Chemical mass transfer in magmatic processes IV. A revised and internally consistent thermodynamic model for the interpolation and extrapolation of liquid-solid equilibria in magmatic systems at elevated temperatures and pressures. *Contributions to Mineralogy and Petrology* **119**, 197-212.

Göpel C., Manhès G., and Allègre C. J. (1994) U-Pb systematics of phosphates from equilibrated ordinary chondrites. *Earth and Planetary Science Letters* **121**, 153-171.

Grady M. M. (2000) *Catalogue of Meteorites: with specific reference to those represented in the collection of the Natural History Museum, London*. Cambridge University Press.

Harvey R. P., Benett M. L., and McSween H. Y. (1993) Pyroxene equilibrium temperatures in metamorphosed ordinary chondrites. (abstract). *Lunar and Planetary Science Conference,* **24**, 615-616.

Heyse J. V. (1978) The metamorphic history of LL-group ordinary chondrites. *Earth and Planetary Science Letters* **40**, 365-381.

Hutchison R., Barton J. C., and Pillinger C. T. (1991) The L6 chondrite fall at Glatton, England, 1991, May 5. *Meteoritics* **26**, 349.

Hutchison R., Bevan A. W. R., and Ashworth J. R. (1980) Thermal history of the H-group of chondritic meteorites. *Nature* **287**, 787-791.

Hutchison R., Bevan W. R., Easton A. J., and Agreli S. O. (1981) Mineral chemistry and genetic relations among H-group chondrites. *Proceedings of the Royal Society of London* **374**, 159-178.

Ishii T., Takeda H., and Yanai K. (1979) Pyroxene geothermometry applied to a three-pyroxene achondrite from Allan Hills, Antarctica and ordinary chondrites. *Mineralogical Journal* **9**, 460-481.

Jackson E. D. (1969) Chemical variation in coexisting chromite and olivine in chromitite zones of the Stillwater Complex. *Economic Geology, Monograph* **4**, 41-71.

Jarosewich E. and Dodd R. T. (1985) Chemical variations among L-chondrites - IV. Analyses, with petrographic notes, of 13 L-group and 3 LL-group chondrites. *Meteoritics* **20**, 23-36.

Jarosewich E. and Mason B. (1969) Chemical analyses with notes on one mesosiderite and seven chondrites. *Geochimica et Cosmochimica Acta* **33**, 411-416.

Johnson C. A. and Prinz M. (1991) Chromite and olivine in type II chondrules in carbonaceous and ordinary chondrites: Implications for thermal histories and group differences. *Geochimica et Cosmochimica Acta* **55**, 893-904.

Keil K. and Fredriksson K. (1964) The iron, magnesium, and calcium distribution in coexisting olivines and rhombic pyroxenes of chondrites. *Journal of Geophysical Research* **69**, 3487-3515.

Kleinschrot D. and Okrusch M. (1999) Mineralogy, petrography, and thermometry of the H5 chondrite Carcote, Chile. *Meteoritics and Planetary Science* **34**, 795-802.

Kretz R. (1961) Co-existing pyroxenes. *Geological Magazine* **98**, 344-345.

Kretz R. (1963) Distribution of magnesium and iron between orthopyroxene and calcic pyroxene in natural mineral assemblages. *Journal of Geology* **77**, 773-785.

Kurat G., Fredriksson B. J., and Nelen J. (1969) Der Meteorit von Siena. *Geochimica et Cosmochimica Acta* **33**, 765-773.

Larimer J. W. (1968) Experimental studies on the system Fe-MgO-SiO_2-O_2 and their bearing on the petrology of chondritic meteorites. *Geochimica et Cosmochimica Acta* **32**, 1187-1207.

Lasaga A. C. (1983) Geospeedometry: an extension of geothermometry. In *Kinetics and Equilibrium in Mineral Reactions*, Vol. 3 (ed. S. K. Saxena), pp. 81-114. Springer, New York Berlin Hiedelberg.

Lehmann J. (1983) Diffusion between olivine and spinel: application to geothermometry. *Earth and Planetary Science Letters* **64**, 123-138.

Lindsley D. H. (1983) Pyroxene thermometry. *American Mineralogist* **68**, 477-493.

Lindsley D. H. and Anderson D. J. (1983) A two-pyroxene thermometer. *Proceedings of the 13th Lunar and Planetary Science Conference, Journal of Geophysical Research, Supplement* **88**, A887-A906.

Lindsley D. H., King H. E., and Turnock A. C. (1974) Compositions of synthetic augite and hypersthene coexisting at 810°C: application to pyroxenes from lunar highlands rocks. *Geophysical Research Letters* **1**, 134-136.

Lofgren G. E. (1980) Experimental studies on the dynamic crystallization of silicate melts. In *Physics of Magmatic Processes* (ed. R. B. Hargraves), pp. 487-551. Princeton University Press.

MacKenzie W. S. (1957) The crystalline modifications of $NaAlSi_3O_8$. *American Journal of Science* **255**, 481-516.

Mason B. (1963) Olivine composition in chondrites. *Geochimica et Cosmochimica Acta* **27**, 1011-1023.

McCoy T. J., Casanova I., Keil K., and Wieler R. (1990) Classification of four ordinary chondrites from Spain. *Meteoritics* **25**, 77-79.

McSween H. Y. and Labotka T. C. (1993) Oxidation during metamorphism of the ordinary chondrites. *Geochimica et Cosmochimica Acta* **57**, 1105-1114.

McSween H. Y. and Patchen A. D. (1989) Pyroxene thermobarometry in LL-group chondrites and implications for parent body metamorphism. *Meteoritics* **24**, 219-226.

McSween H. Y., Sears D. W. G., and Dodd R. T. (1988) Thermal metamorphism. In *Meteorites and the Solar System* (ed. J. F. Kerridge and M. S. Matthews), pp. 102-113. The University of Arizona Press.

Mendybaev R. A., Beckett J. R., Grossman L., and Stolper E. (1996) Kinetics and mechanisms of volatilization of SiC and SiO_2 in the solar nebula (abstract). *Lunar and Planetary Science Conference,* **27**, 865-866.

Miyamoto M., Fuji N. and Takeda H. (1981) Ordinary chondrite parent body: An internal heating model. *Proceeding of the Lunar and Planetary Science Conference* **12**, 1145-1152.

Miyashiro A. (1962) Common occurrence of high temperature plagioclase in chondrites. *Japanese Journal of Geology and Geography* **33**, 235-237.

Mueller R. F. (1964) Phase equilibria and the crystallization of chondritic meteorites. *Geochimica et Cosmochimica Acta* **28**, 189-207.

O'Neill J. R. and Taylor Jr. H. P. (1967) The oxygen isotope and cation exchange chemistry of feldspars. *American Mineralogist* **52**, 1414-1437.

Olsen E. J. and Bunch T. E. (1984) Equilibrium temperatures of the ordinary chondrites: A new evaluation. *Geochimica et Cosmochimica Acta* **48**, 1363-1365.

Onuma N., Clayton R. N., and Mayeda T. K. (1972) Oxygen isotope temperatures of "equilibrated" ordinary chondrites. *Geochimica et Cosmochimica Acta* **36**, 157-168.

Ozawa K. (1984) Olivine-spinel geospeedometry: Analysis of diffusion-controlled Mg-Fe^{2+} exchange. *Geochimica et Cosmochimica Acta* **48**, 2597-2611.

Pellas P. and Fiéni C. (1988) Thermal histories of ordinary chondrite parent asteroids. (abstract). *Lunar and Planetary Science Conference,* **29**, 915-916.

Pellas P. and Storzer D. (1981) ^{244}Pu fission track thermometry and its implication to stony meteorites. *Proceedings of the Royal Society of London* **374**, 253-270.

Rubin A. E. (1990) Kamacite and olivine in ordinary chondrites: Intergroup and intragroup relationships. *Geochimica et Cosmochimica Acta* **54**, 1217-1232.

Rubin A. E. (1992) A shock-metamorphic model for silicate darkening and compositionally variable plagioclase in CK and ordinary chondrites. *Geochimica et Cosmochimica Acta* **56**, 1705-1714.

Sack R. O. and Ghiorso M. S. (1989) Importance of considerations of mixing properties in establishing an internally consistent thermodynamic database: thermochemistry of minerals in the system Mg_2SiO_4-Fe_2SiO_4-SiO_2. *Contributions to Mineralogy and Petrology* **102**, 41-68.

Sack R. O. and Ghiorso M. S. (1991a) An internally consistent model for the thermodynamic properties of Fe-Mg titanomagnetite-aluminate spinels. *Contribution to Mineralogy and Petrology* **106**, 474-505.

Sack R. O. and Ghiorso M. S. (1991b) Chromium spinels as petrogenetic indicators: thermodynamics and petrological applications. *American Mineralogist* **76**, 827-847.

Saxena S. K. (1976) Two-pyroxene geothermometer: a model with an approximate value. *American Mineralogist* **61**, 643-652.

Scott E. R. D., Lusby D., and Keil K. (1985) Ubiquitous brecciation after metamorphism in equilibrated ordinary chondrites. *Proceeding of the 16th Lunar and Planetary Science Conference, Journal of Geophysical Research, Supplement* **90,** D137-D148.

Scott E. R. D. and Rajan R. S. (1981) Metallic minerals, thermal histories and parent bodies of some xenolithic, ordinary chondrite meteorites. *Geochimica et Cosmochimica Acta* **45**, 53-67.

Scott E. R. D., Taylor J. R., and Keil K. (1986) Accretion, metamorphism, and brecciation of ordinary chondrites: evidence from petrologic studies of meteorites from Roosevelt County, New Mexico. *Proceedings of the 17th Lunar and Science Conference* **91**, E115-E123.

Sears W., Grossman J. N., Melcher C. L., Ross L. M., and Mills A. A. (1980) Measuring metamorphic history of unequilibrated ordinary chondrites. *Nature* **287**, 791-795.

Sears D. W. G., Morse A. D., Hutchison R., Guimon R. K., Jie L., Alexander C. M. O. D., Benoit P. H., Wright I., Pillinger C., Xie T., and Lipschutz M. E. (1995) Metamorphism and aqueous alteration in low petrographic type ordinary chondrites. *Meteoritics* **30**, 169-181.

Snetsinger K. G., Keil K., and Bunch T. E. (1967) Chromite from "equilibrated" chondrites. *American Mineralogist* **52**, 1322-1331.

Stöffler D., Keil K., and Scott E. R. D. (1991) Shock metamorphism of ordinary chondrites. *Geochimica et Cosmochimica Acta* **55**, 3845-3867.

Taylor G. J., Maggiore P., Scott E. R. D., Rubin A. E., and Keil K. (1987) Original structures, and fragmentation and reassembly histories of asteroids: evidence from meteorites. *Icarus* **69**, 1-13.

Williams R. J. (1971) Equilibrium temperatures, pressures, and oxygen fugacities of the equilibrated chondrites. *Geochimica et Cosmochimica Acta* **35**, 407-411.

Wood J. A. (1967) Chondrites: their metallic minerals, thermal histories, and parent planets. *Icarus* **6**, 1-49.

Van Schmus W. R. and Ribbe P. H. (1968) The composition and structure state of feldspar from chondritic meteorites. *Geochimica et Cosmochimica Acta* **32**, 1327-1342.

Van Schmus W. R. and Koffman D. M. (1967) Equilibration temperatures of iron and magnesium in chondritic meteorites. *Science* **155**, 1009-1011.

Van Schmus W. R. and Wood J. A. (1967) A chemical-petrologic classification for the chondritic meteorites. *Geochimica et Cosmochimica Acta* **31**, 747-765.

Yamaguchi A., Scott E. R. D., and Keil K. (1998) Origin of unusual impact melt rocks Yamato-790964 and -790143 (LL-chondrites). *Antarctic Meteorite Research* **11**, 18-31.

Table 1. Ordinary chondrites examined in this study

Meteorite	Class	shock stage[a]	Find/Fall	Thin section[b]
Avanhandava[c]	H4	S2[1]	Fall	USNM 6882-1
Phum-Sambo	H4	S1[2]	Fall	ME2665
Allegan[c]	H5	S1[1]	Fall	USNM 953-2
Guareña[c]	H6	S1[1]	Fall	USNM M69-1
Saratov	L4	S2[1]	Fall	ME2673
Ausson	L5	S2[1]	Fall	ME271
Glatton	L6	S3[2]	Fall	M3-1
Greenwell Springs[c]	LL4	S3[3]	Find	USNM 6379-2
Siena	LL5	S3[2]	Fall	ME1699
Tuxtauc[c]	LL5	S2[1]	Fall	ME2850
Saint Séverin[c]	LL6	S3[3]	Fall	MQM800

[a] Source of shock stage estimates: 1-Grady (2000). 2-This study based on criteria given in Stöffler et al. (1991). 3-Gastineau and McSween, 2001.

[b]Source of thin-section: USNM-Smithonian Institution, National Museum of Natural History. ME-Field Museum, Chicago. M3-1, MQM800–D. S. Burnett, Caltech.

[c]Thin sections studied by H. McSween.

Table 2a. Olivine compositions (wt%) in the equilibrated ordinary chondrites studied in this work

	Avanhandava	Phum-Sambo	Allegan	Guareña	Saratov	Ausson	Glatton	Greenwell Spr.	Siena	Tuxtauc	St. Séverin
class	H4	H4	H5	H6	L4	L5	L6	LL4	LL5	LL5	LL6
#[a]	5/15	7/23	4/17	8/30	4/21	3/21	6/24	6	4/18	7/39	6/27
SiO_2	39.84(27)[b]	38.97(60)	39.65(61)	39.22(9)	38.46(15)	37.83(7)	39.21(16)	37.77(35)	38.15(72)	37.09(37)	37.22(39)
Cr_2O_3	0.04(3)	0.18(22)	0.11(10)	0.31(29)	0.17(5)	0.13(10)	0.19(13)	0.19(13)	BDL[f]	0.27(12)	0.26(29)
FeO[c]	16.86(38)	17.22(49)	16.07(22)	17.00(69)	21.29(28)	22.41(17)	21.59(62)	25.41(12)	23.80(54)	26.50(20)	25.61(111)
MgO	43.25(21)	42.23(95)	43.72(104)	42.45(56)	39.13(19)	37.99(27)	40.19(67)	35.51(45)	37.63(98)	34.50(27)	35.18(99)
MnO	0.45(2)	0.46(2)	0.47(2)	0.45(2)	0.46(2)	0.46(1)	0.49(2)	0.45(3)	0.46(2)	0.46(1)	0.43(3)
Total	100.44	99.06	100.02	99.43	99.51	98.81	101.67	99.35	99.05	98.82	98.69
Fa[d]	0.179(4)	0.186(4)	0.178(4)	0.183(8)	0.234(3)	0.249(1)	0.232(8)	0.286(2)	0.254(5)	0.301(2)	0.292(9)
Fa[e]	0.17-0.18	0.19	0.17-0.19	0.19-0.20	0.23-0.24	0.24-0.25	0.24	0.28-0.29	0.27-0.29	0.30-0.31	0.29-0.30

[a] x/y-x refers to the number of grains analyzed, y refers to the total number of analyses. Points were analyzed randomly in the central regions of grains.

[b]Numbers enclosed in parentheses indicate standard deviations of the distribution of average grain compositions.

[c]FeO listed is all Fe expressed as FeO.

[d]Mole fraction of end-member fayalite (Fa) for this study calculated based on four oxygens assuming all Fe to be Fe^{2+}.

[e]Range of compositions for literature sources (Byerly et al., 1988; Gastineau and McSween, 2001; Hutchison et al., 1991; Jarosewich and Dodd, 1985; Jarosewich and Mason, 1969; Keil and Fredriksson, 1964; Kurat et al., 1969; Mason, 1963; McCoy et al., 1990; Rubin, 1990).

[f]BDL – Below Detection Limit.

Table 2b. Spinel compositions (wt%) in the equilibrated ordinary chondrites studied in this work

	Avanhandava	Phum-Sambo	Allegan	Guareña	Saratov	Ausson	Glatton	Greenwell Spr.	Siena	Tuxtauc	St. Séverin
class	H4	H4	H5	H6	L4	L5	L6	LL4	LL5	LL5	LL6
#[a]	6/41	8/58	7/32	8/41	5/22	5/27	7/40	6/37	4/20	7/31	7/38
TiO_2	1.54(14)[b]	1.50(19)	1.85(22)	2.02(14)	1.55(6)	1.88(49)	2.34(21)	1.75(25)	2.01(24)	3.05(44)	3.85(11)
Cr_2O_3	56.87(64)	56.12(52)	56.36(98)	56.86(47)	58.05(14)	55.14(125)	56.24(27)	55.51(115)	55.11(104)	53.51(20)	52.90(42)
V_2O_3	0.01(1)	0.73(4)	0.70(2)	0.70(3)	0.74(2)	0.73(6)	0.73(3)	0.05(5)	0.03(3)	0.72(1)	0.64(2)
Al_2O_3	6.63(18)	6.74(18)	7.12(100)	6.59(16)	3.72(10)	6.17(31)	6.09(16)	6.25(48)	6.15(47)	6.11(24)	5.28(4)
FeO[c]	28.53(47)	29.05(39)	27.71(33)	28.42(35)	30.26(29)	30.48(69)	29.82(31)	31.00(19)	31.00(59)	31.81(43)	32.30(39)
MgO	3.20(19)	2.99(15)	3.21(38)	3.24(21)	1.81(7)	2.44(32)	2.29(20)	1.72(12)	2.16(21)	2.08(6)	2.04(28)
MnO	BDL[g]	0.96(4)	1.00(3)	0.91(6)	0.78(2)	0.72(2)	0.75(3)	BDL	0.16(26)	0.57(1)	0.62(1)
total	96.79	98.04	97.95	98.74	96.91	97.56	98.25	96.31	97.36	97.85	97.62
Sp[d]	0.024(1)	0.023(1)	0.025(1)	0.024(1)	0.008(0)	0.017(2)	0.016(1)	0.013(0)	0.016(1)	0.014(1)	0.012(2)
Her	0.115(4)	0.120(3)	0.123(16)	0.116(4)	0.074(2)	0.116(8)	0.114(4)	0.122(11)	0.118(10)	0.118(5)	0.103(2)
Chr	0.663(8)	0.672(9)	0.663(4)	0.669(8)	0.772(3)	0.695(23)	0.704(7)	0.726(6)	0.704(9)	0.691(5)	0.689(12)
PChr	0.140(8)	0.130(7)	0.138(13)	0.137(9)	0.087(3)	0.104(12)	0.098(8)	0.076(5)	0.093(8)	0.083(2)	0.080(11)
Ulv	0.034(3)	0.034(4)	0.041(4)	0.045(3)	0.039(2)	0.045(11)	0.056(4)	0.043(6)	0.049(5)	0.075(10)	0.095(3)
Qan	0.007(1)	0.007(1)	0.009(2)	0.009(1)	0.004(0)	0.007(2)	0.008(1)	0.005(1)	0.007(1)	0.009(1)	0.011(1)
Mgt	0.016(7)	0.0146(6)	0.001(1)	0.001(1)	0.016(3)	0.016(9)	0.005(2)	0.016(5)	0.014(5)	0.011(3)	0.010(4)
Chr[e]			0.69						0.54-0.73		
Size (μm)[f]	43.2(185)	39.8(104)	72.8(449)	74.3(447)	26.5(47)	51.4(307)	54.6(218)	42.0(200)	53.9(95)	51.7(172)	50.1(82)

[a] x/y-x refers to the number of grains analyzed, y refers to the total number of analyses. Points were analyzed randomly in the central regions of grains.

[b]Numbers enclosed in parentheses indicate standard deviations of the distribution of average grain compositions.

[c]All Fe expressed as FeO.

[d]Mole fraction of end-member spinel ($MgAl_2O_4$; Sp), hercynite ($FeAl_2O_4$; Her), chromite ($FeCr_2O_4$; Chr), picrochromite ($MgCr_2O_4$; PChr), ulvöspinel (Fe_2TiO_4; Ulv), qandelite (Mg_2TiO_4; Qan), and magnetite (Fe_3O_4; Mgt) were calculated based on mass and charge balance.

[e]Range of compositions from the literature (Bunch et al., 1967; Kurat et al. 1969).

[f]Grain size is the average of 15 measurements of the minimum dimension of spinel grains in a thin section.

[g]BDL – Below Detection Limit.

Table 2c. Pyroxene compositions (wt%) in the equilibrated ordinary chondrites studied in this work

	Avanhandava	Phum-Sambo	Allegan	Guareña	Saratov	Ausson	Glatton	Greenwell Spr.	Siena	Tuxtauc	St. Séverin
class	H4	H4	H5	H6	L4	L5	L6	LL4	LL5	LL5	LL6
#[a]	6/26	8/47	6/34	8/40	5/15	4/26	6/37	5/14	4/13	6/26	7/39
SiO_2	56.48(29)[b]	56.36(89)	56.35(64)	56.05(15)	55.89(33)	55.39(86)	56.84(7)	55.08(39)	54.93(90)	54.36(46)	54.92(37)
TiO_2	0.16(3)	0.14(6)	0.19(1)	0.19(2)	0.07(3)	0.20(1)	0.19(2)	0.18(5)	0.13(4)	0.19(3)	0.20(3)
Cr_2O_3	0.30(29)	0.26(15)	0.36(17)	0.36(12)	0.35(20)	0.25(8)	0.32(10)	0.16(6)	0.16(8)	0.36(21)	0.35(26)
Al_2O_3	0.31(26)	0.18(12)	0.18(3)	0.17(1)	0.19(16)	0.21(10)	0.14(1)	0.36(20)	0.25(27)	0.13(2)	0.16(0)
FeO[c]	11.05(41)	11.11(95)	10.50(18)	11.23(8)	12.62(119)	14.27(93)	13.58(16)	15.39(51)	14.43(67)	16.10(54)	15.94(39)
MgO	30.92(33)	30.39(41)	31.10(55)	30.29(11)	29.79(45)	28.08(32)	29.64(17)	27.24(38)	27.78(71)	26.73(29)	26.68(12)
MnO	0.50(1)	0.49(3)	0.48(1)	0.50(2)	0.43(6)	0.48(1)	0.50(2)	0.46(2)	0.48(2)	0.45(1)	0.45(1)
CaO	0.68(9)	0.98(7)	0.70(4)	0.68(7)	0.50(15)	0.87(8)	0.82(7)	0.59(11)	0.71(5)	0.73(9)	0.85(5)
total	100.40	100.02	99.85	99.47	99.85	99.74	102.04	99.47	99.02	99.06	99.55
Fs[d]	0.171(5)	0.165(7)	0.166(2)	0.176(1)	0.196(15)	0.217(1)	0.207(3)	0.247(16)	0.221(5)	0.251(2)	0.252(5)
Wo	0.013(2)	0.011(1)	0.013(1)	0.013(1)	0.010(3)	0.017(2)	0.015(1)	0.012(2)	0.014(1)	0.015(2)	0.017(1)
Fs[e]			0.16	0.17-0.18	0.24		0.21	0.23-0.24	0.24-.0.27	0.24-0.25	0.24-0.25

[a] x/y-x refers to the number of grains analyzed, y refers to the total number of analyses. Points were analyzed randomly in the central regions of grains.

[b]Numbers enclosed in parentheses indicate standard deviations of the distribution of average grain compositions.

[c]All Fe expressed as FeO.

[d]Mole fraction of end-members ferrosilite (Fs) and wollastonite (Wo) were calculated based on six oxygens assuming all Fe as Fe^{2+}.

[e]Range of compositions found in literature (Bunch and Olsen, 1974; Byerly et al., 1988; Folco et al., 1997; Gastineau and McSween, 2001; Hutchison et al., 1991; Keil and Fredriksson, 1964; Kurat et al., 1969; McCoy et al., 1990; McSween and Patchen, 1989).

Table 2d. Feldspar compositions (wt%) in the equilibrated ordinary chondrites studied in this work

	Avanhandava	Allegan	Guareña	Saratov	Ausson	Glatton	Greenwell Spr.	Tuxtauc	St. Séverin
class	H4	H5	H6	L4	L5	L6	LL4	LL5	LL6
#[a]	8	5	9	4	9	7	8	5	10
SiO_2	65.63(26)[b]	65.10(27)	65.25(28)	67.86(91)	66.27(88)	65.20(104)	64.30(76)	65.69(62)	65.34(9)
Al_2O_3	21.44(28)	21.08(17)	21.39(1)	19.80(43)	22.77(26)	21.32(36)	20.68(85)	20.73(57)	21.16(1)
CaO	2.44(15)	2.42(16)	2.58(1)	0.25(6)	2.30(14)	2.05(9)	1.76(15)	2.09(62)	2.30(11)
Na_2O	11.03(4)	11.08(3)	10.91(7)	11.00(228)	4.91(131)	10.54(130)	10.78(100)	11.27(52)	11.26(13)
K_2O	1.05(9)	1.12(12)	1.02(11)	1.37(149)	0.47(10)	1.68(128)	0.85(20)	0.83(21)	0.78(10)
total	101.68	100.90	101.33	100.30	97.19	100.79	98.51	100.88	101.17
Ab[c]	0.844(1)	0.843(0)	0.839(6)	0.902(94)	0.737(37)	0.822(76)	0.874(15)	0.878(8)	0.863(10)
An	0.103(6)	0.099(3)	0.110(0)	0.012(4)	0.209(23)	0.089(7)	0.079(1)	0.080(15)	0.097(5)
An[d]		0.12-0.27	0.12-0.13						0.10
Size (μm)[e]	17.8(93)	21.0(67)	56.8(179)	11.4(31)	27.6(94)	56.0(183)	8.7(27)	14.1(41)	43.4(125)

[a]Number of grains analyzed, one analysis per grain. Points were analyzed randomly in the center of grains.

[b]Numbers enclosed in parentheses indicate standard deviations of the distribution of average grain compositions.

[c]Mole fraction of end-members albite (Ab) and anorthite (An) were calculated based on 8 oxygens assuming all Fe as Fe^{2+}.

[d]Range of compositions from literature sources (Rubin, 1992; Van Schmus and Ribbe, 1968).

[e]Grain size is the average of 15 measurements of the maximum dimension of feldspar grains in a thin section.

Table 3. Olivine-spinel equilibration temperatures

Meteorite	Class	Average temperatures (°C)	Range of temperatures (°C)	# of pairs
Avanhandava	H4	769(24)[a]	728-791	7
Phum-Sambo	H4	760(21)	735-800	7
Allegan	H5	787(27)	747-806	4
Guareña	H6	796(19)	768-820	8
Saratov	L4	680(15)	659-694	4
Ausson	L5	756(66)	691-823	3
Glatton	L6	749(29)	708-773	6
Greenwell Springs	LL4	713(9)	701-724	6
Siena	LL5	735(42)	692-786	4
Tuxtauc	LL5	771(7)	761-781	7
Saint Séverin	LL6	771(41)	734-829	5

[a] Numbers enclosed in parentheses indicate one standard deviation of the distribution of measurements.

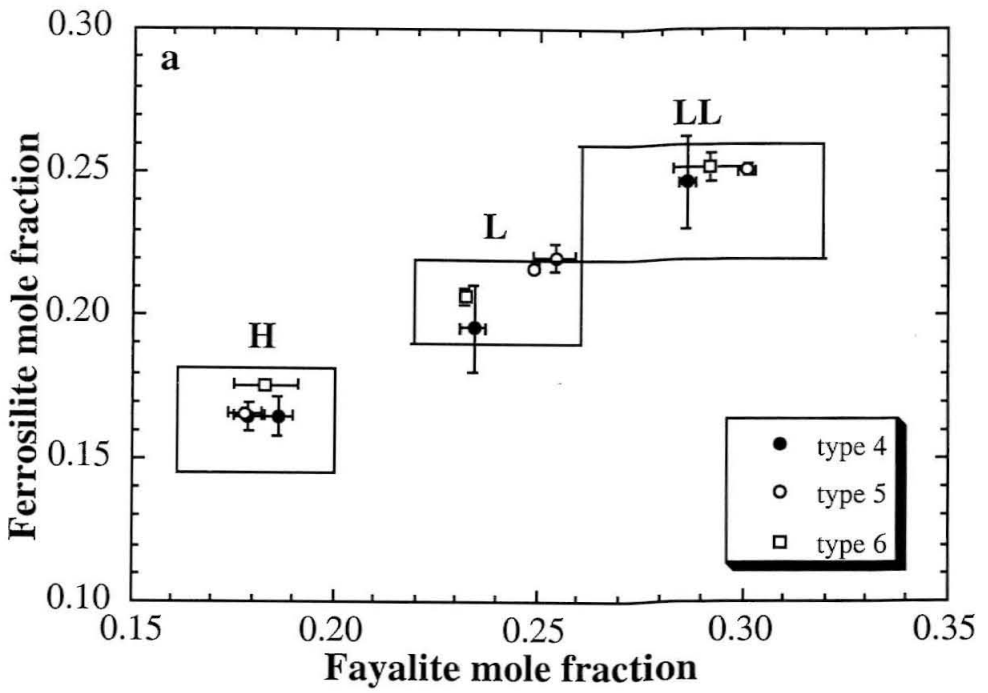
a
H
L
LL
type 4
type 5
type 6
Ferrosilite mole fraction
Fayalite mole fraction
0.10
0.15
0.20
0.25
0.30
0.35

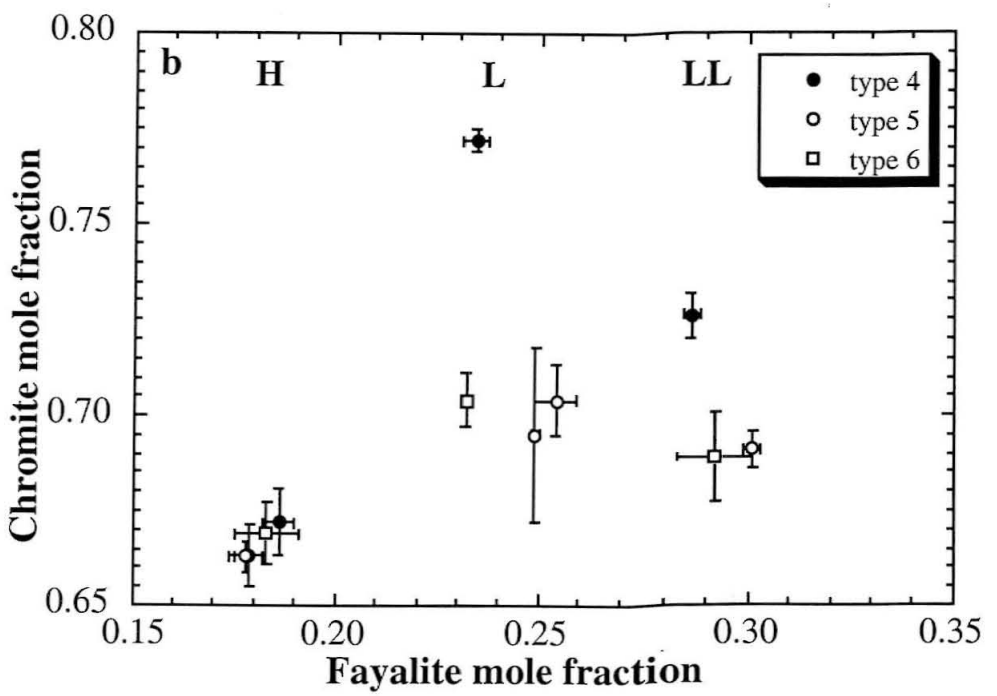
b
H
L
LL
type 4
type 5
type 6
Chromite mole fraction
Fayalite mole fraction
0.65
0.70
0.75
0.80
0.15
0.20
0.25
0.30
0.35

Figure 1. (a) Fayalite (Fa) versus ferrosilite (Fs) content of olivine and low-Ca pyroxenes in equilibrated ordinary chondrites analyzed in this work superimposed on composition fields for H, L, and LL class chondrites from Fredriksson et al. (1968). (b) Fayalite content of olivine versus chromite (Chr) in spinel in equilibrated ordinary chondrites types 4-6 analyzed in this work. The uncertainties in these and subsequent figures represent one standard deviation of the distribution of measurements in each meteorite.

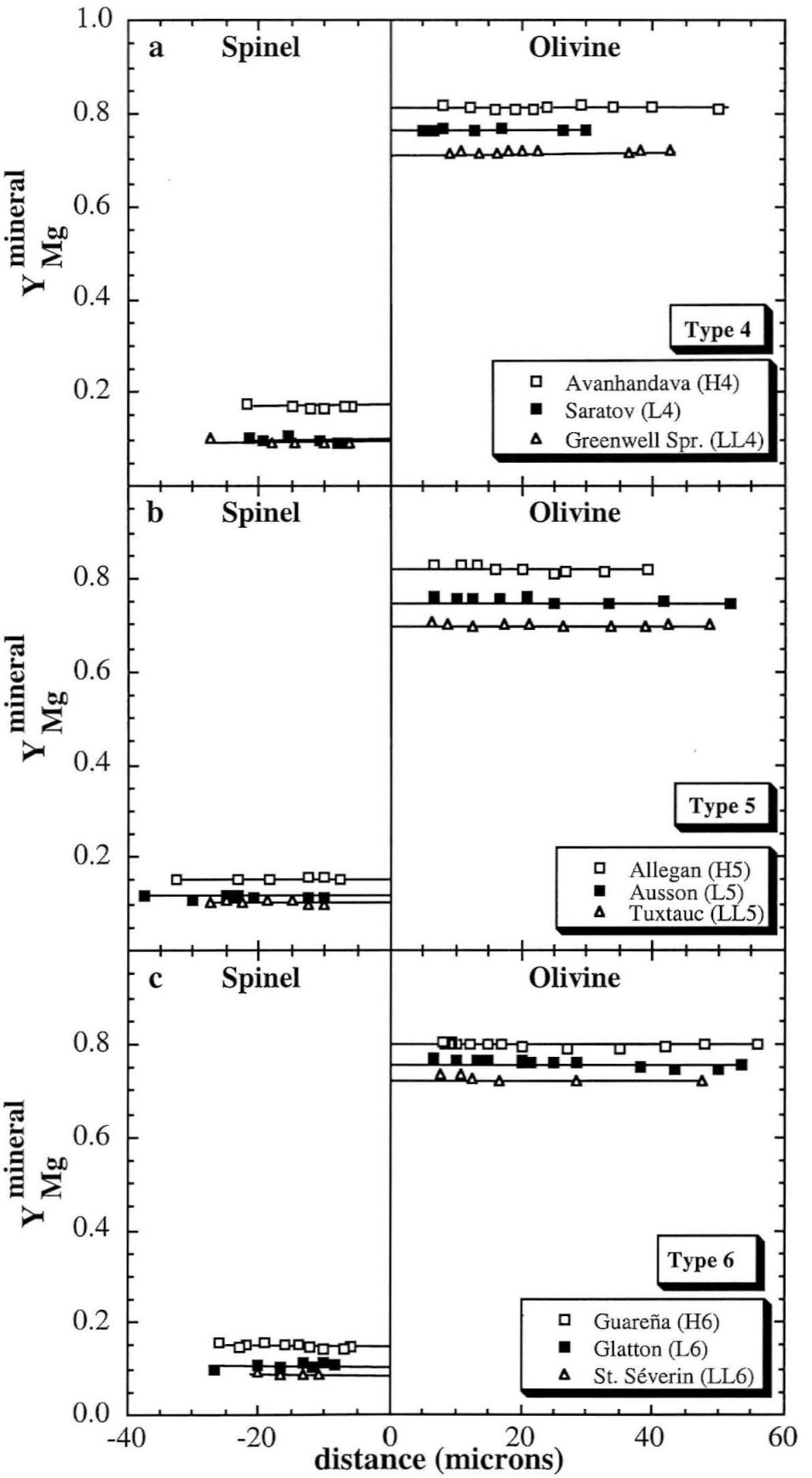
a
Spinel
Olivine
b
Spinel
Olivine
c
Spinel
Olivine
$Y^{mineral}_{Mg}$
1.0
0.8
0.6
0.4
0.2
0.0
Type 4
Avanhandava (H4)
Saratov (L4)
Greenwell Spr. (LL4)
Type 5
Allegan (H5)
Ausson (L5)
Tuxtauc (LL5)
Type 6
Guareña (H6)
Glatton (L6)
St. Séverin (LL6)
-40
-20
0
20
40
60
distance (microns)

Figure 2. $Y_{Mg}^{mineral}$ [molar Mg/(Mg+Fe^{2+})] along a traverse across adjacent olivine and spinel crystals as a function of distance (in μm) from the interface between the two grains. Error bars in $Y_{Mg}^{mineral}$ are approximately equal to the size of the symbols. (a) Type 4 ordinary chondrites. (b) Type 5 ordinary chondrites. (c) Type 6 ordinary chondrites.

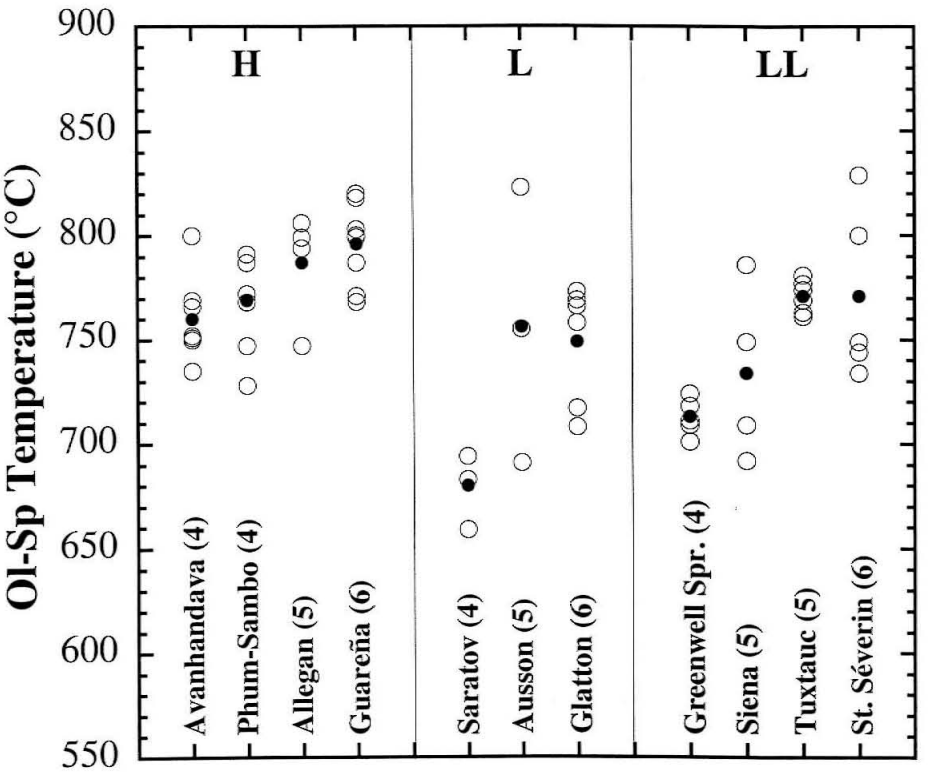

Figure 3. Equilibration temperatures for the equilibrated ordinary chondrites as recorded by olivine-spinel Fe-Mg exchange. Open circles are the temperatures calculated for each olivine-spinel pair in each meteorite. Filled circles represent the average temperature for each meteorite.

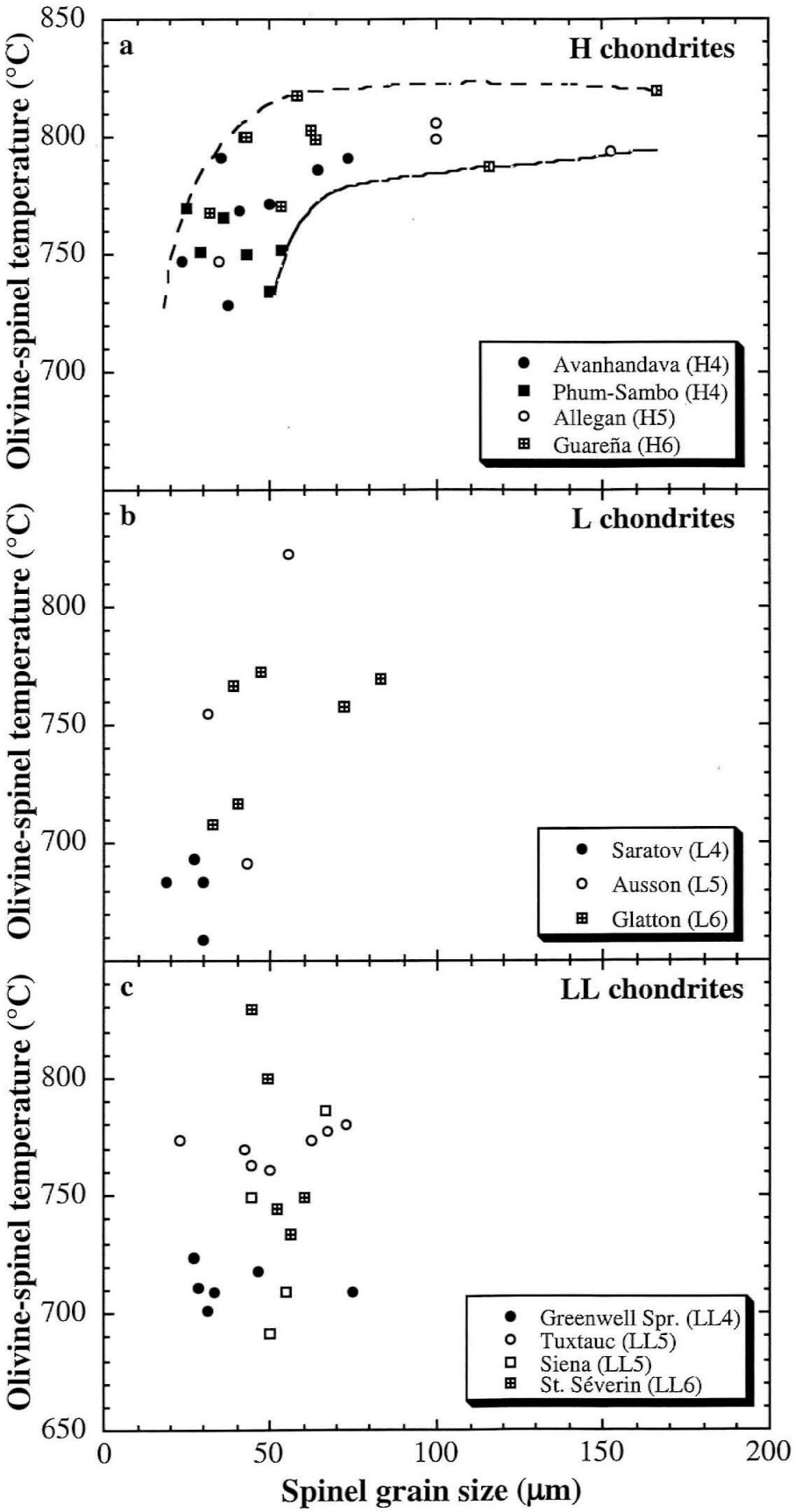
a
H chondrites
Avanhandava (H4)
Phum-Sambo (H4)
Allegan (H5)
Guareña (H6)
b
L chondrites
Saratov (L4)
Ausson (L5)
Glatton (L6)
c
LL chondrites
Greenwell Spr. (LL4)
Tuxtauc (LL5)
Siena (LL5)
St. Séverin (LL6)
Olivine-spinel temperature (°C)
850
800
750
700
650
0
50
100
150
200
Spinel grain size (μm)

Figure 4. Calculated olivine-spinel equilibration temperatures versus minimum distance across the spinel grain in the plane of the thin section. (a) H chondrites. The thick curves envelop the data. (b) L chondrites. (c) LL chondrites.

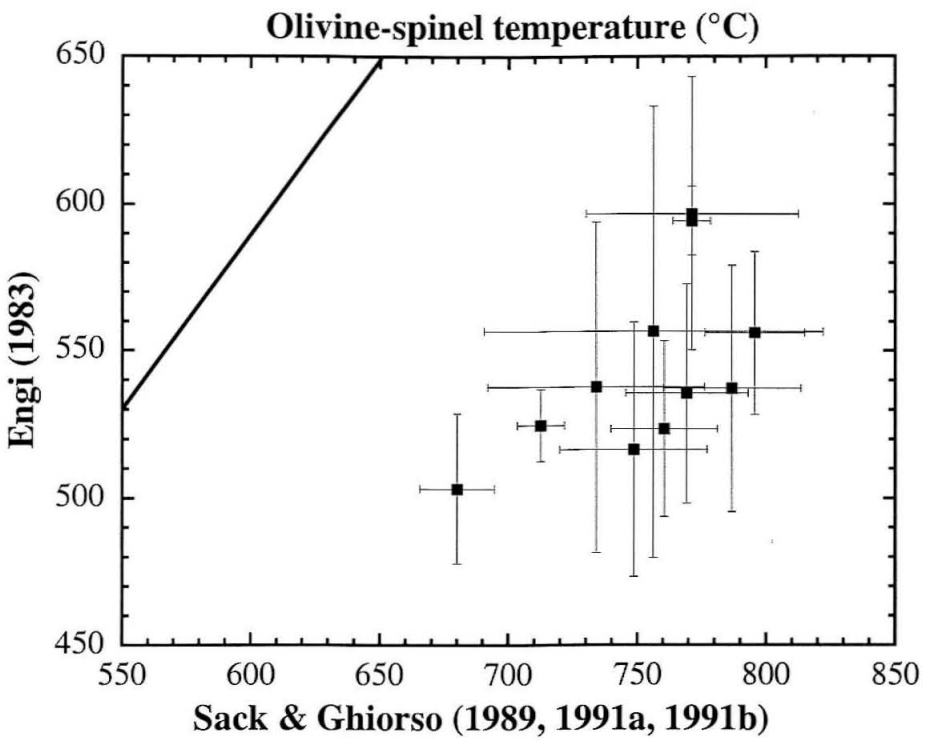

Figure 5. Average olivine-spinel equilibration temperatures for the equilibrated ordinary chondrites analyzed in this work calculated using a formulation by Engi (1983) compared to values calculated using the formulation of Sack and Ghiorso (1989, 1991a,b). Error bars are one standard deviation of the distribution of temperatures in each meteorite. The solid line represents a 1:1 line.

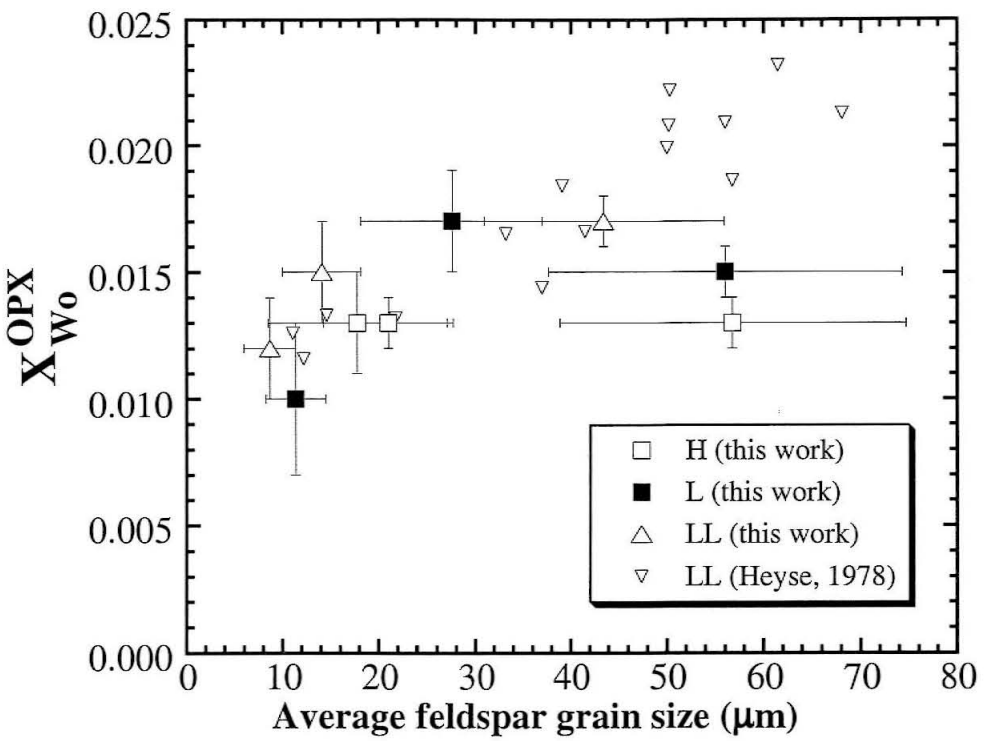

Figure 6. Average wollastonite (Wo) content in low-Ca pyroxenes, X_{Wo}^{OPX}, versus average feldspar grain size in each meteorite. Also shown are results given by Heyse (1978) for LL chondrites.

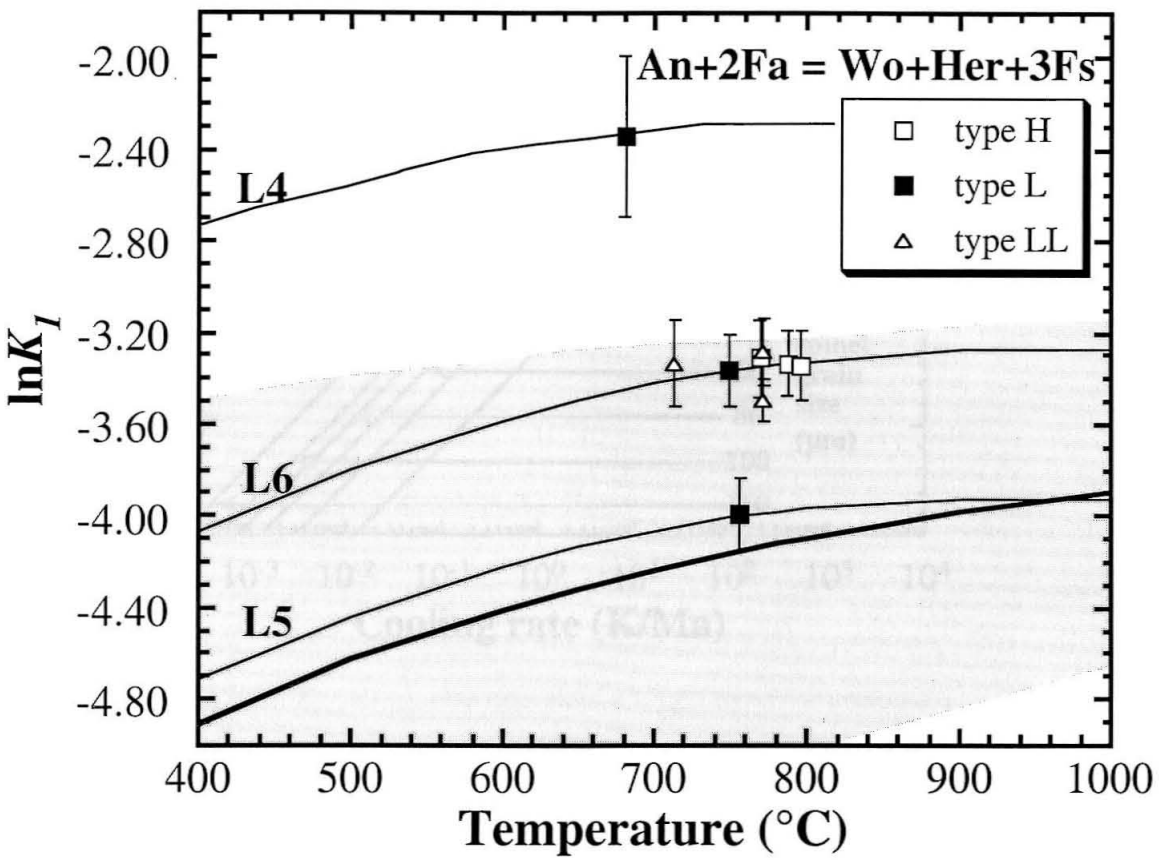

Figure 7. $\ln K_1$ as a function of temperature. The bold curve and shaded field represent $\ln K_1$ for the end-member components, taking into account uncertainties on the free energy of reaction. The lighter curves show the change in $\ln K_1$ with temperature for L chondrites if the average mineral compositions are held constant. Individual symbols denote values of $\ln K_1$ located at the mean olivine-spinel equilibrium temperature for each meteorite. Error bars are one standard deviation calculated by propagating uncertainties on composition only.

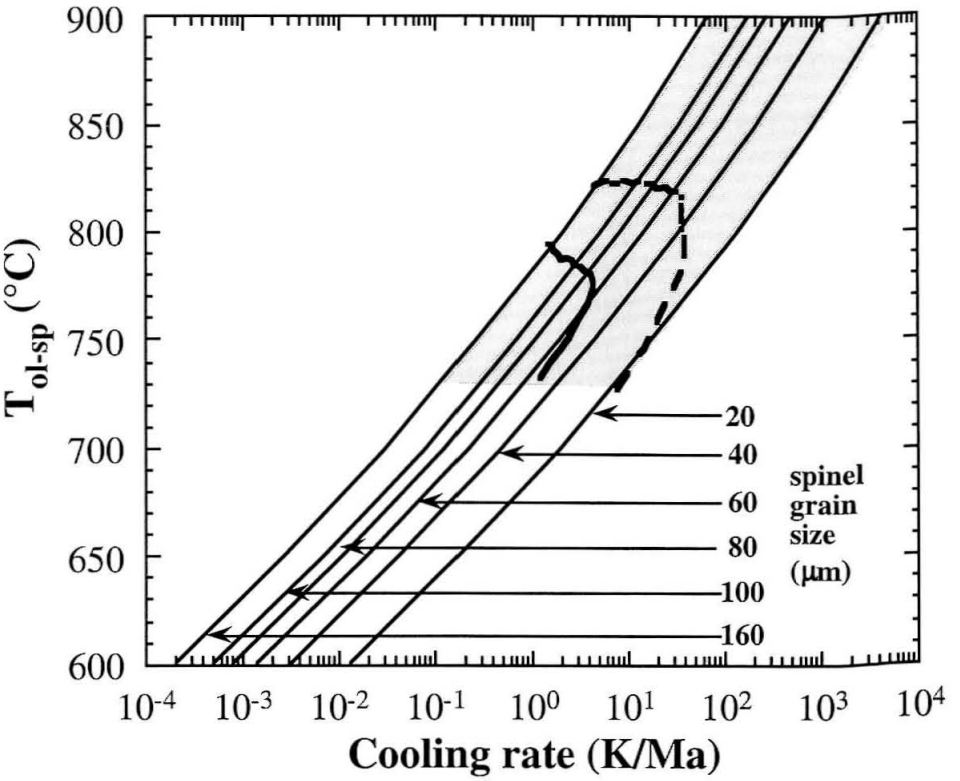
900
850
800
750
700
650
600
T_{ol-sp} (°C)
20
40
60
80
100
160
spinel grain size (μm)
10^{-4} 10^{-3} 10^{-2} 10^{-1} 10^{0} 10^{1} 10^{2} 10^{3} 10^{4}
Cooling rate (K/Ma)

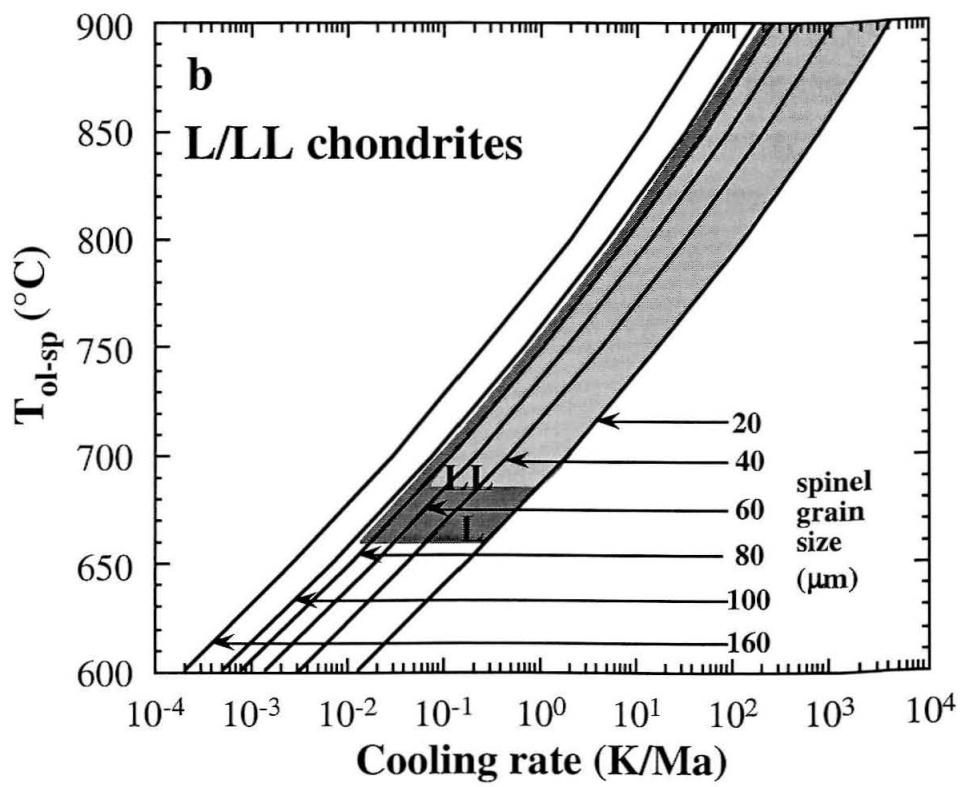
b
L/LL chondrites
900
850
800
750
700
650
600
T_{ol-sp} (°C)
LL
L
20
40
60
80
100
160
spinel grain size (μm)
10^{-4} 10^{-3} 10^{-2} 10^{-1} 10^{0} 10^{1} 10^{2} 10^{3} 10^{4}
Cooling rate (K/Ma)

Figure 8. Calculated cooling rates at a range of equilibration temperatures, $T_{ol\text{-}sp}$, for the Fe-Mg closure temperature between olivine-spinel according to the model of Lasaga (1983) that are required for complete re-equilibration of spinels of a given grain size (minimum distance across the grain in the plane of the thin section). The grains are assumed to cool from $T_{max}>T_{ol\text{-}sp}$ at a rate slow enough to allow continues re-equilibration to some temperature $T_{ol\text{-}sp}$ at which point, the profile is effectively frozen in. The shaded boxes represent estimated cooling rates experienced by the chondrites in each group at temperature range $T_{ol\text{-}sp}$(chondrite)-900°C . (a) H chondrites. The thick curves represent the envelope of data from Fig. 4a. (b) L and LL chondrites.

Chapter 4. The activity of chromite in multicomponent spinels. Part II: Implications for the metamorphic history of equilibrated H chondrites

Abstract—Activities of chromite in multicomponent spinels whose compositions represent spinels in H chondrites were experimentally determined by equilibrating Pt-alloys with the spinels at known temperature and f_{O_2}, and found to be similar within errors to literature evaluation. Combined with activities of the ferromagnesian silicates and alloy, evaluated from literature formulations, temperature-f_{O_2} relationships were determined for two assemblages, olivine-pyroxene-alloy and spinel-alloy, in each meteorite. Previously determined olivine-spinel equilibration temperatures were used to constrain the absolute f_{O_2}.

$\mathrm{Log}_{10} f_{O_2}$ values based on the assemblage olivine-pyroxene-alloy are –1.75±0.02 log units below Iron-Wüstite (IW) buffer, regardless of petrographic type. The $\log_{10} f_{O_2}$ values calculated based on the alloy-spinel coexistence are at least ~1.5 log units more oxidizing than those based on the olivine-pyroxene-alloy if olivine-spinel equilibration temperatures (728-820°C) are assumed. This probably indicates that closure for spinel-alloy equilibria occurred under retrograde conditions at temperatures below 700°C.

1. INTRODUCTION

The ordinary chondrites are classified into three chemically distinct groups, H, L, and LL, each of which is further subdivided into petrographic types ranging from 3 (least equilibrated) to 7 (most equilibrated) based on differences in texture and the degree of

chemical homogeneity (Van Schmus and Wood, 1967). Estimating the metamorphic conditions experienced by these meteorites is fundamental to understanding the evolution of fluids and the thermal and structural histories of the parent bodies (e.g., Bennett and McSween, 1996; McSween and Labotka, 1993; Miyamoto et al., 1981).

The oxygen fugacity is a key measure of physical conditions during metamorphism. Metal is ubiquitous in ordinary chondrites implying reducing conditions and qualitatively, a general increase in the ratio of bulk oxidized to metallic iron from H to L to LL chondrites suggests increasing oxidation, H chondrites being the most reduced and LL the least reduced (e.g., Dodd, 1969; Fredriksson et al., 1968). Possible variations in relative oxidation states within each group have also been suggested based on systematic changes in the composition and abundance of Fe-bearing phases (e.g., Dodd, 1969; Fredriksson et al., 1968; Larimer, 1968; McSween and Labotka, 1992; Mueller, 1964; Rubin et al., 1988; Williams, 1971).

In a few studies the oxygen fugacity has been calculated explicitly. There is general agreement that oxygen fugacities during metamorphism of ordinary chondrites were near or below those of the Iron-Wüstite (IW) buffer but the results are inconsistent in detail. Brett and Sato (1984) measured intrinsic oxygen fugacities in type 3 to type 6 H, L, and LL chondrites and found that increasing metamorphism in the equilibrated ordinary chondrites was accompanied by increasing degrees of reduction while McSween and Labotka (1993) argued that progressive metamorphism from type 4 to type 6 H and L chondrites was characterized by oxidation. In both studies, the proposed shifts in oxidation/reduction were subtle but a knowledge of the direction is fundamental to

understanding fluid composition and mobility of elements during metamorphism of the ordinary chondrite parent bodies.

Temperature is intimately connected to the issue of redox conditions because many methods of calculating the oxygen fugacity require that temperature be known. For example, by accepting the commonly held assumption that peak metamorphic temperatures increased with petrographic type from <600°C for type 4 to 600-650°C for type 5 to 650-800°C for type 6 chondrites (e.g., Dodd, 1981; Heyse, 1978), McSween and Labotka (1993) were able to show that progressive increase in temperature was accompanied by progressive oxidation. If as suggested by Kessel et al. (2001c) there is no direct correlation between petrographic type and metamorphic temperature, their conclusions would require re-examination. The direct relationship between metamorphic temperature and f_{O_2} also implies that our ability to constrain f_{O_2} depends on the accuracy in determining the temperature. For example, Williams (1971) estimated equilibrium temperatures of 880°±150°C in type 5 and 6 equilibrated ordinary chondrites. This large uncertainty in temperature propagates into large uncertainties on his calculated values of $\log_{10} f_{O_2}$ (~±1.2 log units).

In this paper, we evaluate the redox conditions experienced by equilibrated H chondrites through application of spinel-alloy and olivine-pyroxene-alloy oxygen barometry. We first determine chromite activities in spinels whose compositions approximate those in equilibrated ordinary chondrites using a technique developed by Kessel et al. (2001b). We then evaluate temperature-oxygen fugacity relationships in equilibrated H chondrites using activity models for spinels and Fe-alloys and compositions of meteoritic phases. A similar approach is used for coexisting olivine,

pyroxene, and alloy. Finally, based on the re-evaluated peak metamorphic temperatures of Kessel et al. (2001c), we obtain absolute values of oxygen fugacities for H chondrites and consider the possibility that progressive oxidation or reduction occurred during metamorphism.

2. METHODS

2.1. Experimental starting material

Kessel et al. (2001b) developed an experimental method based on oxide-alloy equilibration (Chamberlin et al., 1995) by which the activity of chromite in complex multicomponent spinels can be determined by equilibrating the spinel with Pt-alloy under a controlled temperature and oxygen fugacity. In this study, we use the technique to determine the activity of chromite in multicomponent spinels whose compositions correspond to those in ordinary chondrites.

Six spinel end-members, chromite ($FeCr_2O_4$), picrochromite ($MgCr_2O_4$), ulvöspinel (Fe_2TiO_4), qandelite (Mg_2TiO_4), hercynite ($FeAl_2O_4$), and spinel ($MgAl_2O_4$), were synthesized from the oxides. The synthesis procedures of chromite and picrochromite are given in Kessel et al. (2001b). Ulvöspinel was prepared following procedures similar to those of Senderov et al. (1993): reagent grade powders of Fe_2O_3 (JMC Puratronic) and TiO_2 (JMC Puratronic) were weighed out in appropriate ratios and ground in an automated alumina mortar under ethanol for ~7 hr. The resulting mixture was pressed into 13 mm diameter pellets, placed inside an alumina crucible, suspended using Pt wire from a sample holder at the hot spot of a vertical furnace and held in a flowing H_2-CO_2 gas at 1300°C and $\log_{10} f_{O_2}$=–10.5 for 45 hr. Qandelite was prepared

following the procedure of Sugimoto et al. (1997): reagent grade MgO (JMC Puratronic) was held in an alumina crucible in air at 1000°C for 40 hr and then ground together with TiO_2 in the required molar ratio in an automated alumina mortar under ethanol for ~6 hr. The mixture was then pressed into 13 mm diameter pellets, placed inside an alumina crucible and held at 1300°C in air for 48 hr. Hercynite was prepared following the procedure of Petric et al. (1981): reagent grade powders of Fe_2O_3, Fe (Alfa Products), and Al_2O_3 (JMC Puratronic) were ground in the required molar ratio in an automated alumina mortar under ethanol for ~6 hr. The mixture was pressed into 7 mm diameter pellets, placed inside loosely capped alumina ceramic cylinders, and sealed inside an evacuated quartz tube. The quartz tube was then heated at 1100°C for 4 days. Preparation of $MgAl_2O_4$ spinel was similar to that described in Mattioli et al. (1987). Reagent grade MgO in an alumina crucible was heated at 1000°C for 40 hr and then ground together with Al_2O_3 in the required molar ratio in an automated alumina mortar under ethanol for ~6 hr. The mixture was pressed into 13 mm diameter pellets, placed on a Pt foil inside an alumina boat, which was suspended in a horizontal furnace for 48 hr at 800°C in air. The furnace temperature was then increased to 1400°C at which the sample was held for additional 48 hr. Homogeneity of the products and the degree to which oxides were converted to spinel end-members were determined using a Scintag Pad-V x-ray diffractometer and electron microprobe analyses of the synthesized spinels.

Figure 1 shows a literature compilation of spinel compositions found in H chondrites of petrographic types 3 through 6, presented as mole fractions of three different components in spinel as a function of chromite content. Spinels in L and LL chondrites exhibit similar trends. In each group, the range of compositions decreases

with increasing petrographic type but no systematic changes in composition are observed. Five spinel compositions, shown as filled circles in Fig. 1, were chosen to capture the basic features of the observed trend. One composition is pure chromite and the other four are multicomponent spinels. The four intermediate spinel compositions were prepared by mechanically mixing the six spinel end-members in various proportions using an automated alumina mortar under ethanol for 2 hr. Each mix was pressed into 13 mm diameter pellets, placed inside an alumina crucible suspended from a sample holder at the hot spot of a vertical furnace and held in a flowing H_2-CO_2 gas at 1300°C and $\log_{10} f_{O_2}$=–10.8. After 120 hr, the alumina crucibles were raised up into the cold region near the top of the furnace and allowed to cool. The pellets were taken out of the crucible and re-ground to produce the starting material used for the experiments. The spinels were analyzed by electron probe and the compositions, in good agreement within uncertainties with the nominal values, are given under the "initial" columns of Table 1.

2.2. Experimental preparation and analytical procedures

The experimental setup and calibration procedures are described in detail by Kessel et al. (2001a,b). All of the experiments were conducted at 1300°C and 1 atm in a Deltech DT-31 furnace or a home-built $MoSi_2$ furnace with gas-mixing capabilities. The oxygen fugacity was set by mixing CO_2 and H_2 gases and measured using an yttria-doped-zirconia solid electrolyte oxygen sensor ($SIRO_2$®, Ceramic Oxide Fabricators, Ltd., Australia) with an uncertainty of ±0.05 log units. Temperature was measured using a Pt-$Pt_{90}Rh_{10}$ (type S) thermocouple and is estimated to be accurate to within ±3°C. In each experiment, seven crucibles made from 0.625 cm diameter and 1 cm long Al_2O_3 rods (Vesuvius McDanel) were suspended from a sample holder in the vicinity of the

furnace hot spot. One crucible contained a pellet of Cr_2O_3 (7 mm diameter, 1 mm thick) pressed around 3 pieces of pure Pt wire [3-5 mm long, 75 μm diameter wire (99.9999%, Alfa® ÆSAR)]. A second crucible contained a pellet of $FeCr_2O_4$+Cr_2O_3, a third crucible contained a pellet of $FeCr_2O_4$, and each of the remaining four crucibles contained two pellets of one of the synthesized multicomponent spinels. Each of the spinel-bearing pellets was pressed around two pieces of previously synthesized Pt-Fe wires of known composition.

Experiments were conducted for 8-14 days to ensure equilibrium of the Pt-alloys with the surrounding oxides [see discussion in Kessel et al. (2001b)]. Experiments were terminated by raising the crucibles into the cold region of the furnace under the flowing gas mixture. Once cooled, samples were removed from the furnace. A small piece of each pellet containing a Pt-alloy surrounded by oxides was mounted in epoxy to allow examination of oxide textures and compositions in the vicinity of the Pt-alloy. The second wire from each pellet was physically separated from the adjacent oxides and mounted vertically. This sample was used to determine alloy composition and check for homogeneity across the wire. Alumina impregnated papers were used to expose the wires and oxides, and diamond powder (<0.25 μm) to achieve the final polished surfaces.

Platinum-alloys were analyzed for Pt, Fe, Cr, Ti, Mg and Al, using a JEOL733 Superprobe with an accelerating voltage of 20 keV, following procedures described in Kessel et al. (2001b). Pure metals were used as standards for Pt, Fe, Cr, and Ti, and $MgAl_2O_4$ for Mg and Al. Magnesium (<40 ppm), Al (<30 ppm), and Ti (<100 ppm) in the alloys were below detection limit in all experiments. The spinel composition in the

vicinity of the wires was analyzed for Fe, Cr, Ti, Mg, and Al, using an accelerating voltage of 15 keV, a beam current of 10 nA, and Fe_2O_3, Cr_2O_3, TiO_2, and $MgAl_2O_4$, as standards. A ZAF correction procedure (Armstrong, 1988) was applied to the results.

The results of experiments containing Pt-alloy equilibrated with Cr_2O_3 and those equilibrated with $FeCr_2O_4$+Cr_2O_3 are given in Kessel et al. (2001b) and discussed as part of a set of experiments whose results were used to construct a ternary Pt-Fe-Cr model. The compositions of Pt-alloys equilibrated with multicomponent spinels are used in this paper to evaluate the activity-composition relationship of chromite in spinels corresponding to spinel compositions in ordinary chondrites.

2.3. Meteoritic samples and analyses

We studied three equilibrated ordinary chondrites, Avanhandava (H4), Allegan (H5), and Guareña (H6). All are falls characterized by low shock intensity and unbrecciated character [Table 1 in Kessel et al. (2001c)] and the thin sections are identical to samples studied by H. McSween (private communication, 2001). Each thin section was examined by SEM and spinels in contact with metal grains were located. The compositions of spinel and metal grains, as well as olivines and pyroxenes in the vicinity, were obtained using a JEOL733 Superprobe. Average compositions for these phases are reported in Kessel et al. (2001c). Metal grains were analyzed for Fe, Si, Ni, Co, S, and P using, except for S (FeS_2) and P (GaP), pure metals as standards. With a beam current of 25 nA, counts were collected for 30 seconds on peak and 15 seconds at each background position on the standards. For alloys in the meteorites, Fe, Ni, and P were analyzed using the same counting time as for the standards. Counting times for Co, Si and S were 10 times longer at each position. A ZAF correction procedure (Armstrong,

1988) was applied to the results. Sulfur and P were below detection limit (0.004 and 0.015 elemental wt%, respectively) in all analyses.

Chromium contents of metal grains were analyzed using a Cameca IMS 6f ion microprobe at Arizona State University. A focused O^- primary beam was used to sputter $^{56}Fe^+$ and $^{52}Cr^+$ ions from the metal grains in the carbon coated thin sections. An area of 20x20 μm was first presputtered for 20 minutes with a 3 nA ion current to eliminate surface Cr contamination. Then a 0.5 nA beam was focused in the center of the rastered area, masked by a field aperature, and the spot measured for 30 minutes. Although the beam diameter was nominally 1-2 microns, the halo extended 10-15 μm away from the beam in all directions with intensity sufficient to contribute Cr ions from high-Cr phases. Thus, no data could be collected closer than ~20 μm from the edges of the metal grains. The secondary-ion mass spectrometer was operated at a mass resolving power of ~4800, sufficient to exclude contributions from $^{51}VH^+$ on ^{52}Cr and $^{55}MnH^+$ on ^{56}Fe. Data were corrected for electron-multiplier deadtime and a background count-rate of about 0.008 cps. Three Fe wires with Cr contents ranging 100 to 976 ppm Cr were used as standards. The detection limit for Cr was found to be ~3 ppb.

3. RESULTS

3.1. Activity-composition relationship of chromite in multicomponent spinels

The experimental conditions and results for each set of experiments are listed in Table 2. Experiments were conducted at 1300°C and 1 bar, with oxygen fugacities ranging from $\log_{10} f_{O_2}$=–11.77 to –9.27, corresponding to –1.0 to +1.5 log units relative

to IW buffer. As described above, each of the two spinel-bearing pellets in each crucible was pressed around two Pt-Fe wires, each pellet with wires of different initial Pt/Fe ratios. Starting with Pt/Fe ratios above and below the expected equilibrium alloy composition enabled us to conduct forward and reversal experiments simultaneously. Alloy compositions were determined by analyzing the wires separated from the adjacent oxides using EPMA. The mole fractions of Fe and Cr in the alloys, X_{Fe}^{PtFeCr} and X_{Cr}^{PtFeCr}, respectively, were calculated from the measured wt% Fe and Cr by averaging three to five analyses made on the wires separated from the oxides in each pellet. The uncertainties were calculated as the standard deviation of the distribution of measured alloy compositions from each wire. The initial and equilibrium Pt-alloys compositions are given in Table 2. Most Pt-alloys at a given f_{O_2} and spinel composition converged to the same composition within 1σ and all are within 2σ, giving us considerable confidence that equilibrium was attained during our experiments. The composition of each of the spinels in equilibrium with the Pt-alloys was determined for the most oxidizing and most reducing experiments by analyzing the oxides in the vicinity of the wires (Table 1). These "final" spinel compositions are in good agreement with the initial spinel compositions within analytical errors.

The equilibrium between a Pt-Fe-Cr alloy and a Cr-bearing spinel in the presence of an oxygen-bearing vapor can be represented by the reaction:

$$Fe^{alloy} + 2Cr^{alloy} + 2O_2^{gas} = FeCr_2O_4^{spinel}. \qquad (1a)$$

The free energy of reaction for 1a can be expanded in terms of component activities (e.g., Kessel et al., 2001b) and solved for the activity of chromite in the spinel, $a^{spinel}_{FeCr_2O_4}$, yielding:

$$a^{\text{spinel}}_{FeCr_2O_4} = \exp[-\Delta G^{\circ}_1 / RT](a^{alloy}_{Fe})(a^{alloy}_{Cr})^2 (f_{O_2})^2. \quad (1b)$$

In Eqn. 1b, a^j_i refers to the activity of component i in phase j, R is the gas constant, T is the temperature in Kelvin, and ΔG°_1 is the free energy of formation of $FeCr_2O_4$ from the elements. If ΔG°_1, a^{PtFeCr}_{Fe}, and a^{PtFeCr}_{Cr} are known, then the activity of chromite can be computed for an experiment given the run conditions from Eqn. 1b. We used ΔG°_1 and the alloy ternary model of Kessel et al. (2001b) to calculate $a^{\text{spinel}}_{FeCr_2O_4}$ for each spinel composition in each of our experiments. The chromite activities and activity coefficients for alloys obtained through the identity $\gamma^j_i = a^j_i / X^j_i$, where X^j_i is the mole fraction of component i in phase j, are given in Table 2. In Fig. 2, $a^{\text{spinel}}_{FeCr_2O_4}$ is shown as a function of $X^{spinel}_{FeCr_2O_4}$. Errors (1σ) on $a^{\text{spinel}}_{FeCr_2O_4}$ calculated using Eqn. 1b are 14-20% based on propagating the errors on temperature, f_{O_2}, and alloy composition. We note that results for each composition are independent of f_{O_2} (the ordering of the symbols in Fig. 2 is variable), suggesting that there are no large systematic errors in the calculated alloy compositions and that the spinel did not break down over the range of f_{O_2}'s investigated. Also shown in Fig. 2 are two curves calculated using the program MELTS (Ghiorso and Sack, 1995). Both are smoothed curves obtained for spinel compositions examined in this study. The first curve (dotted) for 1300°C, which is directly comparable to our experiments, is in excellent agreement with our data. The second curve (dashed)

represents the corresponding activity-composition relationships according to MELTS at 800°C. This temperature is relevant to near peak metamorphic temperatures of equilibrated ordinary chondrites (Kessel et al., 2001c; McSween and Patchen, 1989).

3.2. Meteoritic mineral compositions

We examined three equilibrated H chondrites as part of this study. Compositions of olivine, spinel, and pyroxene grains located in the matrix material outside chondrules are given in and discussed by Kessel et al. (2001c). Four to seven metal grains in contact with spinel were analyzed in each meteorite and the average compositions for kamacite and taenite grains in each meteorite are given in Table 3. Most of the selected grains appear as isolated kamacite surrounded by spinel and silicates in the plane of the thin section, one to two grains in each meteorite contains a small taenite zone close to the rim surrounded by kamacite and one of the grains in Avanhandava was found to be entirely composed of taenite. Kamacite compositions are homogeneous within analytical error (1σ) in each meteorite and among meteorites with average Ni content of 6.24±0.25 and Co of 0.598±0.017 wt% (1σ). A subtle decrease in average Ni concentration is observed from types 4 and 5 to type 6 correlated with an increase in the Co content. The taenite compositions are also homogeneous in all three meteorites with average Ni and Co contents of 49.28±0.72 and 0.129±0.012 wt%. The implied preferential partitioning of Co into kamacite is consistent with observations of previous workers (e.g., Afiattalab and Wasson, 1980)

Chromium contents of kamacite and taenite are extremely low, at or below detection limit (3 ppb) in all of our measurements. We therefore assign an upper limit of

3 ppb Cr in both kamacite and taenite in all three chondrites for the purpose of constraining f_{O_2} during metamorphism of equilibrated H chondrites. Chromium contents of alloys in chondrules from unequilibrated ordinary chondrites can reach 0.8 wt% (e.g., Zanda et al., 1994), which suggests that Cr was scavenged from metal during metamorphism.

Alloy compositions and structure in equilibrated ordinary chondrites are the result of their thermal history (e.g., Wood, 1967). Afiattalab and Wasson (1980) used mass balance calculations and estimated a Ni content of 10.2% in the bulk metal fraction in H chondrites with 12% of the total metal currently being taenite in composition. Similar estimates were presented by Willis and Goldstein (1983) for Guareña (H6) of 10% bulk Ni content with 20% of it being taenite. We assume 10% Ni in bulk metal in H chondrites. According to the Fe-Ni phase diagram (e.g., Reuter et al., 1989), such an alloy should exist as a single-phase taenite (γ-fcc) above ~700°C. During cooling through 400°C, the taenite enters a two-phase field of taenite and kamacite (α-bcc) where kamacite nucleates from taenite by volume diffusion of Ni out of the taenite into kamacite. As cooling continues, the Ni content of taenite increases along the $(\alpha+\gamma)/\gamma$ solvus to ~40 wt%, while the Ni content in kamacite changes only slightly along the $\alpha/(\alpha+\gamma)$ solvus up to ~7 wt%. Below 400°C, taenite continues going through subsolidus transformations. Since Ni diffusion in both kamacite and taenite is slow at temperatures below ~400°C, these phases are rare but evident as thin rims around alloy grains or as partial transformations of the alloy cores.

4. METAMORPHIC HISTORY OF EQUILIBRATED H CHONDRITES

4.1. Oxidation state during metamorphism

We studied two phase assemblages, olivine-pyroxene-alloy and spinel-alloy, for possible constraints on the oxygen fugacities experienced by equilibrated H chondrites near peak metamorphic conditions. Knowledge of the activity-composition relationships of the solid phases in each assemblage and the temperature dependence of the equilibrium constant allow calculation of the dependence of f_{O_2} on temperature.

Activities of oxygen-bearing phases were calculated using the program MELTS based on the mineral compositions in each meteorite [average compositions in each meteorite are given in Table 2a-c of Kessel et al. (2001c)]. The activities of Fe and Cr in the alloy were calculated based on the extrapolated bulk metal composition (Table 3) following the formulation of Miettinen (1999), for ternary Fe-Ni-Cr, ignoring other minor components, such as Co, in the meteoritic alloy. The equilibrium constants for both assemblages were calculated from the free energy of formation of the components derived from the program MELTS. Since the free energy at temperature given by MELTS is an apparent value relative to the elements at 298.15 K and 1 bar, equilibrium constants were corrected to reference the elements at the temperature of interest and 1 bar, using a procedure similar to that described in Kessel et al. (2001b).

4.1.1. Olivine-pyroxene-alloy oxygen barometer

When alloy coexists with olivine and pyroxene, the reaction

$$Fe^{alloy} + FeSiO_3^{pyroxene} + \frac{1}{2}O_2^{gas} = Fe_2SiO_4^{olivine} \qquad (2a)$$

is operative, from which an expression for f_{O_2} can be obtained:

$$f_{O_2} = \left(\frac{a_{Fe_2SiO_4}^{olivine}}{\exp[-\Delta G_2^\circ / RT] a_{Fe}^{alloy} a_{FeSiO_3}^{pyroxene}} \right)^2 . \quad (2b)$$

The activities of the solid phases are given in Table 4 together with the average oxygen fugacity calculated for each chondrite at olivine-spinel equilibration temperatures. Figure 3 shows $\log_{10} f_{O_2}$ calculated using Eqn. 2b as a function of olivine-spinel equilibration temperature for each individual mineral assemblage (Kessel et al., 2001c). The same redox conditions (IW-1.75±0.02) apply to all meteorites, regardless of petrographic type or metamorphic temperature.

The principle advantages of using the coexistence of olivine, pyroxene, and alloy are the common occurrence and relatively simple activity-composition models required for these three phases. The primary disadvantages are that appropriate equilibration temperatures based on this phase assemblage are poorly constrained and the equilibrium requires the same closure temperature for both olivine-alloy and pyroxene-alloy. This later requirement is not likely to hold in detail because of the very different diffusivities for cations in these phases. Olivine-orthopyroxene thermometry, based on Fe-Mg partitioning between the two phases, is relatively insensitive to temperature (e.g., Larimer, 1968) and therefore unsuitable for accurate thermometry. Either the temperature must be determined independently or large uncertainties in f_{O_2} must be accepted.

4.1.2. Spinel-alloy oxygen barometer

The second equilibrium examined involves the coexistence of spinel and alloy as described by reaction 1. In our experiments, temperature and f_{O_2} were known and the equilibrium was used to constrain alloy (Kessel et al., 2001b) or chromite (see above and

Kessel et al., 2001b) activities. For ordinary chondrites, the activities are assumed to be known and it is temperature- f_{O_2} that is desired. The equilibrium constant for reaction 1 calculated using the program MELTS after correction to refer to the free energy of formation of chromite from the elements via the free energy of formation of Cr_2O_3 from Holzheid and O'Neill (1995) [see detailed calculation in Kessel et al. (2001b)] is identical within 1σ to that calculated from the free energy of formation of chromite from Cr_2O_3, Fe, and O_2, given by Jacob and Iyengar (1999). Activities of the solid phases based on the meteoritic mineral compositions [Table 2b of Kessel et al. (2001c) and Table 3] using a limiting value of 3 ppb for Cr and the equilibrium constant are given in Table 4 together with the average oxygen fugacity calculated for each chondrite assuming that peak metamorphic conditions are recorded by olivine-spinel (Kessel et al., 2001c) and spinel-alloy compositions. All calculated f_{O_2} values are at or below the f_{O_2} of IW buffer for Fe-alloy containing 10% Ni, the relevant value for ordinary chondrites (Fig. 3). There is an apparent progressive increase in relative oxidation with increasing metamorphic grade, from –1.12 - –0.32 relative to IW in type 4 to –0.28 - –0.22 in type 5 to –0.60 - +0.02 in type 6. This apparent trend is, however, an artifact of the calculations because only a single limiting alloy composition was used. The calculated f_{O_2}'s are also considerably more oxidizing than values inferred from olivine-pyroxene-alloy, an issue we discuss below.

Oxygen barometry based on the coexistence of spinel and alloy has the advantage of requiring equilibrium between only two phases, but there are also a few disadvantages that require discussion. First, multicomponent spinels are characterized by relatively complex thermodynamic properties. Our experimentally determined activities at 1300°C

are in excellent agreement with those calculated using the program MELTS (Ghiorso and Sack, 1995) which gives us some confidence in using the MELTS model to calculate activities at 800°C. A second obstacle, particularly in equilibrated ordinary chondrites, is the low concentration of Cr in the alloys. Chromium is below the detection limit of 3 ppb in all of the meteoritic alloys studied here, so that only upper limits on the oxidation state can be determined. Values of $\log_{10} f_{O_2}$ constrained by spinel-alloy coexistence as a function of temperature are shown in Fig. 3 for a range of Cr concentration in the alloy between 0.1 and 3 ppb. A Cr content of 1 ppb instead of 3 ppb would increase our calculated f_{O_2} values by ~0.8 log units at constant temperature. It is important to note that because there is only a limiting constraint on Cr concentration, our spinel-alloy data carry no implications for relative oxidation among the ordinary chondrites.

The last issue to be considered is the assumption that spinel-alloy closure temperature for Cr exchange approximated peak metamorphic conditions as inferred from olivine-spinel thermometry. The metal composition at high temperature was taken in this work to represent the composition near peak metamorphic conditions. At the olivine-spinel equilibration temperatures, 730-820°C, $\log_{10} f_{O_2}$ values constrained by the spinel-alloy assemblages are 1.2-1.5 log units more oxidizing than those constrained by the olivine-pyroxene-alloy assemblages (Fig. 3). This apparent inconsistency between the two approaches can be resolved if the spinel-alloy equilibrium records lower temperatures <~660°C, where extensions of the $\log_{10} f_{O_2}$-temperature curves intersect. A detailed analysis would require taking into account the partitioning of elements between alloy phases. Lower closure temperatures recorded by the spinel-alloy equilibrium than

those by olivine-spinel equilibrium are most likely a retrograde effect dictated by the kinetics of spinel dissolution at the spinel-alloy interface.

4.2. Comparison with previous work

4.2.1. Olivine-pyroxene-alloy oxygen barometer

The phase assemblage olivine+pyroxene+alloy in equilibrated ordinary chondrites has been used previously to constrain temperature-f_{O_2} relationships. Mueller (1964) applied ideal solutions to both olivine and pyroxene and calculated T-$\log_{10} f_{O_2}$ curves as a function of olivine composition. Larimer (1968) experimentally derived an expression for f_{O_2} as a function of temperature for the mineral assemblage by applying regular solutions for both olivine and pyroxene. In both of these studies, the activity coefficients of olivine and pyroxene were taken as independent of temperature and the metal phase was regarded as pure Fe. No specific calculations were provided for mineral compositions in meteorites but, based on the range of silicate compositions given in Ringwood (1961), Mueller (1964) suggested $\log_{10} f_{O_2}$ of IW–2.03 (2.03 log units below IW) at 1100 K. Williams (1971) used the compositions of coexisting olivine and pyroxene in types 5 and 6 equilibrated ordinary chondrites to estimate equilibrium temperatures of 880°±150°C, regardless of group or petrographic type. He used this temperature to calculate $\log_{10} f_{O_2}$ of IW–0.47 based on the equilibrium between olivine, pyroxene, and metal. Reisener et al. (submitted) examined the T-f_{O_2} relationships in one H5 and three H6 chondrites as constrained by the olivine-pyroxene-metal assemblage by applying regular solutions to the olivine, pyroxene, and metal. Based on the mineral

compositions in these meteorites, they derived $\log_{10} f_{O_2}$ values of IW–1.71 at 800°C, in good agreement with our results.

McSween and Labotka (1993) examined a compilation of compositions and abundance of olivine, pyroxene, and metal in types 4 to 6 H and L equilibrated ordinary chondrites. They argued that three observations indicate increasing Fe^{2+}/Fe^0 and hence increasing oxidation with increasing petrographic type. First, Fe/(Fe+Mg) of olivine and pyroxene increase with petrographic type, as observed by others (e.g., Rubin et al., 1988, Rubin, 1990). The idea here is that if equilibrated ordinary chondrites have constant bulk Fe, Mg, and Si, then oxidation of metallic iron will lead to increasing Fe in the dominant ferromagnesian silicates. A considerable scatter, however, is observed in the data compilation presented by McSween and Labotka (1993) with standard deviations comparable to the scale of the trends. Even taking apart the errors involved, an increase in Fe in olivine and pyroxene with increasing petrographic type is observed only in LL chondrites. The trend for L chondrites is less obvious and there is no systematic trend for H chondrites. McSween and Labotka's (1993) second observation is that there is an increase in the abundance of olivine and a decrease in the abundance of pyroxene and metal with increasing petrographic type. They interpreted this as indicating that oxidation drove reaction 2 to the right, leading to an increase in the olivine/pyroxene ratio and a decrease in the amount of metal. This observation is based on a comparison of average normative mineral abundances in each petrographic type in each group calculated from the bulk chemistry (McSween et al., 1991). However, a close look at the averages suggests that a significant trend exists only in LL chondrites. An increase in olivine/pyroxene ratio is observed in L chondrites with increasing petrographic type but

this is not accompanied by a corresponding change in Fe metal abundance. There is no systematic change in either olivine/pyroxene or metal with petrographic type in the H chondrites. The ambiguity in the data cited by McSween and Labotka (1993) is also seen in other work with Jarosewich (1990) finding an increase in the olivine/pyroxene ratio and decrease in the amount of metal and Dodd (1976) finding the opposite correlation. The third line of evidence presented by McSween and Labotka (1993) is an increase in average Ni and Co contents of metal grains with increasing petrographic type. This was taken to indicate that oxidation of metallic iron occurred during metamorphism resulting in decreasing Fe and increasing concentrations of siderophile elements such as Ni and Co in the metal. In McSween and Labotka's (1993) compilation, however, H chondrites have identical metal compositions within error regardless of petrographic type and there are insufficient data for any judgement regarding LL chondrites. There may be a subtle increase in Ni and Co in the bulk metal of L chondrites but they are the same within error. We conclude that the reported range of both mineral compositions and abundance in each petrographic type in the three chondrite groups is wider than the suggested differences between the types making such correlations statistically unresolvable.

In an attempt to put the above arguments on a more quantitative foundation, McSween and Labotka (1993) calculated relative oxygen fugacities constrained by the mineral compositions. They treated olivine and pyroxene as ideal solutions and assumed a constant composition for the metallic phase, taken as pure iron, so that all activities of the solid phases are independent of temperature. Given this set of assumptions, deviations of $\log_{10} f_{O_2}$ from the Fayalite-Iron-Ferrosilite (FIF) buffer are a function only of the olivine and pyroxene composition. They translated increases in Fe/(Fe+Mg) of

olivine and pyroxene with petrographic type into a corresponding increase in $\log_{10} f_{O_2}$ from FIF–1.38 for type 4 to FIF–1.37 for type 5 to FIF–1.35 for type 6 H chondrites and FIF–1.13 for types 4 and 5 to FIF–1.11 for type 6 L chondrites. Errors were not assessed but McSween and Labotka (1993) nevertheless argued for a subtle but progressive oxidation with petrographic type in both H and L parent bodies. Temperatures were not incorporated directly into their calculations but by assuming increasing metamorphic temperature with petrographic type McSween and Labotka (1993) were able to link the increasing oxidation with increasing metamorphic temperatures. They suggested that the progressive oxidation resulted from reactions with an aqueous vapor, possibly derived from ices originally accreted into the parent body interior.

The range of mineral compositions found in each petrographic type leads to a range of activities at any given temperature and thus a range of $\log_{10} f_{O_2}$, regardless of activity-composition model. For example, the range of olivine and pyroxene compositions found in Guareña alone in Kessel et al. (2001c) resulted in an uncertainty of ± 0.06 in $\log_{10} f_{O_2}$ relative to IW (Table 4). The differences in $\log_{10} f_{O_2}$ relative to FIF of up to 0.02 log units reported by McSween and Labotka (1993) are smaller than the standard deviation of $\log_{10} f_{O_2}$ as propagated from the range of mineral compositions in each petrographic type and therefore can not be regarded as increasing oxidation with type. Their linkage between increasing oxidation and increasing metamorphic temperatures is also not valid at present because petrographic type and metamorphic temperature are not directly correlated (e.g., Kessel et al., 2001c; McSween and Patchen, 1989).

4.2.2. Intrinsic f_{O_2} measurements

Walter and Doan (1969) and Brett and Sato (1984) measured intrinsic oxygen fugacities in equilibrated ordinary chondrites using a solid-electrolyte double-cell method. The EMF was determined during a few cycles of heating and cooling of the sample in the furnace and was converted to absolute $\log_{10} f_{O_2}$ values. These measurements provide a temperature-oxygen fugacity relationship for each meteorite. Provided temperatures are independently known, $\log_{10} f_{O_2}$ is readily calculated. In a preliminary report, Walter and Doan (1969) examined one H6 chondrite and one L6 chondrite, obtaining IW–3 and IW–1.5 at 800°C. Brett and Sato (1984) measured intrinsic oxygen fugacity in two H chondrites, types 4 and 6, one L5 chondrite, and two LL chondrites, types 3 and 5. The oxygen fugacity-temperature curves for these meteorites parallel each other and the IW buffer with $\log_{10} f_{O_2}$ referenced to 800°C ranging from IW–0.98 for H4 to IW–1.04 for H6, IW–0.56 for L5, and from IW–0.35 for LL3 to IW–0.86 for LL5. Brett and Sato (1984) noted that the range for all meteorites, 0.7 log units, was similar to their errors on individual measurements and calculated that redox conditions for all equilibrated ordinary chondrites are approximately the same. Their results imply redox conditions about 2 order of magnitudes more oxidizing than inferred by McSween and Labotka (1993). McSween and Labotka (1993) criticized the results of Brett and Sato (1984) by arguing that calculated $\log_{10} f_{O_2}$ values more oxidizing than the FIF buffer are metastable and therefore inconsistent with the mineral assemblage of equilibrated ordinary chondrites. On this basis, they rejected intrinsic f_{O_2} measurements of Brett and Sato (1984). Both the direction and magnitude of deviations

from FIF are, however, a function of the mineral compositions and activity-composition models. For example, recalculating $\log_{10} f_{O_2}$ values for the mineral compositions given by McSween and Labotka (1993) using activity-compositions for olivine and pyroxene using MELTS leads to FIF+0.29 to FIF+0.32 for H chondrites and FIF+0.44 to FIF+0.64 for L chondrites, all of which are more oxidizing than FIF. While there is clearly a discrepancy between results of McSween and Labotka (1993) and our data for olivine-pyroxene-alloy on the one hand and intrinsic f_{O_2} measurements of Brett and Sato (1984) on the other, the arguments of McSween and Labotka (1993) are not formally valid.

The main disadvantage of intrinsic f_{O_2}measurements is the vulnerability to autoreduction and oxidation leading to false readings. Due to the low oxygen buffering capacity of the rock, oxygen released from rusted minerals, mainly metal grains, will dominate the recorded signal and result in higher than primary f_{O_2} values. Any oxidation of graphite grains during heating will consume available oxygen to produce CO_2 and lead to more reducing values. Although Brett and Sato (1984) examined only chondrites that were seen to fall and visibly rusted grains were removed, measured EMF may reflect incorporation of oxidized regions in the rocks. Some support for the idea that auto-oxidation occurred during measurements of Brett and Sato (1984) is seen in the data for Semarkona (LL3), Cherokee Springs (LL5), and Guareña (H6), all of which yielded higher f_{O_2} values when heating/cooling cycles were repeated. Analogous problems were apparently encountered in the intrinsic f_{O_2} measurements of Arculus and coworkers (Arculus et al., 1984; Arculus and Delano, 1981) on upper mantle rocks. Mattioli and Wood (1986) reported thermobarometric estimates of upper mantle f_{O_2} 1.5 log units

more oxidizing than intrinsic f_{O_2} measurements on the same samples. They explained this discrepancy as reflecting autoreduction during heating of the samples leading to low anomalously f_{O_2} values.

5. CONCLUSIONS

Based on equilibrium of olivine, pyroxene, and alloy in equilibrated H chondrites, all experienced similar f_{O_2}'s, IW-1.75±0.02, regardless of petrographic type and metamorphic temperature. Oxygen fugacities calculated using spinel-alloy are at least ~1.5 log units more oxidizing than those based on the olivine-pyroxene-alloy at the same temperature. The higher f_{O_2} values calculated for spinel-alloy coexistence indicate lower closure temperatures than for olivine-spinel equilibration temperature and are probably recording retrograde conditions.

Acknowledgements – This work was supported by NASA grant NAG–10423. Discussions with Mike Baker and Hap McSween inspired part of this work and led to significant improvements in the quality of this study. We are grateful for time provided for work using the ion probe by Gary Huss and thank him for helping with the measurements. Ma Chi and Yunbin Guan are thanked for their help with the analytical work. Thin sections were generously provided by the Smithsonian Institution and the Field Museum.

REFERENCES

Afiattalab F. and Wasson J. T. (1980) Composition of the metal phases in ordinary chondrites: Implications regarding classification and metamorphism. *Geochimica et Cosmochimica Acta* **44**, 431-436.

Arculus R. J., Dawson J. B., Mitchell R. H., Gust D. A., and Holmes R. D. (1984) Oxidation states of the upper mantle recorded by megacryst ilmenite in kimberlite and type A and B spinel lherzolites. *Contributions to Mineralogy and Petrology* **85**, 85-94.

Arculus R. J. and Delano J. W. (1981) Intrinsic oxygen fugacity measurements: techniques and results for spinels from upper mantle peridotites and megacryst assemblages. *Geochimica et Cosmochimica Acta* **45**, 889-913.

Armstrong J. T. (1988) Quantitative analysis of silicate and oxide materials: Comparison of Monte Carlo, ZAF, and $\phi(\rho Z)$ procedures. In *MicroBeam Analysis* (ed. D. E. Newbury), pp. 239-246. San Francisco Press, Inc.

Bennett M. E. and McSween H. Y. (1996) Revised model calculations for the thermal histories of ordinary chondrite parent bodies. *Meteoritics and Planetary Science* **31**, 783-792.

Bischoff A. and Keil K. (1983) Ca-Al-rich chondrules and inclusions in ordinary chondrites. *Nature* **303**, 588-592.

Bischoff A., Plame H., and Spettel B. (1989) Al-rich chondrules from the Ybbsitz H4-chondrite: evidence for formation by collision and splashing. *Earth and Planetary Science Letters* **93**, 170-180.

Brett R. and Sato M. (1984) Intrinsic oxygen fugacity measurements on seven chondrites, a pallasite, and a tektite and the redox state of meteorite parent bodies. *Geochimica et Cosmochimica Acta* **48**, 111-120.

Bunch T. E., Keil K., and Snetsinger K. G. (1967) Chromite composition in relation to chemistry and texture of ordinary chondrites. *Geochimica et Cosmochimica Acta* **31**, 1569-1582.

Buseck P. R. and Keil K. (1966) Meteoritic rutile. *American Mineralogist* **51**, 1506-1515.

Chamberlin L., Beckett J. R., and Stolper E. (1995) Palladium oxide equilibrium and the thermodynamic properties of $MgAl_2O_4$ spinel. *American Mineralogist* **80**, 285-296.

Dodd R. T. (1969) Metamorphism of the ordinary chondrites: A review. *Geochimica et Cosmochimica Acta* **33**, 161-203.

Dodd R. T. (1974) The metal phase in unequilibrated ordinary chondrites and its implications for calculated accretion temperatures. *Geochimica et Cosmochimica Acta* **38**, 485-494.

Dodd R. T. (1976) Iron-silicate fractionation within ordinary chondrite groups. *Earth and Planetary Science Letters* **28**, 479-484.

Dodd R. T. (1981) *Meteorites, A petrologic-chemical synthesis*. Cambridge University Press.

Fredriksson K., Nelen J., and Fredriksson B. J. (1968) The LL-group chondrites. In *Origin and Distribution of the Elements* (ed. L. H. Ahrens), pp. 457-466. Pergamon Press.

Ghiorso M. S. and Sack R. O. (1995) Chemical mass transfer in magmatic processes IV. A revised and internally consistent thermodynamic model for the interpolation and extrapolation of liquid-solid equilibria in magmatic systems at elevated temperatures and pressures. *Contributions to Mineralogy and Petrology* **119**, 197-212.

Heyse J. V. (1978) The metamorphic history of LL-group ordinary chondrites. *Earth and Planetary Science Letters* **40**, 365-381.

Holzheid A. and O'Neill H. St. C. (1995) The Cr-Cr_2O_3 oxygen buffer and the free energy of formation of Cr_2O_3 from high-temperature electrochemical measurements. *Geochimica et Cosmochimica Acta* **59**, 475-479.

Ikeda Y., Yamatomo T., Kojima H., Imae N., Kong P., Ebihara M., and Prinz M. (1997) Yamato-791093, a metal-sulfide-enriched H-group chondritic meteorite transitional to primitive IIE irons with silicate inclusions. *Antarctic Meteorite Research* **10**, 335-353.

Jacob K. T. and Iyengar G. N. K. (1999) Thermodynamics and phase equilibria involving the spinel solid solution $Fe_xMg_{1-x}Cr_2O_4$. *Metallurgical and Materials Transactions B* **30**, 865-871.

Jarosewich E. (1990) Chemical analyses of meteorites: A compilation of stony and iron meteorite analyses. *Meteoritics* **25**, 323-337.

Johnson C. A. and Prinz M. (1991) Chromite and olivine in type II chondrules in carbonaceous and ordinary chondrites: Implications for thermal histories and group differences. *Geochimica et Cosmochimica Acta* **55**, 893-904.

Keil K. (1980) Origin and history of the polymict-brecciated Tysnes Island chondrite and its Carbonaceous and non-carbonaceous lithic fragments. *Chemie die Erde* **39**, 1-26.

Kessel R., Beckett J. R., and Stolper E. M. (2001a) Thermodynamic properties of the Pt-Fe system. *American Mineralogist*. **86**, 1003-1014.

Kessel R., Beckett J. R., and Stolper E. M. (2001b) Chromite activities in multicomponent spinels. Part I: Experimental technique. *Geochimica et Cosmochimica Acta*.

Kessel R., Beckett J. RB., and Stolper E. M. (2001c) The thermal history of equilibrated ordinary chondrites and the relationship between textural maturity and temperature. *Geochimica et Cosmochimica Acta*.

Kleinschrot D. and Okrusch M. (1999) Mineralogy, petrography, and thermometry of the H5 chondrite Carcote, Chile. *Meteoritics and Planetary Science* **34**, 795-802.

Larimer J. W. (1968) Experimental studies on the system Fe-MgO-SiO_2-O_2 and their bearing on the petrology of chondritic meteorites. *Geochimica et Cosmochimica Acta* **32**, 1187-1207.

Mattioli G. S. and Wood B. J. (1986) Upper mantle oxygen fugacity recorded by spinel lherzolites. *Nature* **322**, 626-628.

Mattioli G. S., Wood B. J., and Carmichael I. S. E. (1987) Ternary-spinel volume in the system $MgAl_2O_4$-Fe_3O_4-$\gamma Fe_{3/8}O_4$: Implications for the effect of P on intrinsic f_{O_2} measurements of mantle-xenolith spinels. *American Mineralogist* **72**, 468-480.

McSween H. Y., Bennett M. E., and Jarosewich E. (1991) The mineralogy of ordinary chondrites and implications for asteroid spectrophotometry. *Icarus* **90**, 107-116.

McSween H. Y. and Labotka T. C. (1992) Changes in redox state during ordinary chondrite metamorphism. (abstract). *Lunar and Planetary Science Conference,* **23**, 89-90.

McSween H. Y. and Labotka T. C. (1993) Oxidation during metamorphism of the ordinary chondrites. *Geochimica et Cosmochimica Acta* **57**, 1105-1114.

McSween H. Y. and Patchen A. D. (1989) Pyroxene thermobarometry in LL-group chondrites and implications for parent body metamorphism. *Meteoritics* **24**, 219-226.

McSween H. Y., Sears D. W. G., and Dodd R. T. (1988) Thermal metamorphism. In *Meteorites and the Solar System* (ed. J. F. Kerridge and M. S. Matthews), pp. 102-113. The University of Arizona Press.

Miettinen J. (1999) Thermodynamic reassessment of Fe-Cr-Ni system with emphasis on the iron-rich corner. *CALPHAD* **23**, 231-248.

Miyamoto M., Fuji N., and Takeda H. (1981) Ordinary chondrite parent body: An internal heating model. *Proceeding of the Lunar and Planetary Science Conference* **12**, 1145-1152.

Mueller R. F. (1964) Phase equilibria and the crystallization of chondritic meteorites. *Geochimica et Cosmochimica Acta* **28**, 189-207.

Petric A., Jacob K. T., and Alcock C. B. (1981) Thermodynamic properties of Fe_3O_4-$FeAl_2O_4$ spinel solid solutions. *Journal of the American Ceramic Society* **64**, 632-639.

Reisener R. J., Goldstein J. I., and Petaev M. I. (submitted) Olivine zoning and olivine-orthopyroxene-metal equilibration in H5 and H6 chondrites during metamorphic cooling. *Geochimica et Cosmochimica Acta.*

Reuter K. B., Williams D. B., and Goldstein J. I. (1989) Determination of the Fe-Ni phase diagram below 400°C. *Metallurgical Transactions* **20A**, 719-725.

Ringwood A. E. (1961) Chemical and genetic relationships among meteorites. *Geochimica et Cosmochimica Acta* **24**, 159-197.

Rubin A. E. (1990) Kamacite and olivine in ordinary chondrites: Intergroup and intragroup relationships. *Geochimica et Cosmochimica Acta* **54**, 1217-1232.

Rubin A. E., Fegley B., and Brett R. (1988) Oxidation state in chondrites. In *Meteorites and the Early Solar System* (ed. J. F. Kerridge and M. S. Matthews), pp. 488-511. The university of Arizona Press.

Sack R. O. and Ghiorso M. S. (1989) Importance of considerations of mixing properties in establishing an internally consistent thermodynamic database: thermochemistry of minerals in the system Mg_2SiO_4-Fe_2SiO_4-SiO_2. *Contributions to Mineralogy and Petrology* **102**, 41-68.

Sack R. O. and Ghiorso M. S. (1991a) An internally consistent model for the thermodynamic properties of Fe-Mg titanomagnetite-aluminate spinels. *Contribution to Mineralogy and Petrology* **106**, 474-505.

Sack R. O. and Ghiorso M. S. (1991b) Chromium spinels as petrogenetic indicators: thermodynamics and petrological applications. *American Mineralogist* **76**, 827-847.

Senderov E., Dogan A. U., and Navrotsky A. (1993) Nonstoichiometry of magnetite-ulvöspinel solid solutions quenched from 1300°C. *American Mineralogist* **78**, 565-573.

Snetsinger K. G., Keil K., and Bunch T. E. (1967) Chromite from "equilibrated" chondrites. *American Mineralogist* **52**, 1322-1331.

Sugimoto W., Kaneko N., Sugahara Y., and Kuroda K. (1997) Preparation of stoichiometric and nonstoichiometric magnesium titanate spinels. *Journal of the Ceramic Society of Japan* **105**, 101-105.

Van Schmus W. R. and Wood J. A. (1967) A chemical-petrologic classification for the chondritic meteorites. *Geochimica et Cosmochimica Acta* **31**, 747-765.

Walter L. S. and Doan A. S. (1969) Determination of oxygen activities of chondritic meteorites. *Geological Society of America Abstracts and Programs*, 232-233.

Williams R. J. (1971) Equilibrium temperatures, pressures, and oxygen fugacities of the equilibrated chondrites. *Geochimica et Cosmochimica Acta* **35**, 407-411.

Willis J. and Goldstein J. I. (1983) A three-dimensional study of metal grains in equilibrated, ordinary chondrites. *Proceedings of the 14th Lunar and Planetary Science Conference, Journal of Geophysical Research Supplement* **88**, B287-B292.

Wood J. A. (1967) Chondrites: their metallic minerals, thermal histories, and parent planets. *Icarus* **6**, 1-49.

Zanda B., Bourot-Denise M., Perron C., and Hewin R. H. (1994) Origin and metamorphic redistribution of silicon, chromium, and phosphorus in the metal of chondrites. *Science* **265**, 1846-1849.

Zinovieva N. G., Mitreikina O. B., and Granovsky L. B. (1997) Origin mechanism of hercynite-kamacite objects: evidence for liquid immiscibility phenomena in the Yamato-82133 ordinary chondrite (H3). *Antarctic Meteorite Research* **10**, 299-311.

Table 1. Composition of experimental spinel[a]

	OCb[b]			OCc			OCd			OCe		
	nominal	initial	final	nominal	initial	final	nominal	initial	final	nominal	initial	final
#[c]	–	9	28	–	9	28	–	9	25	–	9	28
FeO[d]	30.59	30.38(33)[e]	29.37(116)	30.18	30.16(223)	29.28(124)	28.60	29.39(45)	27.72(62)	24.17	25.38(33)	24.27(57)
MgO	1.78	1.68(3)	1.87(16)	2.40	2.20(43)	2.61(42)	3.62	3.50(34)	3.71(27)	6.55	6.37(45)	6.37(32)
Al_2O_3	2.83	3.27(66)	3.45(61)	5.93	6.01(92)	6.17(31)	6.51	6.49(92)	6.60(22)	6.03	5.97(33)	6.08(38)
Cr_2O_3	62.58	62.49(94)	63.32(121)	59.19	59.46(235)	59.83(89)	58.74	58.07(169)	59.63(51)	60.89	59.66(78)	61.09(53)
TiO_2	2.23	2.19(30)	1.99(29)	2.31	2.18(66)	2.11(27)	2.53	2.55(61)	2.34(33)	2.35	2.62(36)	2.19(29)
Ulv[f]	0.054	0.053(7)	0.047(6)	0.054	0.050(15)	0.047(6)	0.054	0.055(13)	0.048(8)	0.040	0.046(7)	0.038(5)
Chr	0.803	0.796(17)	0.787(14)	0.718	0.719(36)	0.707(18)	0.661	0.660(29)	0.647(22)	0.566	0.555(18)	0.560(12)
Her	0.054	0.062(12)	0.064(12)	0.109	0.108(14)	0.109(6)	0.110	0.110(15)	0.106(7)	0.081	0.083(5)	0.083(5)
PChr	0.078	0.078(2)	0.090(8)	0.100	0.095(18)	0.112(17)	0.140	0.140(11)	0.160(26)	0.253	0.253(15)	0.262(11)
Qan	0.005	0.005(1)	0.005(1)	0.006	0.007(2)	0.008(1)	0.012	0.012(3)	0.012(2)	0.020	0.021(2)	0.018(2)
Sp	0.006	0.006(1)	0.007(1)	0.013	0.015(4)	0.017(2)	0.022	0.023(4)	0.026(3)	0.040	0.038(4)	0.039(3)
Mgt	0.000	0.000(0)	0.000(0)	0.000	0.007(16)	0.000(0)	0.000	0.000(0)	0.000(0)	0.000	0.004(8)	0.000(0)

[a] Compositions are normalized to 100 wt%.

[b]OCb-e refer to the spinel compositions chosen to represent the composition trend in H chondrites as shown in Fig. 1. Data for OCa, which is pure chromite are given Kessel et al. (2001b).

[c]Total number of analyses. Points were analyzed randomly on grains in the vicinity of the Pt-alloy.

[d]All Fe expressed as FeO.

[e]Numbers enclosed in parentheses indicate standard deviations of the distribution of average grain compositions.

[f]Mole fraction of end-member ulvöspinel (Ulv), chromite (Chr), hercynite (Her), picrochromite (PChr), qandelite (Qan), spinel (Sp), and magnetite (Mgt) were calculated based on mass and charge balance.

Table 2. Experimental conditions and results for Pt-Fe-Cr alloys+OC spinels at 1300°C

Run[a,b]	X_{Fe}^{alloy} (initial)	X_{Fe}^{alloy}[c] (final)	X_{Cr}^{alloy} (final)	$\ln\gamma_{Cr}^{alloy}$[d]	$\ln\gamma_{Fe}^{alloy}$	$a_{FeCr_2O_4}^{spinel}$[f]	X_{Fe}^{alloy} (initial)	X_{Fe}^{alloy} (final)	X_{Cr}^{alloy} (final)	$\ln\gamma_{Cr}^{alloy}$	$\ln\gamma_{Fe}^{alloy}$	$a_{FeCr_2O_4}^{spinel}$
RK275-21	0.539(4)[e]	0.510(1)	0.00572(3)	-2.25	-1.59(10)	0.98						
RK276-21/45	0.539(4)	0.579(1)	0.00175(1)	-1.54	-1.11(19)	0.70	0.408(3)	0.575(2)	0.00187(1)	-1.58	-1.14(18)	0.71
RK277-21/45	0.539(4)	0.556(2)	0.00230(2)	-2.59	-1.27(16)	0.61						
RK278-21/45	0.539(4)	0.558(3)	0.00208(1)	-1.76	-1.26(16)	0.53	0.408(3)	0.559(3)	0.00211(3)	-1.74	-1.25(16)	0.56
RK279-21/45	0.539(4)	0.556(1)	0.00215(1)	-1.77	-1.27(16)	0.54	0.408(3)	0.558(2)	0.00209(2)	-1.76	-1.26(16)	0.53
RK268-43	0.447(8)	0.479(3)	0.00378(7)	-2.65	-1.88(7)	0.94						
RK269-21/43	0.539(4)	0.499(2)	0.00240(2)	-2.42	-1.72(9)	0.75	0.447(8)	0.494(1)	0.00267(1)	-2.49	-1.76(8)	0.76
RK270-21/43							0.447(8)	0.485(1)	0.00280(1)	-2.59	-1.84(8)	0.61
RK271-21/43	0.539(4)	0.517(2)	0.00157(2)	-2.22	-1.58(11)	0.56	0.447(8)	0.509(5)	0.00172(1)	-2.32	-1.64(10)	0.52
RK272-21/43	0.539(4)	0.492(1)	0.00225(1)	-2.51	-1.78(8)	0.51	0.447(8)	0.481(4)	0.00273(2)	-2.63	-1.87(7)	0.52
RK249-43	0.447(8)	0.426(1)	0.00268(2)	-3.34	-2.43(4)	0.95						
RK250-43/44	0.447(8)	0.442(1)	0.00175(1)	-3.15	-2.27(5)	0.72	0.371(3)	0.443(2)	0.00172(4)	-3.14	-2.26(5)	0.72
RK251-43/44	0.447(8)	0.4459(4)	0.00148(1)	-3.10	-2.23(5)	0.59	0.371(3)	0.442(1)	0.00159(8)	-3.15	-2.27(5)	0.59
RK252-43/44	0.447(8)	0.447(1)	0.00139(1)	-3.08	-2.22(5)	0.55	0.371(3)	0.449(1)	0.00139(1)	-3.06	-2.20(5)	0.59
RK253-43/44	0.447(8)	0.429(2)	0.00192(14)	-3.31	-2.41(4)	0.53	0.371(3)	0.430(3)	0.00191(9)	-3.30	-2.40(4)	0.54
RK242-30	0.400(4)	0.355(1)	0.00143(3)	-4.34	-3.31(1)	0.95						
RK243-21/30	0.539(4)	0.374(2)	0.00085(3)	-4.07	-3.06(2)	0.76	0.400(4)	0.373(2)	0.00086(5)	-4.09	-3.08(2)	0.75
RK244-21/30	0.539(4)	0.365(3)	0.00094(2)	-4.20	-3.18(2)	0.63	0.400(4)	0.367(1)	0.00088(4)	-4.17	-3.15(2)	0.62
RK245-21/30	0.539(4)	0.367(2)	0.00085(1)	-4.17	-3.15(2)	0.57	0.400(4)	0.370(1)	0.0008(3)	-4.13	-3.12(2)	0.57
RK246-21/21	0.539(4)	0.359(1)	0.00095(1)	-4.28	-3.25(1)	0.51	0.400(4)	0.362(2)	0.00096(3)	-4.24	-3.21(1)	0.59

Table 2. Continued. Experimental conditions and results for Pt-Fe-Cr alloys+OC spinels at 1300°C.

Run[a,b]	X_{Fe}^{alloy} (initial)	X_{Fe}^{alloy} [c] (final)	X_{Cr}^{alloy} (final)	$\ln\gamma_{Cr}^{alloy}$ [d]	$\ln\gamma_{Fe}^{alloy}$	$a_{FeCr_2O_4}^{spinel}$ [f]	X_{Fe}^{alloy} (initial)	X_{Fe}^{alloy} (final)	X_{Cr}^{alloy} (final)	$\ln\gamma_{Cr}^{alloy}$	$\ln\gamma_{Fe}^{alloy}$	$a_{FeCr_2O_4}^{spinel}$
RK261-33	0.359(3)	0.322(1)	0.00109(2)	-4.82	-3.77(1)	0.98						
RK262-14/33	0.314(3)	0.331(1)	0.00077(1)	-4.69	-3.64(1)	0.75	0.359(3)	0.330(1)	0.000784(3)	-4.70	-3.65(1)	0.75
RK263-14/33	0.314(3)	0.334(4)	0.00066(2)	-4.64	-3.60(1)	0.64	0.359(3)	0.334(1)	0.00067(2)	-4.65	-3.60(1)	0.63
RK264-14/33							0.359(4)	0.337(4)	0.00059(1)	-4.60	-3.56(1)	0.56
RK265-14/33							0.359(4)	0.326(2)	0.00074(5)	-4.76	-3.71(1)	0.55

[a]RKx-y/z: experiment #x with initial Pt-Fe alloy #y in first pellet and #z in second pellet; y, z refer to the run in Kessel et al. (2001a) in which the initial alloy was produced. In each set of conditions, consecutive rows refer to spinel compositions in equilibrium with the Pt-alloys – OCa (pure chromite), OCb, OCc, OCd, OCe (compositions given in Table 1). Empty entries for experiments OCb-e indicate loss of Pt-alloy.

[b]Experimental conditions [$\log_{10} f_{O_2}$/time(hr)]: -11.63/402 (RK275-279); -11.20/431 (RK268-272); -10.61/313 (RK249-253); -9.67/216 (RK242-246); -9.22/309.5 (RK261-265).

[c] X_i^j=mole fraction of *i* in *j* based on three analyses for Cr and five for Fe in the Pt-alloys.

[d] γ_i^j= activity coefficient of *i* in *j*; model values calculated based on the Pt-Fe-Cr ternary model of Kessel et al. (2001b).

[e]Numbers enclosed in parentheses indicate one standard deviation of the mean calculated by error propagation.

[f]Activity of chromite in the spinel as calculated from reaction 1b.

Table 3. Meteoritic alloy composition

	Avanhandava (H4)		Allegan (H5)		Guareña (H6)	
	Kamacite	Taenite	Kamacite	Taenite	Kamacite	Taenite
#[a]	5/31	1/7	4/55	2/6	7/61	1/4
Fe[d]	93.11(103)	50.49(88)	91.89(83)	48.76(36)	92.27(74)	48.90(18)
Ni	6.35(21)	48.52(23)	6.41(31)	49.96(63)	5.95(40)	49.35(29)
Co	0.581(7)	0.118(6)	0.596(9)	0.142(10)	0.615(11)	0.127(6)
Si	0.012(11)	0.031(19)	0.011(8)	0.001(2)	0.018(8)	0.003(1)
Cr[b]	BDL[c]	BDL	BDL	BDL	BDL	BDL
Total	100.06	99.16	98.90	98.87	98.86	98.38

[a]x/y-x refers to the number of grains analyzed using the electron probe, and y refers to the total number of analyses. Points were analyzed randomly in the central regions of grains. Chromium was analyzed separately using SIMS (see footnote b).

[b]Average of 1-6 analyses in 1-2 grains in each meteorite, using ion probe (ASU).

[c]Below Detection Limit (3 ppb).

Table 4. Thermodynamic values and calculated metamorphic conditions of H chondrites

	Avanhandava (H4)	Allegan (H5)	Guareña (H6)
		Activities[a]	
Fayalite	0.156(6)	0.144(2)	0.158(9)
Ferrosilite	0.109(5)	0.110(0)	0.115(2)
Chromite	0.608(2)	0.606(0)	0.606(2)
Fe	0.904	0.904	0.904
Cr($x10^{-8}$)	3.88(70)	3.20(7)	3.25(40)
		Metamorphic conditions	
Temperature (°C)[b]	769(24)	787(27)	796(19)
$\log_{10} f_{O_2}$ (1a)[c]	-20.15(95)	-19.12(12)	-19.17(69)
$\log_{10} f_{O_2}$ (2a)	-21.32(66)	-20.61(11)	-20.60(54)
ΔIW (1a)	-0.59(32)	-0.25(4)	-0.27(23)
ΔIW (2a)	-1.77(4)	-1.75(2)	-1.72(6)

[a]Activities of silicates and oxides are from MELTS based on the meteoritic mineral compositions in Kessel et al. (2001c). Activities in metal are from Miettinen (1999) based on extrapolated bulk metal composition (see text). All are computed for the olivine-spinel temperatures quoted in each column.

[b]Average olivine-spinel equilibration temperature (Kessel et al., 2001c).

[c]Constrained by spinel-metal assemblages (reaction 1a) and by olivine-pyroxene-metal assemblage (reaction 2a).

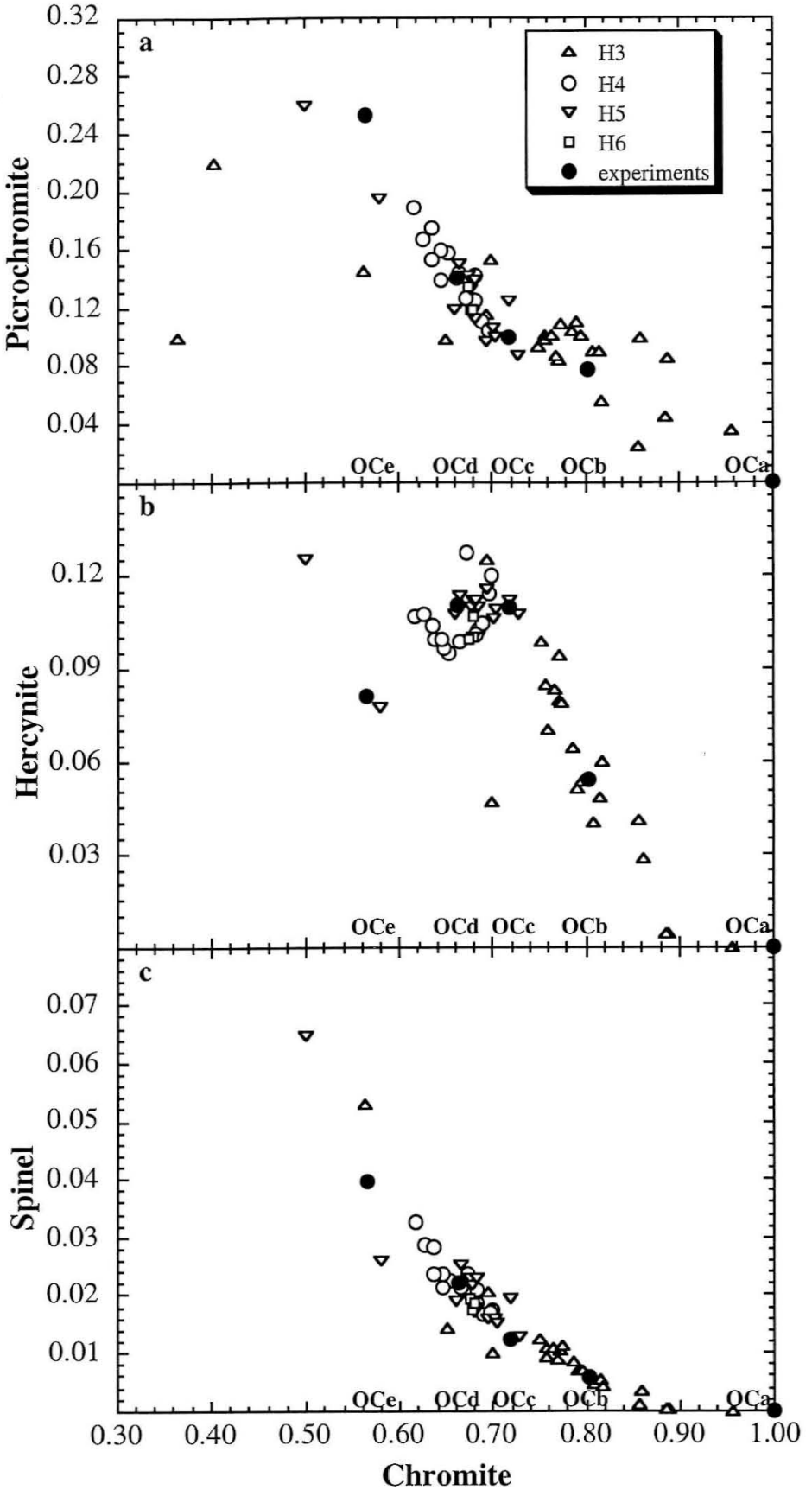
a
b
c
H3
H4
H5
H6
experiments
Picrochromite
Hercynite
Spinel
Chromite
OCe
OCd
OCc
OCb
OCa
0.32
0.28
0.24
0.20
0.16
0.12
0.08
0.04
0.12
0.09
0.06
0.03
0.07
0.06
0.05
0.04
0.03
0.02
0.01
0.30
0.40
0.50
0.60
0.70
0.80
0.90
1.00

Figure 1. Composition of spinel in H chondrites as a function of chromite content. Data sources: Bischoff and Keil, 1983; Bischoff et al., 1989; Bunch et al., 1967; Buseck and Keil, 1966; Ikeda et al., 1997; Johnson and Prinz, 1991; Keil, 1980; Kleinschrot and Okrusch, 1999; Snetsinger et al., 1967; Zinovieva et al., 1997. Also shown (filled circles labeled OCa-d) are compositions of spinels used in the experiments. (a) Picrochromite. (b) Hercynite. (c) Spinel.

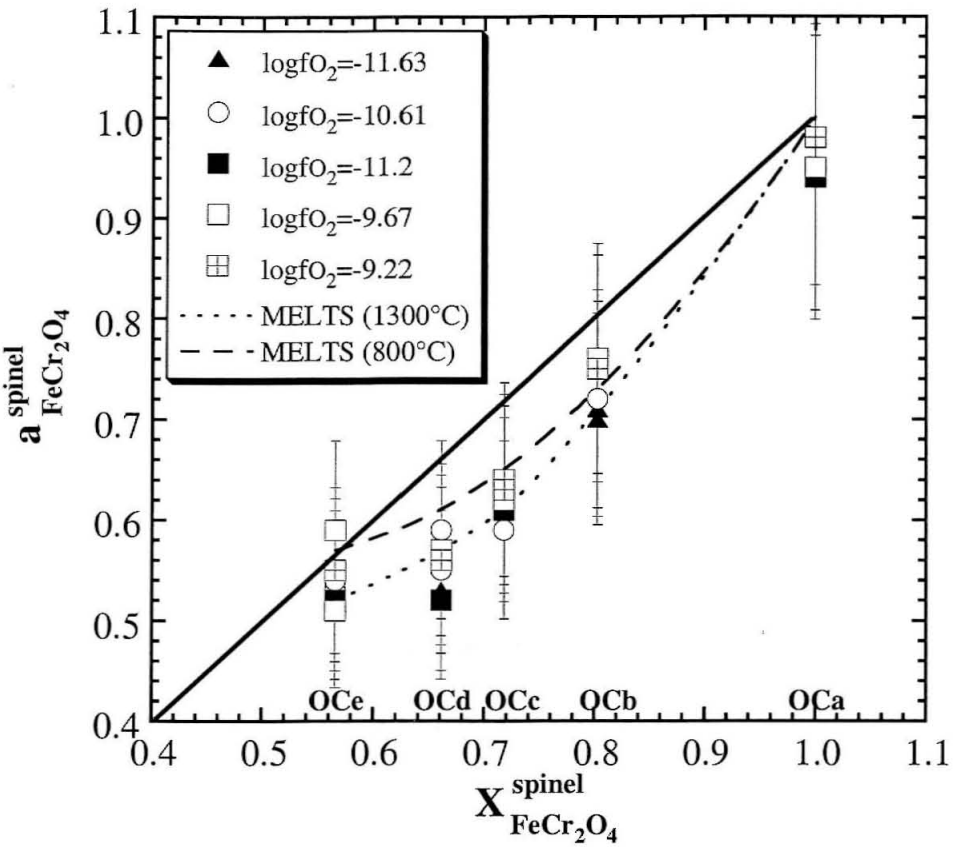

Figure 2. Activity of chromite in spinels whose compositions represents equilibrated H chondrites as a function of $X^{spinel}_{FeCr_2O_4}$. Symbols represent results of experiments from this study with error bars of 15% of value. The solid thick line represents a 1:1 line and the dashed curves represent activity-composition relationships obtained by smoothing line segments joining values calculated for our spinel compositions using the program MELTS at 1300°C and 800°C.

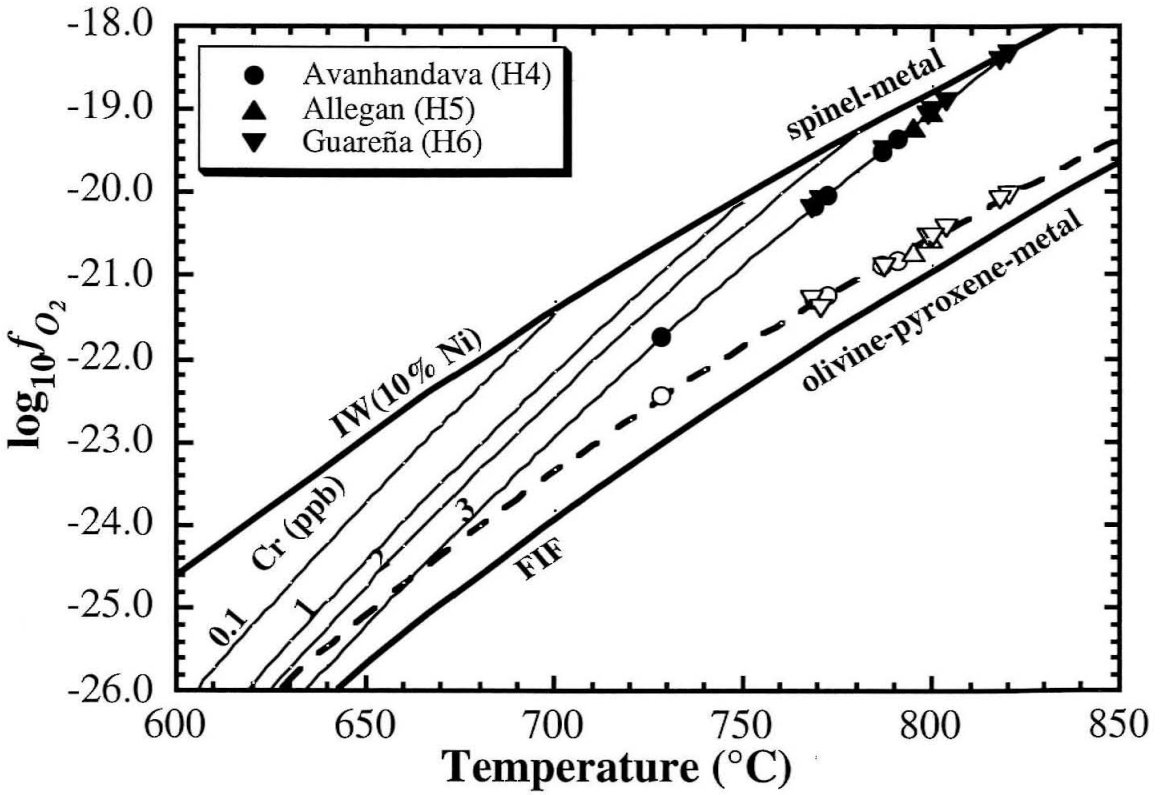

Figure 3. Values of $\log_{10} f_{O_2}$ as a function of olivine-spinel equilibration temperatures as constrained by the individual spinel-metal assemblages (filled symbols) and olivine-pyroxene-metal assemblages (open symbols). The Iron-Wüstite (IW) for a Fe-alloy containing 10% Ni and Fayalite-Iron-Ferrosilite (FIF) buffer is also shown as a reference. The solid curves are spinel-alloy based $\log_{10} f_{O_2}$ as a function of temperature for a range of Cr content. Dashed curve through the olivine-pyroxene-alloy results is shown as well. Curves involving alloy solid solutions are metastable below ~700°C.

SUMMARY

Spinel in equilibrium with other ferromagnesian silicates and metal are commonly used as geothermometers, geobarometers, and oxygen barometers. Knowledge of the thermodynamic properties of the phases allows one to relate the mineral compositions to temperature, pressure, and oxygen fugacity. Existing activity-composition models for multicomponent spinels are based on extrapolation of experiments on binary and ternary spinel subsystems. In this work an experimental technique was developed for evaluating chromite activities in multicomponent spinels.

The approach is based on equilibrating the spinel of interest with a Pt-alloy under a controlled temperature and oxygen fugacity, f_{O_2}, as expressed by the reaction:

$$Fe^{alloy} + 2Cr^{alloy} + 2O_2^{gas} = FeCr_2O_4^{spinel}. \quad (1a)$$

The activity of chromite in the spinel can be determined provided the activities of Fe and Cr in the equilibrated Pt-alloy and the equilibrium constant are known at the experimental conditions, according to the expression:

$$a_{FeCr_2O_4}^{spinel} = \exp[-\Delta G_1^{o} / RT](a_{Fe}^{alloy})(a_{Cr}^{alloy})^2 (f_{O_2})^2. \quad (1b)$$

A wide range of Pt-alloy compositions was created and used to construct an activity model for the ternary Pt-Fe-Cr system, from which activities of Fe and Cr in Pt-alloys can be obtained. The ternary activity model formulation used is based on the characterization of each bounding binary system, Pt-Fe, Pt-Cr, Fe-Cr, with the addition of a ternary interaction terms.

The activity-composition relationship in the Pt-Fe system was evaluated by equilibrating Pt wires with Fe-oxides at temperature range 1200-1400°C and $\log_{10} f_{O_2}$

from 1.6 to 7.7 log units above Iron-Wüstite (IW) buffer. The system is described as an asymmetric regular solution with interaction parameters of W_{PtFe}=–138.0±3.3 and W_{FePt}=–90.8±24.0 kJ/mol (1σ). The activity-composition relationship in the Pt-Cr system was evaluated by equilibrating Pt wires with Cr_2O_3 at 1300°C and $\log_{10} f_{O_2}$ from –0.9 to +2.9 log units relative to IW. Similar to the Pt-Fe system, the Pt-Cr system is characterized as an asymmetric regular solution with interaction parameters of W_{PtCr}=–129.1±1.2, W_{CrPt}=–80.9±4.4, and D_{PtCr}=+94.4±2.5 kJ/mol (1σ). The thermodynamic properties of the Fe-Cr system were taken from the literature. Combining the interaction parameters of the three bounding binaries, the ternary interaction parameters were constrained for a set of experiments in which the activity of Cr in Pt-Fe-Cr-alloys was fixed by coexisting Cr_2O_3 and vapor. With C_{Cr} set equal to zero, the remaining ternary interaction parameters are C_{Pt}=+115.7 and C_{Fe}=–68.6 kJ/mol.

To test the validity of the above ternary model, the free energy of formation of $FeCr_2O_4$ was evaluated at 1300°C from a set of experiments in which Pt-alloys were equilibrated with end-member $FeCr_2O_4$ and Cr_2O_3. The activities of Fe and Cr in the Pt-alloys were calculated using the ternary Pt-Fe-Cr model and the free energy of formation of chromite from the elements was found to be –923.5±2.1 kJ/mol (1σ). The free energy of formation of chromite from $Fe+Cr_2O_3+O_2$ was found to be –202.7±0.4 kJ/mol (1σ). Our results are consistent previous studies, providing a measure of the internal consistency of our ternary alloy model.

The activity-composition relationship of chromites in $(Fe,Mg)Cr_2O_4$ at 1300°C was evaluated from a set of experiments in which Pt-alloys were equilibrated with

$(Fe,Mg)Cr_2O_4+Cr_2O_3$. The activity of $FeCr_2O_4$ in $Fe_XMg_{1-X}Cr_2O_4$ was calculated in two ways. First, the equilibrium between Pt-alloy and coexisting Cr_2O_3 provided a direct method for calculating the activity of Cr in the Pt-alloy. In the second method, the activity of Cr in the Pt-alloy was calculated using the ternary Pt-Fe-Cr model. These experiments show that $(Fe,Mg)Cr_2O_4$ spinels can be described as a one-site symmetric regular solution with an interaction parameter of $W_{(Fe,Mg)Cr_2O_4}$=+2.14±0.62 kJ/mol (1σ). The agreement between both methods of calculation and with literature data demonstrates that the experimental approach described above is valid. The uncertainties in chromite activities derived based on the equilibrium between Cr_2O_3 and Pt-alloys are 6-7% (1σ). The uncertainties in chromite activities calculated from the composition of the Pt-alloy are larger (14-20%) due to the large uncertainty in the activity of Cr in Pt-alloys. However, this method of calculation provides a way for determining the activity of chromite even under conditions where Cr_2O_3 is not stable.

The above technique for evaluating the chromite activity in multicomponent spinels was used as part of a study on the metamorphic history of equilibrated ordinary chondrites. Peak metamorphic temperatures experienced by H, L, and LL equilibrated ordinary chondrites spanning petrographic types 4 to 6 were evaluated based on the equilibrium between olivine and spinel. Spinel-alloy and olivine-pyroxene-alloy oxygen barometers were used to evaluate the f_{O_2}-temperature relationships of equilibrated H chondrites.

Olivine-spinel equilibration temperatures were calculated by equating Fe-Mg exchange potentials of the two phases. All equilibrated ordinary chondrites studied

exhibit temperatures in the range of 659-829°C. This range of temperatures is much smaller than commonly assumed for these meteorites (600-950°C). Equilibration temperatures for the H chondrites are similar within error, 778±26°C, although mean, minimum, and maximum temperatures slightly increase with petrographic type. Maximum olivine-spinel temperatures recorded in L and LL chondrites are lower than in H chondrites and the type 4 chondrites record significantly lower temperatures than types 5 and 6. These results demonstrate that type 4 chondrites record variable temperatures that are lower than or equal to those of types 5 and 6 chondrites, implying a decoupling of metamorphic temperature from petrographic type. This decoupling indicates that the classification used to assign a type, which is based on textural and chemical maturation, is not an indication of metamorphic temperatures.

Flat composition profiles in spinel grains in contact with olivine constrain cooling rates near 800°C of 1-3 K/Ma. This cooling rate is slow enough to allow continuous re-equilibration of spinel grains to an olivine-spinel equilibration temperature that is lower than peak temperature, at which point, the profile is effectively frozen in. The olivine-spinel equilibration temperature is a function of the spinel grain size, such that larger grains, abundant in types 5 and 6 chondrites, record temperatures of ~800°C while smaller grains, rare in types 5 and 6 but abundant in type 4 chondrites, record lower temperatures. These results suggest a single stage thermal history at high temperatures for types 5 and 6 and some type 4 chondrites within each chondrite group. The lack of correlation between petrographic type and cooling rate can not be used as an argument in favor of a rubble-pile model because chondrite type and temperature are largely decoupled. By the same token,

increasing degree of metamorphism does not necessarily correspond to increasing depth within the parent body.

The oxidation state of equilibrated H chondrites was calculated based on spinel-alloy and olivine-pyroxene-alloy phase assemblages. Activities of chromite in multicomponent spinels whose compositions represent spinels in H chondrites were experimentally determined and found to be similar within errors to literature evaluation. Combined with activities of the ferromagnesian silicates and alloy, evaluated from literature formulations, $\log_{10} f_{O_2}$-temperature relationships and olivine-spinel equilibration temperatures were used to constrain the absolute f_{O_2}.

$\mathrm{Log}_{10} f_{O_2}$ values based on the assemblage olivine-pyroxene-alloy are –1.75±0.02 log units below Iron-Wüstite (IW) buffer, regardless of petrographic type. Oxygen fugacities calculated using spinel-alloy are at least ~1.5 log units more oxidizing than those based on the olivine-pyroxene-alloy at the same temperature. The higher f_{O_2} values calculated for spinel-alloy coexistence indicate lower closure temperatures than for olivine-spinel equilibration temperature and are probably recording retrograde conditions.